NOVEL DRUG INTERACTION FOR IMPROVING INTRACELLULAR ACCUMULATION AND EFFICACY OF CHEMOTHERAPEUTICS IN RETINOBLASTOMA AND MITOCHONDRIAL LOCALIZATION OF TRANSPORTERS IN CORNEAL EPITHELIAL CELLS

A DISSERTATION IN
Pharmaceutical Sciences
and
Chemistry

Presented to the Faculty of University
of Missouri - Kansas City in partial fulfillment
of the requirements for the degree

DOCTOR OF PHILOSOPHY

by
MEGHA BAROT
M. Pharm., Sardar Patel University, India, 2006

Kansas City, Missouri
2013

NOVEL DRUG INTERACTION FOR IMPROVING INTRACELLULAR ACCUMULATION AND EFFICACY OF CHEMOTHERAPEUTICS IN RETINOBLASTOMA AND MITOCHONDRIAL LOCALIZATION OF TRANSPORTERS IN CORNEAL EPITHELIAL CELLS

Megha Barot, Candidate for the Doctor of Philosophy Degree,

University of Missouri-Kansas City, 2013

ABSTRACT

Chemoreduction is the key treatment for retinoblastoma management. However, anticancer agents suffer from poor cell permeability and chemoresistance due to major interaction with multidrug resistant (MDR) efflux proteins (MDR1 and MRP2) over-expressed on retinoblastoma tumor. Ocular cells have shown good tolerability against antimicrobial moxifloxacin (fourth generation fluoroquinolone) at higher dose level. As majority of fluoroquinolones become ineffective due to efflux mediated acquired drug resistance therefore, we have first determined an interaction of moxifloxacin with efflux (MDR1 and MRP2) transporters. Our results provides direct evidence that moxifloxacin is an overlapping substrate of MDR1 and MRP2 efflux transporters. Since, literature has evident co-administration of overlapping drug substrate as a viable strategy to overcome MDR. Therefore, we have tested moxifloxacin potential to overcome chemoresistance in retinoblastoma. Our results showed that 2-2.5 fold increased uptakes of three anticancer drugs (etoposide, topotecan and vinblastine) were observed in the presence of moxifloxacin across model cell lines suggesting moxifloxacin mediated evasion of efflux pumps. Significant reductions in efflux ratio of these anticancer agents were also observed in the presence of moxifloxacin indicating moxifloxacin mediated improved anticancer

transport. Following cytotoxicity study, tenfold reduction in IC50 value of topotecan and etoposide and twofold reduction in IC50 value of vinblastine was observed in the presence of moxifloxacin. Significant enhancement of anticancer mediated caspase-3 enzyme activity and reduction in proinflammatory cytokines (IL-8 and IL-6) release were also observed in the presence of moxifloxacin. There is a need to further explore this finding to confirm its clinical feasibility, if proven, ultimately it will aid to reduce the chemotherapeutic dose and associated dose-limiting toxicities.

Considering the fact that most drug targets are indeed contained within specific intracellular compartments, the ability of a drug to accumulate into these sites is a critical determinant in the observed drug response. Mitochondrion is an attractive target for drug-delivery because there is a growing confirmation to support an association between mitochondrial dysfunctions and a number of ocular diseases. A range of possibilities exist for the selective drug delivery to the mitochondria one among such is a transporter targeted strategy. Localization of various influx and efflux transporters is generally considered to be restricted to cell surface level. However, cellular compartments may also be a potential site for these transporters. The functional localization of both efflux (MDR1) and influx (PepT-1) transporters in the mitochondrial membrane of primary corneal epithelial cells was studied. Isolation and purification of mitochondria was performed by optimized cell fractionation method. Functional activity of MDR1 and PepT-1 transporter was assessed by performing *in vitro* uptake studies on isolated mitochondria. Molecular characterization of both transporters was confirmed by western blot and confocal analysis. This knowledge of mitochondrial existence of MDR1 and PepT-1transporter may aid in the development of subcellular ocular drug delivery strategies.

APPROVAL PAGE

The faculty listed below, appointed by the Dean of the School of Graduate Studies have examined a dissertation titled "Novel Drug Interaction For Improving Intracellular Accumulation and Efficacy of Chemotherapeutics in Retinoblastoma and Mitochondrial Localization of Transporters in Corneal Epithelial Cells," presented by Megha Barot, candidate for the Doctor of Philosophy degree, and certify that in their opinion it is worthy of acceptance.

Supervisory Committee

Ashim K. Mitra, Ph.D., Committee Chair
Department of Pharmaceutical Sciences

Chi Lee, Ph.D.
Department of Pharmaceutical Sciences

Kun Cheng, Ph.D.
Department of Pharmaceutical Sciences

J. David Van Horn, Ph.D.
Department of Chemistry

Santosh Kumar, Ph.D.
Division of Pharmacology

CONTENTS

ILLUSTRATIONS

Figure Page

TABLES

Table Page

ACKNOWLEDGEMENTS

First of all I would like to express deep sense of gratitude to my research adviser Dr. Ashim K. Mitra for being a pillar of support and inspiration throughout my graduate studies. It is with deep reverence that I thank him for boosting my confidence in difficulties and providing me all possible resources during the course of training. I am also grateful to Drs. Chi Lee, Kun Cheng, David Van Horn and Santosh Kumar for serving on my supervisory committee and also for their timely help and guidance throughout my graduate work.

I take the opportunity to express my humble thanks to Dr. Russell B. Melchert, Dean of the School of Pharmacy at UMKC for his constant support and motivation. I am highly indebted to Dr. Dhananjay Pal for his valuable guidance and Mrs. Ranjana Mitra for her motherly love and encouragement. I heartily appreciate the selfless help extended to me by my husband Mitan. His endless standing with me during entire research has enabled me to stand confidently against all the challenges. I would also like to thank Drs. Ripal Gaudana and Deep Kwatra for their valuable advice and timely cooperation during my research at UMKC. I am also thankful to all my labmates and frineds for their support and creating a cheerful environment throughout my graduate studies. A special note of thanks to Joyce Johnson, Sharon Self, and Ashley Ismert at School of Pharmacy and Connie Mahone, and Nancy Hover at School of Graduate Studies for moral support and administrative help.

I take an opportunity to appeal my profound gratitude to my parents, younger siblings, late grandparents and my in-laws for their everlasting love, strong moral support, encouragement and personal sacrifice without which I was unable to reach the present status of education. Finally, I offer flowers of gratitude to the almighty Radhasoami who has been the source of strength throughout my life.

DEDICATED TO ALMIGHTY GOD, FAMILY AND MITAN

CHAPTER 1

LITERATURE REVIEW

1.1 Barriers for Posterior Segment Ocular Drug Delivery

Drug delivery, particularly to the posterior ocular segment remains an extremely challenging task due to its restrictive barrier functionalities. Blood-ocular barriers act as a physical barrier between the local blood vessels and ocular tissues and fluids. These barriers also control the passage of various solutes and effectively impedes the transport of various ocular therapeutic agents [1]. Research on the posterior segment diseases, such as age-related macular degeneration (AMD), diabetic macular edema (DME), retinitis pigmentosa, endophthalmitis and proliferative vitreoretinopathy is of high clinical significance.

Drug delivery to the retina remains a challenging task due to various limitations and inefficiency associated with topical and systemic administrations. Various forms of local formulation strategies for intravitreal and transscleral drug delivery to the retina have recently emerged [2,3]. While intravitreal delivery is the primary mode of therapy to the retina, it also carries various risks that include cataract, endophthalmitis, retinal puncture and detachment [4-8]. Transscleral delivery is an alternative form of local therapy to the retina which includes, sub-conjunctival, sub-tenon's, retrobulbar, peribulbar and intrascleral administrations (Fig. 1). Transscleral delivery offers localized drug delivery with a less invasive procedure compared to intravitreal administration [2].

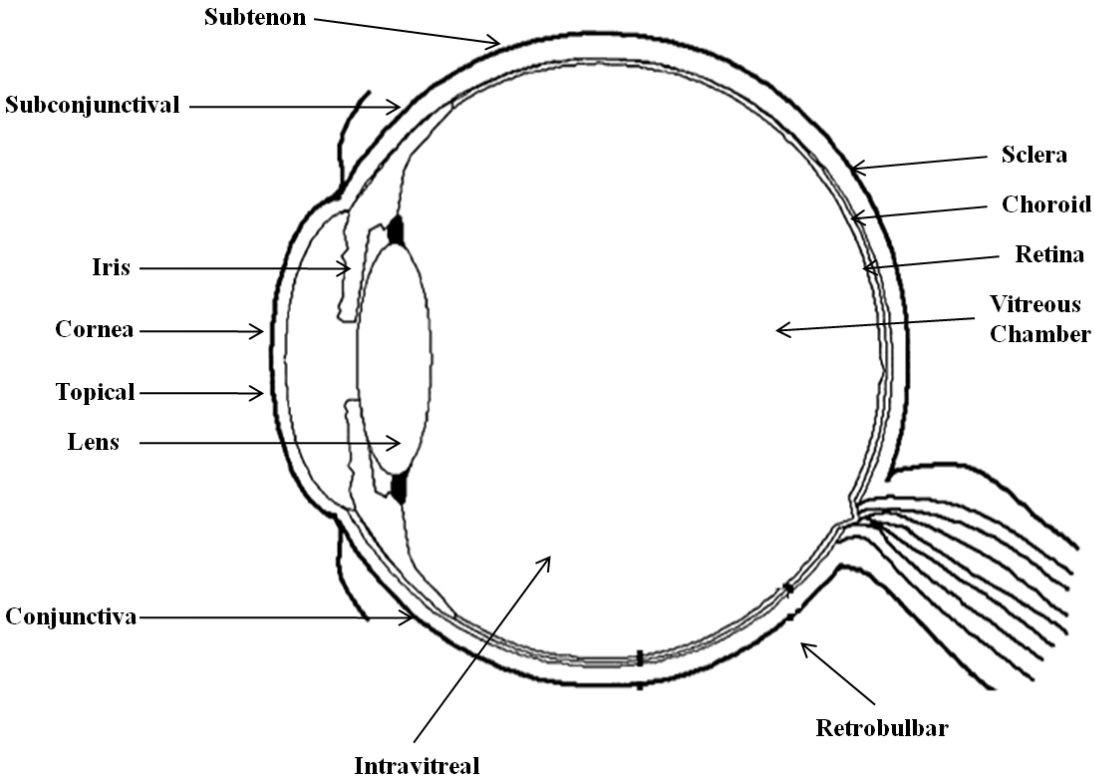

Figure 1. Structure of eye depicting anatomy and routes of administration.

Posterior segment drug delivery requires actives to permeate through various ocular tissue layers (sclera, Bruch's membrane-choroid, and retinal pigment epithelium) before reaching the neural retina. As a result, a very steep concentration gradient is established and very low amounts are detected in the retina. This steep gradient is due to barriers that hinder molecules from successfully reaching the retina. Ocular barriers may be classified as static and dynamic barriers. Static barriers comprise of those ocular tissues that pose a physical barrier to drug diffusion such as sclera, Bruch's membrane-choroid, retinal pigment epithelium and conjunctiva. Dynamic barriers include drug clearance mechanism through blood and lymphatic vessels [2].

1.1.A Static Barriers

Sclera

The sclera is elastic and microporous tissue consists of proteoglycans and closely packed collagen fibers [2,9]. Collagen fibrils embedded in a glycosaminoglycan matrix is the major component of the sclera, with type I being the major collagen type [10,11]. The structure of the sclera, pore diameter and intracellular space may help to determine the behavior of drug movement [2]. Due to the regional difference in collagen architecture, posterior sclera is almost twice as thick as the anterior sclera [12] and has only 60% of the stiffness of the anterior sclera [13]. Posterior sclera is composed of loose weave of collagen fibers having a greater degree of extensibility in comparison to the more uniform weave orientation of anterior sclera which explains its higher permeability for solutes [14]. Lateral orientation of the scleral fibers may also affect drug transport, as diffusion within the sclera in the lateral direction appears to be a slower process that produces localized drug distribution on a millimeter scale over h to days [15]. Moreover due to hypocellular nature of

the sclera, it has very low level of proteolytic enzymes or protein-binding sites that can degrade or sequester drugs. Slower hydrolysis of various prostaglandin ester prodrugs further indicate low protease activity in sclera compared to the cornea [10,16]. *Ex-vivo* permeability of sclera has been extensively reported in the literature suggesting relatively high scleral permeability relative to the cornea (Table 1) [16-20].

Table 1. Comparison of scleral versus corneal drug permeability [16-20].

Drug	Permeability Coefficient (10^{-6} cm/sec)		Scleral Permeability
	Cornea	Sclera	(fold increase)
Prostaglandins	1.7 (± 0.5)	15.6 (± 2.5)	15 times
Insulin and beta-blockers	1.9 (± 0.2)	8.5 (± 2.3)	5 times
Hydrocortisone	4.5 (± 0.7)	21.8 (± 4.3)	5 times
Polyethylene glycol	1.0	8.8	9 times
Carbonic anhydrase inhibitors	-	-	10 times

This fact has resulted in delivery of several drug molecules via transscleral route especially for posterior segment ocular diseases. Several factors influence scleral permeability of molecules. It has been a strong dependence on molecular weight (Table 2), with smaller molecules exhibiting higher permeabilities then larger molecules [20-23]. However, Ambati *et al*. have demonstrated scleral permeability for higher molecular weight dextrans, IgG and bovine serum albumin [21,24]. This anomaly may be explained by an orientation effect of asymmetrical particles in a matrix. Degrees of asymmetry of molecules rise with ascending molecular weight [22]. Thus facilitated diffusion in the matrix will be more pronounced like an extended polymer such as dextrans [14,24]. However, molecular radius was found to be much better predictor of scleral permeability than molecular weight. Globular protein albumin (3.62 nm) has higher scleral permeability than the linear dextran (4.5 nm) of the same molecular weight across rabbit sclera [10,21]. Results from log-linear regression analysis shows that molecular radius is a better predictor of scleral permeability ($r^2 = 0.87$, $P = 0.001$) than molecular weight ($r^2 = 0.31$, $P = 0.16$). Experimental data (Table 2) demonstrated that scleral permeability roughly decreases exponentially with molecular radius [21,25].

Table 2. Effect of solute's molecular weights and molecular radii on scleral permeability [20-23].

Compound	Molecular Weight (D)	Radius (nm)	Permeability Coefficient (10^{-6} cm/sec)	Species
Sucrose	342	0.48	21.6 ± 6.0	Human
Dextran-10	10000	0.23	6.4 ± 1.7	Human
Dextran-40	40000	0.73	4.9 ± 2.4	Human
Dextran-70	70000	0.81	1.9 ± 0.4	Human
Sodium Fluorescein	376	0.50	84.5 ± 16.1	Rabbit
FITC-D, 4	4400	1.30	25.2 ± 5.1	Rabbit
FITC-D, 20	19600	3.20	6.8 ± 4.2	Rabbit
FITC-D, 40	38900	4.50	2.8 ± 1.6	Rabbit
FITC-BSA	67000	3.62	5.5 ± 2.1	Rabbit
Rhodamine D,70	70000	6.40	1.4 ± 0.8	Rabbit
FITC-D, 70	71200	6.40	1.4 ± 0.9	Rabbit
FITC-IgG	150000	5.23	4.6 ± 2.2	Rabbit
FITC-D,150	150000	8.25	1.4 ± 0.9	Rabbit

Boubriak *et al*. have reported that a diffusion coefficient increases in the sclera as hydration increases [22]. Large surface area (16-17 cm^2) of the sclera and a high degree of hydration renders it conducive to water-soluble substances [11]. An increase in a solute's lipid solubility is reported to lower the scleral permeability across rabbit and human sclera [26,27]. Other authors also reported higher scleral permeability for hydrophilic molecules [28,29]. Anionic molecules possess higher permeability then cationic molecules in bovine, porcine and rabbit sclera (Table 3) [30-32].

Scleral permeability is also altered by physical changes such as surgical thinning, cryotherapy, transscleral diode laser and variations in transscleral pressure [23]. Surgical thinning of the sclera predictably increases permeability whereas cryotherapy and diode laser treatment may not alter the permeability or ultrastructure of sclera [23]. Effect of simulated transscleral pressure on scleral permeability has been demonstrated across human and rabbit sclera which suggest decreasing in scleral permeability at higher intraocular pressure despite the tendency for a lowering in scleral thickness with higher pressure [9,33,34].

Table 3. Effect of physicochemical properties of solutes on ocular tissue permeability.

Ocular Tissue	Molecular Radius	Lipophilicity	Charge
Sclera	Permeability exponential decreases with increasing molecular radii [21,25]	Permeability decrease with increasing lipophilicity [11,26,27]	Permeability increase with negatively charged solute [30-32]
Bruch's membrane-choroid	Permeability decreases with increasing molecular radii [35]	Permeability decrease with increasing lipophilicity [30,36]	Permeability increase with negatively charged solute [30,37]
Retinal pigment epithelium	Permeability exponential decreases with increasing molecular radii [35]	Permeability increase with increasing lipophilicity [35]	-

Bruch's Membrane-Choroid (BC)

The choroid is a vascular tunic part of the eye that supplies blood to the outer two-thirds of the retina. Similar to sclera, the choroid is also made up of collagen and can be considered as a matrix. Higher melanin content of choroid differentiates it from sclera [30,38]. In terms of solute permeability, the choroid-Bruch's layer generally offers greater resistance than does the sclera due to the presence of melanin and lipodial plasma membranes of endothelial cells. Due to rapid blood flow, choroid-Bruch's layer could be an even more formidable barrier *in vivo*, which can potentially remove solutes before reaching the neural retina [30,39].

Bruch's membrane and choroid permabilities have always been studied in tandem due to the difficulty of separating the two tissue layers [2,30]. Choroid-Bruch's layer permeability has been studied across the bovine and porcine tissue which has shown dependency on a solute's lipophilicity and molecular radii [30,35,36]. A trend line of decreasing choroid-Bruch's layer permeability with increasing solute lipophilicity or molecular radii appear to be steeper than sclera. Overall results suggest that mechanistically, transport across the choroid-Bruch's layer occurs in a fashion similar to transport across the sclera, differing only in magnitude, with the former being a more significant barrier for lipophilic solutes [2,30,36]. In addition to lipophilicity and molecular radii, molecular charge is another factor that should be taken into consideration. It has been shown that similar to sclera, choroid-Bruch's layer is also more permeable to negatively charged solutes over positively charged solutes (Table 3) [30,37].

Resistance to solute transport across the choroid has been observed due to age-related changes in human Bruch's membrane [30,40]. However, no significant change in

permeability or ultrastructure of sclera has been observed due to ageing [23]. It has been reported that Bruch's membrane thickens (from 2 to 4.7 μm between first to tenth decades of life) and the choroidal layer thins out (11 μm per 10 years) with aging in the human eye [41]. Moreover, age-related linear diminution in hydraulic conductivity has been reported. Taurine and other amino acid transport across the choroid-Bruch's layer in humans has been studied [40,42,43]. These results indicated that the aged Bruch's membrane offers a major resistance to solute transport [40,42]. Permeability of human Bruch's membrane to serum proteins was also reported to diminish about 10-fold from the first to ninth decade of life [44].

Taken together these reports indicate that the choroid-Bruch's layer is a significant barrier to transscleral delivery of drugs. If the choroid is the intended target for treatment such as choroidal neovascularization, higher level of free drug in the choroid can be achieved by designing hydrophilic and anionic drugs and/or prodrugs relatives to lipophilic and cationic ones [30]. If retina is the intended target in addition to choroid-Bruch's layer then there may be a further reduction in drug transport because of the presence of RPE which will be further discussed in the following section.

Retinal Pigment Epithelium (RPE)

The retina is a multilayered membrane of neuroectodermal origin and can be broadly divided into the neural retina and the RPE. Neural retina is involved in signal transduction, leading to vision. RPE, on the other hand, is a single cell layer lies at the interface between the neural retina and the choroid. It plays a vital role in supporting, and maintaining the viability of the neural retina [3,45]. The RPE is compared of a monolayer of highly specialized cuboidal cells located between the neural retina and the choroid [46]. It restricts

the absorption and permeation of drugs from choroid to the retina, to its intercellular junctions it is considered to be a tight barrier [35].

RPE can be easily removed and its permeability function assessed by comparing tissue permeability values with and without removal of RPE [2,47]. RPE permeability determines the transport of solute from the choroidal circulation to neural retina following systemic administration. Moreover, RPE permeability may also depend on drug binding to the melanin pigment or tissue proteins, active transport processes and metabolism [35,48,49]. In monkeys, the movement of horseradish peroxidase (44 kDa molecules) stopped at the tight RPE junctions [50,51]. However, in another study following subconjunctival administration, it was observed that the fluorescein-conjugated pigment epithelium-derived factor (PEDF) and ovalbumin proteins permeated to the cultured RPE monolayer of monkey even in the presence of fully formed tight junction. This data suggests that subconjunctival protein delivery may be feasible for delivering of proteins like PEDF and ovalbumin [47].

With hydrophilic molecules and macromolecules, RPE may be the rate-limiting barrier for the retinal drug delivery. Permeability of bovine RPE for hydrophilic carboxyfluorescein and FITC-dextrans shows exponential decrease with increase in molecular radius. In addition, permeability of lipophilic compounds (metoprolol and atenolol) is significantly higher whereas scleral permeability is less sensitive to solute lipophilicity. Moreover, macromolecules (dextran) transported passively across the retina have shown similar permeability values in the outward (retina choroid) and inward directions. However, carboxyfluorescein active transport shows difference in that outward permeability is higher than inward direction. It appears that the RPE presents a tighter barrier than

sclera for hydrophilic small and large molecules, therefore scleral permeability alone is not sufficient to predict the drug delivery rate to the retina [2,35].

Conjunctiva

The conjunctiva is a thin, mucus-secreting transparent epithelial barrier; relatively well vascularized tissue covering the anterior one-third of the globe. It consists of two layers: an outer epithelium and its underlying stroma (substantia propria). The epithelial cells connect with each other by tight junctions at the apical side and act as a permeability barrier. The conjunctiva acts as a simple protective role in the eye by functioning as a passive physical barrier. It also participates in the maintenance of tear film stability by secretion of electrolytes, fluid, and mucins [52-54].

Paracellular transport, through the tight junctions of the conjunctival epithelial cells may be the rate-limiting step for diffusion of macromolecular drugs [52,54]. Since hydrophilic drug penetrates occurs via paracellular pathway (between the cells through the tight junctions), the total penetration surface area for any hydrophilic drug is extremely small compared to the surface area offered by transcellular pathway for absorption of lipophilic drugs [52,55]. Hence paracellular pathway of epithelial barriers (like cornea and conjunctiva) where adjacent cells are held together at the apical membrane by tight junctions, can act as the rate-limiting step for diffusion of hydrophilic macromolecule drugs including peptides and proteins [52,56,57]. Data from equivalent pore analysis suggests that conjunctiva may allow the permeation of hydrophilic compounds having molecular weight less than 20 kDa. The theoretical radius of such equivalent pores is predicted to be ~ 5.5 nm [58]. Transport studies of a series of hydrophilic molecules e.g. D-mannitol (182 Da), 6-carboxyfluorescein (376 Da), and fluorescein isothiocyanate-labeled dextrans (4400, 9400, 21300, and 38600 Da

respectively) across the conjunctiva have shown a decline in permeability coefficients with increase in molecular weight of a solute. This results confirms that the conjunctiva may allow reasonable permeation of hydrophilic substances with a molecular weight less than 20 kDa, whereas cornea appears to offer significant resistance to inulin (5 kDa) and FD (20 kDa) solutes [56,58]. Moreover, conjunctival surface area is larger (~ 9 and 17 times) than cornea in rabbits and human, respectively. This may be another contributing factor for greater absorption of hydrophilic drugs via conjunctival route, as conjunctiva is much leakier with numerous tight junctions than cornea [52,59].

Tissue resistance is a good indicator of passive barrier properties of a given biological barrier. Kompella *et al*. have shown that the freshly excised pigmented rabbit conjunctiva portrays a moderately tight epithelium with a transepithelial electrical resistance (TEER) of ~ 1.3 kU cm^2. The conjunctival tissues excised from pigmented rabbits have a lower TEER than the tighter rabbit cornea with a TEER value of ~ 7.0 – 9.0 kU cm^2 [60-62]. This data further explains that the rabbit conjunctiva in general is more permeable to hydrophilic solutes than cornea, as demonstrated earlier using *in-vivo* study [63]. Thus, the conjunctival-scleral pathway is favored for delivery of hydrophilic drugs because this mode of administration may evade the anterior chamber and drug may get direct access to the intraocular tissues of the posterior segments [52].

In addition to structural barrier, the penetration of peptide drugs across the conjunctiva is also restricted by external enzymatic barrier [64]. For example, ocular delivery of enkephalins, substance P, and insulin are significantly degraded due to enzymatic activity [64-66]. Co-administration of protease inhibitor(s) may be one of the approaches to enhance absorption of peptide and protein drugs. The presence of camostat mesylate (an

aminopeptidase inhibitor) and leupeptin (a serine protease inhibitor) in the mucosal fluid resulted in transport of intact arginine vasopressin across the pigmented rabbit conjunctiva [67].

1.1.B Dynamic Barriers

Conjunctival Blood Flow

Tissues themselves (i.e. sclera, non-perfused choroid and retina) may not be the sole barrier to drug transport into the eye, and other factors, such as lymph and blood circulation play an important role in diminishing drug delivery to the posterior segment. The conjunctiva is well vascularized and several studies have reported that drug from conjunctival tissue may be cleared through blood and lymphatic vessels [39,68].

Longer retention of subconjunctivally injected microparticles compared to nanoparticles and higher half-life of albumin compared to ^{22}Na in subconjunctival tissue suggest that molecular size may control the rate of conjunctival/episcleral clearance [69,70]. The barrier location and clearance parameters of ocular tissue need to be considered when designing a transscleral drug delivery system. Rapid transscleral movement into the vitreous, under complete cessation of lymph and blood clearances following euthanasia, was demonstrated by hydrophilic contrast agents and magnetic resonance imaging [71]. Robinson *et al.* have also demonstrated that selective elimination of the conjunctival/episcleral clearance mechanisms results in higher amounts of intraocular drug penetration. Rabbits receiving a sub-Tenon's injection of triamcinolone acetonide with an incised 'conjunctival window' inhibit local blood and lymphatic clearance in the conjunctiva. Under this condition higher drug levels in the vitreous were observed than rabbits that did not have the incision [2,39].

Studies were also performed to compare the delivery of sodium fluorescein to the retina following periocular injection and a unidirectional episcleral exoplant. The exoplant allowed release of dye on the episcleral side but not on the conjunctival side. Higher amounts of sodium fluorescein were detected in the retina following a unidirectional episcleral explant than periocular injection. The results from these studies suggest that conjunctival/episcleral clearance mechanisms play a significant role in the reduction of intraocular drug penetration [2,72].

Choroidal Blood Flow

Choroidal blood flow is among the highest per unit volume in the body. The choriocapillaris containing large fenestrations deliver oxygen and nutrients to the eye, suggesting that the choroidal blood flow could act as a sink for molecules and prevent therapeutic agents from reaching the target. A very few reports have been available in the literature showing effect of choroidal circulation on drug delivery to posterior segment tissues [73,74]. Using episcleral implants on rabbits, Kim *et al*. have observed significant vitreous concentrations in e*x-vivo* experiments but negligible vitreous concentrations during *in-vivo* experiments. The authors had attributed the observed difference to the choroidal blood flow and assumed the choroid to be a complete sink in their computational model [71].

Robinson *et al*. have used cryotherapy as a method to eliminate choroidal blood flow locally. A single freeze-thaw cycle with cryotherapy forms a chorioretinal scar but leaves the conjunctiva and sclera intact. Results from this study showed that elimination via the conjunctival lymphatic/blood vessels was more effective in reducing vitreal concentrations than elimination by choroidal vessels. Hence, this study suggests that choroidal blood flow may not significantly contribute to drug elimination following transscleral delivery [39].

Balachandran *et al.* supports this finding with Thiele modulus that suggests that a large fraction of the dose diffuses through the choroid without being washed away by the blood flow. Hence, clearance by the blood flow is not as important factor for drug loss as previously thought. The results of the study show that a loss to choroidal circulation is not as important impeding factor as thought previously. In contrast, the mass transfer from the scleral surface was found to be significant and therefore, design of the drug vehicle to be placed on the episcleral region needs more attention [73].

Blood Retinal Barrier (BRB)

The integrity of the BRB has been recognized as an important component of normal vision. Disruption of this barrier may cause various retinal vascular diseases and macular pathologies, causing blindness. BRB serves as a selective partitioning barrier and restricts drug movement between the retina and blood circulation. It also maintains a highly specialized environment of the neural tight junction. BRB is located in the posterior part of the globe and is composed of two parts. The tight junctions of the retinal pigment epithelium serves as a outer part of the barrier while the endothelial cells and pericytes of the retinal blood vessels serve as a inner part of the barrier [75,76]. Under normal pathological conditions, BRB serves as "non-leaky" firm tight junctions and restricts diffusion of various small molecules like glucose, amino acid [77], sodium ions and fluorescein into the retina [78,79].

Inner Blood Retinal Barrier

The inner part of the BRB is similar to the blood-brain barrier except presence of higher density of interendothelial junctions and endothelial vesicles. In addition, it also possesses a slightly higher vascular permeability. Inner BRB also expresses about four times

as many pericytes, which may limit leakiness of the vasculature despite a reduced transcellular resistance [80]. It has been suggested that pericytes can add to the tightness of the inner barrier. Lower pericyte density has been observed as one of pathological change in diabetic retinopathy where retinal vessels leak [81]. A break in the BRB at optic disc has been observed which may allow diffusion of hydrophilic substances from choroid into optic nerve head [78]. The barrier property of retinal vascular endothelium has been observed for fluorescein (376 D) and also for larger molecules including thorium oxide, horseradish peroxidase (40 kD) and microperoxidase (1.9 kD) [76,81,82]. The significance of the BRB to retinal disease has been demonstrated by fluorescein angiography. Clinical investigation can detect relationships between the breakdown of the BRB and diverse retinal disease [83]. In a healthy eye, very small quantity of fluorescein or its metabolite fluorescein glucuronide transport is noted across the barrier. However, more fluorescein leakage occurs in diabetic retinopathy then in nonpathological state. Although fluorescein molecules in smaller diameter and eighteen times more lipid soluble then fluorescein glucuronide, the permeability of both molecules was found to be similar. This observation suggests that neither molecular dimension nor lipid solubility is the rate limiting factor for enhanced BRB transport in diabetic retinopathy. Rather, the leakiness appears across the water-filled pores in the barrier. Moreover ultrastructural changes can be seen in capillaries that invade the retina during phototoxic retinopathy [84,85].

Outer Blood Retinal Barrier

It is comprised of junctions at apical border between adjacent retinal pigment epithelial cells. These tight junctions are composed of multiple layers of anastomosing strands. It has been reported that the BRB breakdown in diabetic RPE is due to alterations of

plasma membrane permeability rather than a loss of tight junctions. In the dystrophic rat retina, there is no change in the plasma membrane permeability, rather there is a loss in the number of junction strands [76].

1.2 Ocular Transporters

Recent progress in transporter identification has greatly contributed to the field of ocular drug delivery. Various transporters have been explored and recognized for transferring exogenous and endogenous nutrients across the cell membranes [86]. Various efflux (Table 4) and influx (Table 5) transporters have been identified on the various region of the eye. A major role of influx transporters is to deliver essential nutrients and therapeutic molecules across various ocular barriers. However, an efflux transporter relatively lowers ocular bioavailability of therapeutic drug by pushing molecules out of the cell. Anticancer, antifungal, antiviral, steroids and fluoroquinolones are known substrates of efflux transporters, which lowers ocular bioavailability [87-90]. Several strategies have been applied to evade drug efflux, among which transporter targeted prodrug derivatization is one of the most successfully utilized approach for improving ocular bioavailability of therapeutic agents [91,92].

Table 4. Efflux transporters in various ocular tissues [91].

Ocular Tissue	P-glycoprotein	Multidrug Resistance Associated Proteins	Breast Cancer Resistance Protein
Cornea	human and rabbit cornea	rabbit cornea, human corneal epithelial cells (HCEC)	HCEC
Conjunctiva	rabbit conjunctival cells	human conjunctiva	-
Retina	rabbit retina	-	-
Retinal pigment epithelium (RPE)	human RPE	human RPE cells	human RPE cells

Table 5. Influx transporters in various ocular tissues [91].

Influx Transporters	Substrates	Ocular Tissues
PepT1	Dipeptides	cornea, conjunctiva, retina, RPE, BRB
GLUT1	Glucose	cornea, conjunctiva, retina, RPE, BRB
ENT1	Nucleoside	cornea, conjunctiva, retina, RPE, BRB
MCT	Monocarboxylate	cornea, retina, RPE, BRB
SVCT2	Ascorbic acid	cornea, retina, RPE, BRB
SMVT	Biotin	cornea, retina, RPE, BRB
Riboflavin	Riboflavin	cornea, retina, RPE
LAT1, LAT2	Large neutral amino acids	cornea, retina, RPE, BRB
ASCT1	Neutral amino acids	cornea, retina, BRB
B(0,+)	Neutral and cationic amino acids	cornea, conjunctiva, retina, BRB
RFT	Reduced folate	retina, RPE, BRB
PCFT	Folate	retina, RPE, BRB

PepT = Peptide transporter; GLUT = Glucose transporter; ENT = Equilibrative nucleoside transporter; MCT = Monocarboxylate transporter; SVCT = Sodium-dependent vitamin c transporter; SMVT = sodium-dependent multivitamin transporter; LAT = L-amino acid transporter; ASCT = alanine-serine-cysteine transporter; RFT = Reduced-folate transporter; PCFT = Proton-coupled folate transporter; RPE = Retinal pigment epithelium; BRB = Blood-retinal barrier.

1.3 Retinal Diseases

1.3.A Retinoblastoma

Retinoblastoma is a childhood cancer in the retinal cell layer of the eye. According to the National Cancer Institute, 300 estimated new cases of retinoblastoma have been reported in the US in 2011. Mostly, infants and younger children (< 6 years) are diagnosed with retinoblastoma and it occurs about equally in male and female child, irrespective of races and ethnicities. Retinoblastoma can occur equally in the right or left eye, and in about 1 in 4 cases, both eyes are affected. While the overall five-year survival rate is > 90%, the outlook is not nearly as good if the cancer has spread outside of the eye. Retinoblastoma can be hereditary or non-hereditary (sporadic) in nature. The hereditary form requires only one spontaneous mutation whereas, sporadic form requires two separate spontaneous mutations. Retinoblastoma that occurs in only one eye is usually non-hereditary compared to hereditary form which occurs in both eyes [93]. There are two retinoblastoma tumor types: endophytic tumors originate from the retina into the vitreous while exophytic tumors occur in the subretinal space of the eye [94]. Typical symptoms of retinoblastoma include crossed eye, pain, redness, bulging forward of the eyes, a white spot in the pupil, tearing, cataract, differences in pupil size and iris color. Treatment strategies for retinoblastoma have gradually evolved over the past few decades. The most important goal is to save the patients life, followed by preservation of vision and the cosmetic appearance of the eye.

Treatment options include enucleation (surgery), external beam radiotherapy (EBRT), cryotherapy (freezing treatment), photocoagulation (laser treatment), and chemotherapy (intravenous/subconjunctival). The goal of chemotherapy is to shrink the tumor making it treatable with radiation, cryotherapy, or laser photocoagulation. While chemotherapeutic

agents varied according to the preference of the oncologist, most of the current studies have relied on vinblastin, etoposide or carboplatin/topotecan [95,96].

The major cause of treatment failure in retinoblastoma management with systemic chemotherapy has been linked to chemo-resistance induced by tumor expression of the multi-drug resistance (MDR) proteins, most notably MDR1/Pgp and MRPs [97,98]. Major concern is how MDR can be prevented. This has led some investigators to advocate the incorporation of cyclosporine into standard chemotherapeutic regimens, as cyclosporin blocks the MDR1 trans-membrane pump [99]. The logic behind using adjuvant cyclosporin in combination with chemotherapy for retinoblastoma arises from its role in countering multi-antineoplastic drug resistance. Although the successful treatment of retinoblastoma using cyclosporine has been reported, however the high dosage necessary to affect MDR1 expression were found very toxic and debilitating for the patient [100,101]. Therefore, future studies are needed to determine more effective and less toxic drugs that can inhibit MDR for retinoblastoma therapy.

1.3.B Diabetic Retinopathy

Diabetic retinopathy is the most prevalent microvascular complication of diabetes, and remains a leading cause of vision loss in many developed countries. The development of this microvascular disease occurs gradually and silently in as many as 50% of type I and 10% of type II diabetic patients within 15 years of diagnosis [102,103]. Chronic hyperglycemia and other risk factors (hypertension, dyslipidaemia) are believed to trigger a cascade of biochemical and physiological changes that lead to microvascular damage and retinal dysfunction. The retinal manifestations of diabetes mellitus are broadly classified as either nonproliferative diabetic retinopathy (NPDR) or proliferative diabetic retinopathy (PDR).

The progression of NPDR, which covers only intraretinal microvascular changes, starts from mild nonproliferative abnormalities (altered retinal vascular permeability) to moderate and severe nonproliferative diabetic retinopathy (vascular closure). The eventual progression of PDR is characterized by new blood vessel formation and sometimes fibrous band proliferation on the retinal surface. Macular edema, characterized by retinal thickening from leaky blood vessels, can develop in both stages of retinopathy due to increased retinal vascular permeability which leads to fluid accumulation in the retina [104,105].

Various hyperglycemia-induced metabolic abnormalities, including increased activity of the polyol pathway, advanced glycation end products (AGEs) and protein kinase C (PKC) activation are implicated in the progress of diabetic retinopathy. These metabolic pathways are considered to be interconnected and may mediate oxidative stress. Elevated oxidative stress plays a major role in the pathogenesis of diabetic complications [106,107]. Oxidative stress is the accumulation of reactive oxygen species (ROS) beyond the capacity of a cell to defend, due to increased generation or impaired removal of ROS [108]. The presence of a high content of polyunsaturated fatty acids, and high oxygen uptake and glucose oxidation renders the retina more susceptible to oxidative stress relative than any other tissue [109]. Critical events suggested in the pathogenesis of diabetic retinopathy are hyperglycemia, changes in the redox homeostasis and oxidative stress. Increased oxidative stress is reported in diabetic retina of animal models (diabetic and galactosemic rats). Elevated retinal levels of lipid peroxides, superoxide and hydrogen peroxide and down-regulation of the mRNA of the enzymes responsible for scavenging superoxide, superoxide dismutase (SOD), and glutathione reductase were reported in diabetic rat and mouse models [110-112]. A decreased level of intracellular antioxidant (GSH) and impairment of antioxidant defense enzymes in

the retina was also reported in diabetic rats [113]. Furthermore, increased oxidative stress is also observed in bovine retinal endothelial cells (BREC) and pericytes incubated in high glucose medium and in other non-vascular retinal cells including transformed retinal Muller cells (rMC-1) and photoreceptors [110,114]. These animal experiments clearly suggested an important role of oxidative stress in the development of retinopathy in diabetes. Moreover, animal studies have confirmed that oxidative stress not only contributes to the development of diabetic retinopathy but also offers resistance to reversal of the conditions after glycemic control [115]. However, the mechanism by which oxidative stress can contribute to the pathogenesis of diabetic retinopathy remains to be elucidated.

1.3.C Glaucoma

Glaucoma is a neurodegenerative disease of the optic nerve characterized by the accelerated death of retinal ganglion cells (RGCs) and their axons which ultimately leads to progressive vision loss. Elevated intraocular pressure (IOP) and age are key risk factors for glaucoma. Reducing IOP is the only current treatment option available to retard glaucoma progression in clinical practice. However, control of IOP by itself may not be sufficient to arrest the progression of glaucoma and strategies that compliment IOP control for protecting the optic nerve are required [116,117].

1.3.D Age-related Macular Degeneration (AMD)

AMD is a progressive neurodegenerative disease that primarily affects the central region of the retina (macula) and is a leading cause of blindness in the elderly. The presence of macroscopically visible soft drusen, with areas of hyper- or depigmentation are characteristic early symptoms of AMD, whereas atrophy of photoreceptors and retinal pigment epithelium (RPE), or choroidal neovascularization are evident during later stages of

the disease [118-120]. Age-related growing oxidative damage to the RPE due to an imbalance between generation and elimination of ROS may be responsible for the pathophysiology of AMD [121,122]. Treatment of AMD has always been a challenge for ophthalmologists. Therapeutic strategies targeted to the VEGF-signaling pathway has shown some success in the treatment of neovascular wet AMD, however there are no proven medical treatments for the more common 'dry' AMD. Potential use of antioxidants for delaying later stage progression of AMD has been confirmed by the AREDS study [123]. However, success of this study was likely limited by the choice of dietary antioxidants (which was later addressed in a new NEI funded clinical trial) and the subsequent realization that dietary antioxidants provide differential subcellular protection in the epithelial cells [124].

1.4 Role of Mitochondrial Dysfunction in Retinal Diseases

The mitochondrion is a critical organelle for cell function and survival. Its primary roles are ATP production, control of cellular metabolism and regulation of apoptosis (programmed cell death). It consists of inner and outer membranes composed of phospholipid bilayers containing numerous integral proteins (Fig. 2). Mitochondrial density varies among different cell types and is expressed abundantly in highly metabolic active cell types such as retinal pigment epithelium (RPE) [125]. Due to its critical functioning, mitochondrial dysfunction may severely affect tissue homeostasis. Oxidative damage induced by mitochondrial dysfunction is currently the most prevalent ageing theory [125-128].

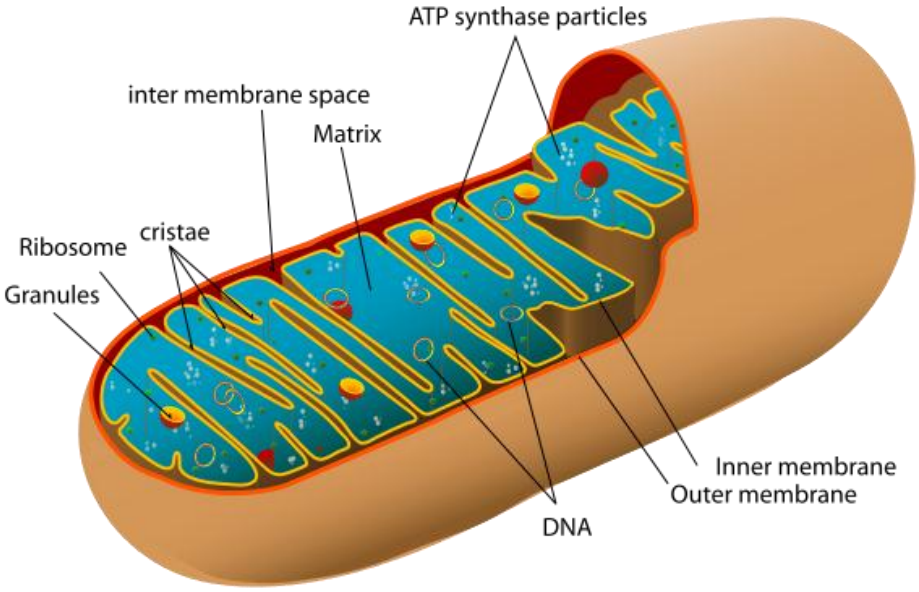

Figure 2. Structure of Mitochondria

(figure reproduced from public domain http://en.wikipedia.org/wiki/File:Animal_mitochondrion_diagram_en.svg).

Acute and chronic mitochondrial dysfunction is associated with a number of age-related degenerative diseases. This section will summarize recent developments in understanding the role of the mitochondria as a weaker link in the antioxidant defenses of retinal cells and a potential contributor to the pathogenesis of retinal degenerations such as diabetic retinopathy, glaucoma and AMD.

1.4.A Mitochondrial Dysfunction in Diabetic Retinopathy

Mitochondria are considered to be the prime endogenous source of superoxides, peroxynitrite, and hydroxyl radicals, and are also a target for damaging effect of oxidants, suggesting the existence of a vicious cycle of oxidative damage [129]. Chronic overproduction of ROS in the retina results in abnormal mitochondrial function in diabetes (Fig. 3) [108,109,130]. Inhibition of antioxidant scavengers is one of the ROS-induced dysfunctions in mitochondria that may lead to enhanced sensitivity of retinal cells to oxidative stress. The isoform of SOD in the mitochondria (MnSOD) along with GSH may be suppressed in diabetic or high glucose-cultured retinal mitochondria [131-133]. Increased mitochondrial DNA damage has been reported in the diabetic retina of mice model [134]. Increased swelling of the mitochondria was observed in the retina of diabetic mice [131]. It is widely accepted that apoptosis of retinal cells is the most common incident in diabetic retinopathy. Kowluru *et al*. have demonstrated that the release of cytochrome c from mitochondria to the cytoplasm and Bax translocation from the cytoplasm to mitochondria that could drive cell apoptosis were increased in retinal capillary cells in diabetes [135]. Thus, it is evident that mitochondria play a crucial role in the development of retinopathy in diabetes, and oxidative stress can modulate mitochondrial cytochrome c release resulting in increased retinal capillary cell death.

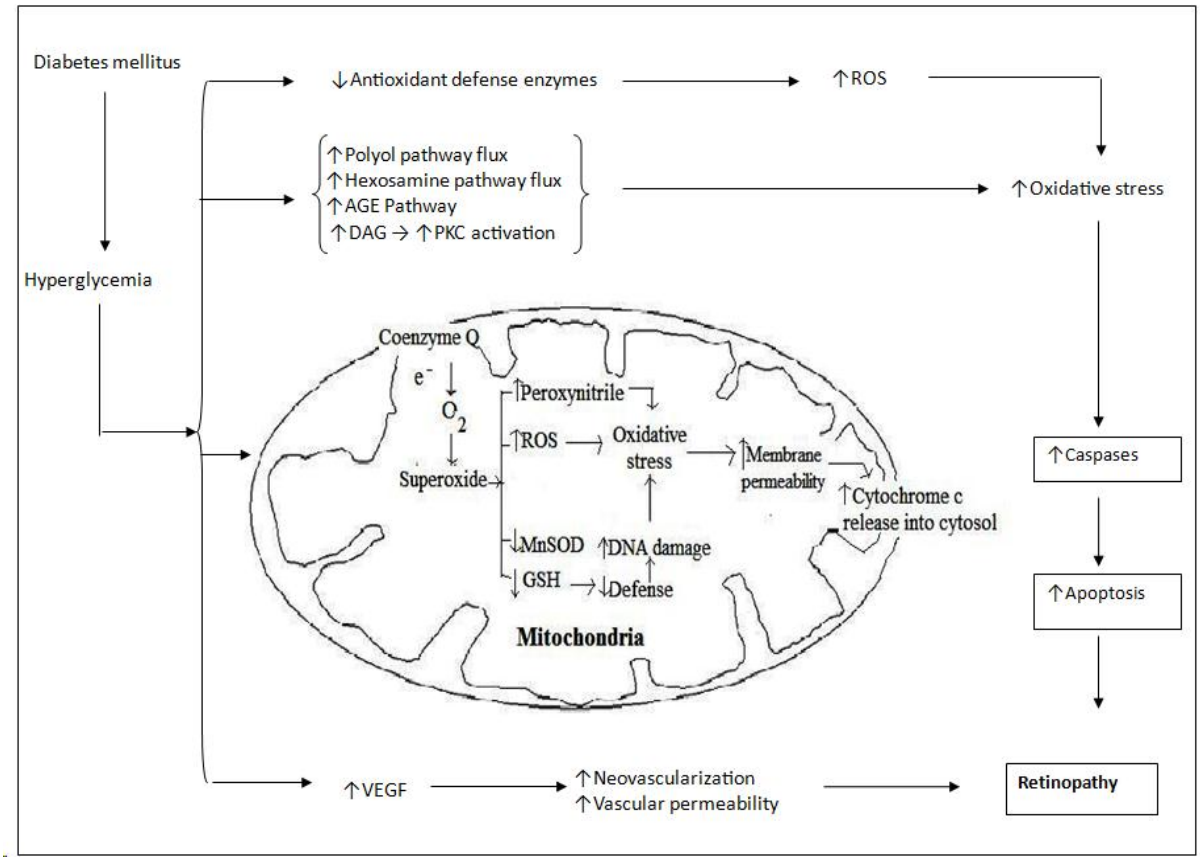

Figure 3. Hyperglycemia mediated mitochondrial dysfunctioning in diabetic retinopathy.

Diabetic retinopathy is a complex disease which is difficult to treat due to its multifactorial nature. An efficient therapy will probably be a combination of drugs targeting multiple pathways involved in the pathogenesis of diabetic retinopathy. Since the disease pathogenesis is partially attributed to mitochondrial dysfunction, treatment options should also consider restoring normal mitochondrial function. Oxidative stress is the significant instigator of hyperglycemia-induced mitochondrial damage. Therefore, treatment strategies to improve mitochondrial function by lowering oxidative stress may be an appropriate alternative [130]. Sheu *et al.* has described a number of antioxidants which can be transported into mitochondria but only a few have been tested in diabetic retinopathy [136]. Considering the role of superoxides in the development of diabetic retinopathy, SOD mimetics may represent a class of treatment to counter the effect of oxidative stress. MnSOD mimics are low-molecular weight, manganese containing, nonpeptidic molecules with similar function, and catalytic rates of native SOD enzymes. Kowluru *et al*. have shown that MnTBAP [manganese (III) meso-tetrakis (4-carboxypheny) porphyrin], can significantly inhibit glucose-induced decrease in GSH levels and translocation of cytochrome c from mitochondria and Bax into the mitochondria of retinal capillary cells. It can also inhibit apoptosis by suppressing caspase-3 activation [130,135]. It is therefore essential to recognize treatment strategies that could inhibit superoxide production which might represent a possible direction for clinical research in diabetes. Although the mimetics appear to be very promising, it is not known whether any of these mitochondria-targeted treatments are beneficial in diabetic retinopathy. Furthermore, pharmacokinetics and the route of administration also need to be addressed. Additional animal studies and clinical trials can resolve such issues [130].

1.4.B Mitochondrial Dysfunction in Glaucoma

Mitochondrial dysfunction is believed to contribute to the pathogenesis of a number of neurodegenerative disorders. Glaucoma has similar etiology to other neurodegenerative diseases, such as selective loss of a single neuronal cell population, age related incidence, and neuronal cell death. The dense distribution of mitochondria around the optic nerve head, the primary site of glaucomatous axonal injury, reflects a high requirement for ATP [116,117]. Ju *et al.* have recently demonstrated the induction of mitochondrial fission, abnormal cristae depletion, and cellular ATP reduction in differentiated RGC-5 cells exposed to high hydrostatic pressure over three days. This observation suggests that elevated pressure, a major risk factor in glaucoma, may disrupt mitochondrial structure and function in RGCs, possibly leading to apoptosis (Fig. 4) [116,137]. An association between glaucoma and mitochondrial dysfunction has also been suggested in a recent clinical study where a 20% reduction in mitochondrial respiratory function and an increase in mitochondrial DNA mutation were observed in peripheral blood of primary open-angle glaucoma patients relative to an age-matched control group [138]. The mitochondria are key regulator of apoptosis and are implicated as the prime factor responsible for neuronal loss in neurodegenerative diseases. Evidence has also suggested that apoptosis is an important mechanism of cell death in glaucoma neurodegeneration. RGC apoptosis occurs in animal glaucoma models and in the retina of glaucoma patients [139,140]. There is growing evidence to support involvement of mitochondria mediated ROS-induced RGC injury. ROS generation is noticed in the retina and optic nerve of glaucoma animal models and in retinal ischemia reperfusion models [141,142]. Furthermore, human studies have also confirmed the involvement of mitochondria-mediated oxidative stress in glaucoma due to up-regulation of various

antioxidant proteins (eg. serum auto-antibodies, glutathione S-transferase and iron-regulating proteins) [143,144].

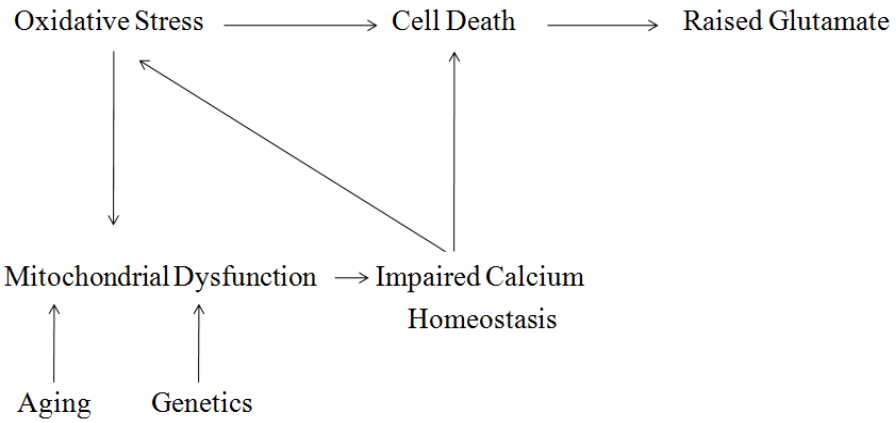

Figure 4. Involvement of mitochondrial dysfunctioning in glaucoma pathogenesis.

As a potential neuroprotective therapy, various antioxidants have been studied in neurodegenerative diseases with partial success. Advances have also been made in targeting antioxidants directly to the mitochondria, a major site of ROS production, by conjugating antioxidants to lipophilic cations [136,145]. The mitochondria-targeted cationic plastoquinone derivative SkQ1 (10-(6′-plastoquinonyl) decyltriphenylphosphonium) has been investigated as a prospective tool for treating experimental glaucoma induced by serial injections of 2% hydroxypropyl methyl cellulose to the anterior segment of the rabbit eye. Once daily drops of 5 μM SkQ1 caused a reduction in glaucomatous changes [146]. SkQ1 appears to be a promising candidate for treating glaucoma. Involvement of mitochondria in glaucoma pathogenesis might therefore represent a new therapeutic target for protecting the optic nerve and preventing vision loss.

1.4.C Mitochondrial Dysfunction in AMD

Strong evidence showing mitochondrial dysfunction in AMD has been reported. An association between AMD and a variant of mitochondrial protein (LOC387715/ARMS2) has been identified [147]. In AMD, genetic variants at two chromosomal loci, 1q32 and 10q26 confer major disease risks. A consensus from multiple studies is that the 1q32 and 10q26 regions simultaneously harbor a first and second major genetic determinant of AMD susceptibility [148-151]. Previous studies have identified chromosome 1q32 as harboring a susceptibility locus (complement factor H) for AMD which does not have any connection to the mitochondria [150,151]. However, signals at 10q26 overlap two nearby genes, LOC387715/ARMS2 (age-related maculopathy susceptibility 2) and HTRA1/PRSS11 (high-temperature requirement factor A1). The LOC387715/ARMS2 gene produces a protein of unknown function that localizes in the mitochondria, and polymorphisms in

LOC387715/ARMS2 alter the risk of AMD by modulating the function of this gene [147-149,152]. Furthermore, changes in the activity or regulation of LOC387715/ARMS2 are likely to be responsible for the impact on AMD disease susceptibility [152].

Retinal pigment abnormalities and RPE atrophy similar to those present in the early AMD phenotypes are detected in 75% of individuals with the MELAS A3243G mitochondrial DNA mutation [153]. mtDNA haplogroups which are associated with either increased or decreased prevalence of age-related maculopathy have been identified [154]. So far there is no report available which confirms the association of similar mtDNA haplotypes with AMD. Based on this finding one can further explore the possible involvement of mtDNA haplogroups in AMD.

In addition, the oxidative stress hypothesis of AMD proposes that cumulative oxidative damage to proteins, lipids, and DNA also leads to disease progression. Changes in selected redox proteins (an indicator of increased oxidative stress) and altered protein expression reflecting impaired mitochondrial biogenesis were found in human donor eyes with the progression of AMD [155,156]. These findings led to the proposition that bioenergetic consequences of mtDNA derangements may be expressed in macular RPE as a maculopathy and contribute to the development of AMD. Evidence of mitochondrial dysfunction from human tissue examination and animal models has also been reported. Feher *et al*. revealed through morphometric studies a significant diminution in number and area of RPE mitochondria as well as loss of cristae and matrix density with age in AMD specimens. These decreases were significantly greater in AMD than in normal aging. This study has further confirmed that besides changes in mtDNA, alterations of mitochondrial membranes

may also play a crucial role in the development of mitochondrial dysfunctions in AMD [157].

Despite evidence of mitochondrial dysfunction in AMD where emphasis is focused on the RPE, only a few studies have been focused the role of mtDNA damage and repair in the retina. Barreau *et al*. has identified mtDNA deletions in aged human retina [158]. Increased mtDNA damage and decreased repair, along with reduced mitochondrial respiration in RPE and choroid of rodents are also observed with progression of ageing [159]. Thus, mtDNA damage in RPE is associated with aging and may be a susceptibility factor in the development of AMD.

Cell culture studies have shown damage to mtDNA but not to nuclear DNA (nDNA) in human RPE cells exposed to oxidizing or alkylating agents [160]. Furthermore, nDNA damage repair appears to be rapid relative to mtDNA repair in the RPE, which appears to be slow and relatively inefficient. The lack of evidence for mtDNA repair in response to oxidative stress further suggests that the mitochondrion is a weaker link in the RPE cell's defense against oxidative damage [161-163]. A collective outcome of mtDNA damage will be the reduction in metabolic activity and/or an increased propensity for apoptosis. However, mtDNA repair capacity appears to be overwhelmed, resulting in diminished mtDNA repair which may play a significant role in the commencement of AMD [159,163]. Further evidence has shown that human RPE cells treated with H_2O_2 resulted in mtDNA damage, which leads to compromised mitochondrial redox function due to impaired repair mechanism [160,163]. This impaired repair mechanism clearly explains the susceptibility of mtDNA to oxidative damage in human RPE cells, together with the age-related decrease of the cellular anti-oxidant system [163].

The susceptibility of RPE mtDNA to oxidative damage along with failure of mtDNA repair provides an intriguing and plausible mechanism for a mitochondria-based model of AMD and retinal degeneration. Figure 5 summarizes the possible mechanisms of AMD from oxidative stress to mtDNA damage [125,163,164].

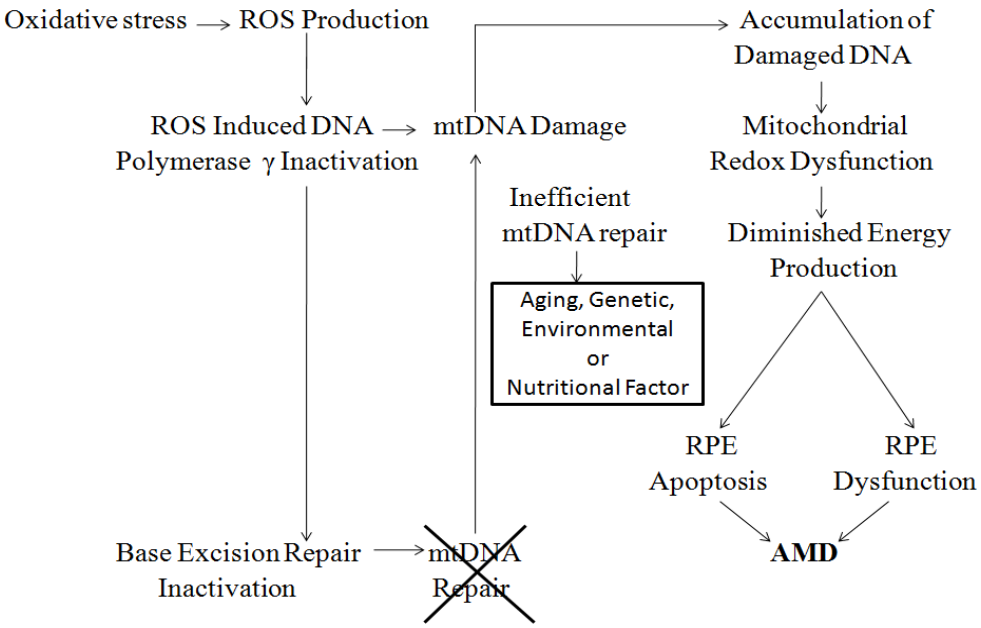

Figure 5. ROS-induced mtDNA damage based model for development of AMD.

In support of the therapeutic concept for retinal degeneration, a study by Jarrett *et al*. has confirmed that dietary interventions can provide oxidative protection to hippocampal mtDNA and can lower ROS levels in rat model of AMD [165]. Reports have further proven that Bcl-2 overexpression, melatonin, ascorbic acid and glutathione-S-transferase can prevent mtDNA damage in cultured RPE [124,166-168]. An alteration of mitochondrial membranes in AMD has immediate clinical significance as several *in vitro* and *in vivo* studies showed that mitochondrial membranes may be a target for the treatment of mitochondrial dysfunction. Compounds with specific affinity for mitochondrial membranes (mitochondriotropic) can restore mitochondrial functions [146]. Alterations of mitochondrial membranes are accompanied by considerable accumulation of lipofuscin which may account for oxidative damage to the RPE [169]. Oxidative damage may result in impaired lipid metabolism and apoptosis, characteristics of late AMD [170]. Improvement in lipid metabolism in the RPE may be an innovative therapeutic approach for preventing AMD. As mitochondria and peroxisomes are implicated in both lipid biosynthesis and catabolism, Feher *et al*. suggested that the most effective dietary intervention may be achieved by targeting these organelles. These researchers developed a new metabolic approach by combining mitochondriotropic compounds, including acetyl-L-carnitine (ALC), n-3 fatty acids, coenzyme Q_{10} and vitamin E, for improvement of retinal function in early AMD. Clinical studies have confirmed this finding, since a combination of ALC, omega-3 fatty acids and coenzyme Q_{10}, after an initial improvement, stabilized several visual functions in early AMD [171]. Recently, these preliminary results were confirmed by a randomized, double-masked, placebo controlled, clinical trial that showed improvement in both visual function and fundus alterations in early AMD [172]. These results regarding the restoration

of mitochondrial function are certainly very promising for a new therapeutic approach for the treatment of AMD.

CHAPTER 2

MOXIFLOXACIN INTERACTION WITH TRANSPORTERS AND ANTICANCER AGENTS FOR RETINOBLASTOMA MANAGEMENT

2.1 Overview

Retinoblastoma is a major, vision-threatening, intraocular malignancy affecting 300 children/year in the USA [173]. Chemoreduction is the key treatment for retinoblastoma which includes topotecan, etoposide and vinblastine. However, chemoresistance is the major cause of treatment failure in retinoblastoma since, anticancer agents suffer from poor cell permeability due to major interaction with multi-drug resistance (MDR) efflux proteins: P-glycoprotein (P-gp/MDR1) and multidrug resistant protein 2 (MRP2). MDR1 and MRP2 belong to the ATP-binding cassette transporter superfamily and act as energy-dependent efflux pumps, decreasing the intracellular drug concentration. Several attempts have been made to overcome MDR using MDR1 or MRP2 inhibitors [100,101]. However, major limitations of MDR1 or MRP2 inhibitors are (i) lack of clinical approval, (ii) undesirable pharmacokinetic interaction with metabolizing enzymes, (iii) negligible improvement in therapeutic drug activity, (iv) off-target effects and (v) detrimental side effects and toxicity at therapeutic dose levels. Furthermore, these inhibitors can blocks only a single efflux transporter functionality out of multiple efflux transporters overexpressed on the tumor cells. Therefore, alternative safe MDR modulators are needed that can simultaneously regulate multiple efflux sites and also improve anticancer efficacy for retinoblastoma therapy.

Moxifloxacin is an 8-methoxy fluoroquinolone with a broad spectrum of bactericidal activity against gram positive and gram negative pathogens. The antibacterial spectrum of moxifloxacin includes all major upper and lower respiratory tract pathogens as well as ocular

pathogens. Ocular cells have shown good tolerance against moxifloxacin even at higher dose levels [174]. Moxifloxacin interferes with bacterial survival by binding to DNA gyrase (topoisomerase II) and topoisomerase IV, essential bacterial enzymes involved in the replication, translation, repair and recombination of deoxyribonucleic acid [175,176].

Recently, the anti-topoisomerase activity of moxifloxacin has also been evident in several eukaryotic and tumor cells [177-179]**.** Furthermore, moxifloxacin has also displayed anti-proliferative, anti-angiogenic, immuno-modulatory and pro-inflammatory cytokines suppression activity, which points to its potential for treating chronic tumors [178,180-184]. Since a majority of fluoroquinolones become ineffective due to bacterial as well as efflux pump mediated acquired resistance, it is important to delineate the interaction of moxifloxacin with major efflux transporters before evaluating its potential for tumor management. This knowledge may provide better direction to overcome MDR caused by efflux transporters. Furthermore, a majority of fluoroquinolones are known substrates of the monocarboxylate transporter (MCT) [185,186]. Therefore, understanding moxifloxacin substrate specificity to the monocarboxylate influx transporter is also important to delineate mechanism of its active transcellular localization. Finally, understanding the interaction of moxifloxacin with anticancer agents may offer new insight for regulation of MDR in retinoblastoma.

This part of dissertation deals with interaction of moxifloxacin with the influx transporter (MCT), efflux transporters (MDR1 and MRP2) and anticancer agents (etoposide, topotecan and vinblastin).

2.2 Statement of the Problem

Chemoresistance is the major cause of treatment failure in retinoblastoma.

Anticancer agents suffer from poor cell permeability and MDR due to major interaction with efflux proteins (MDR1 and MRP2) over-expressed on retinoblastoma tumor. A strategy of utilizing efflux pump inhibitors to overcome MDR has its own limitations since these inhibitors are not clinically approved. Ocular cells have shown good tolerability against clinically accepted fluoroquinolone, moxifloxacinat, at higher dose level. As a majority of fluoroquinolones have become ineffective due to efflux mediated acquired drug resistance therefore, it is important to delineate the interaction of moxifloxacin with major efflux transporters. Moreover, various reports suggest that fluoroquinolones are a known substrate of the monocarboxylate influx transporter. Therefore, knowledge of moxifloxacin substrate specificity to monocarboxylate influx transporter may delineate the mechanism of its active transcellular localization. Furthermore, based on the literature findings which suggest potential role of moxifloxacin in modulating activity of cytotoxic agents, it would be interesting to study its interaction with anticancer agents for the management of retinoblastoma. We hypothesized that in such interactions, moxifloxacin will not only modulate the permeability of anticancer agent across retinoblastoma cells expressing efflux proteins (due to competitive inhibition at efflux sites) but it will also modulate the antiproliferative activity of chemotherapeutics. This approach may simultaneously reduce the chemoresistance, chemotherapeutic dose and associated dose-limiting toxicities.

2.3 Objectives

The objectives of this part of dissertation project are:

a) to study *in vitro* interaction of moxifloxacin with the monocarboxylate influx transporter on ARPE 19 cells using model MCT substrates and inhibitors.

b) to study *in vitro* interactions of moxifloxacin with MDR1 and MRP2 efflux transporters by uptake and bi-directional transport experiments on transfected MDCK cells.

c) to determine IC_{50} values of moxifloxacin inhibition of MDR1- and MRP2-mediated efflux functionality.

d) to study *in vitro* interaction of moxifloxacin with anticancer agents by uptake and bi-directional transport experiments on transfected MDCK cells.

e) to study modulation of anticancer cytotoxicity and anti-apoptotic activity by moxifloxacin in human retinoblastoma cells.

f) to study modulation of anticancer induced cytokines release by moxifloxacin in human retinal pigment epithelial cells.

CHAPTER 3

INTERACTION OF MOXIFLOXACIN WITH INFFLUX TRANSPORTER

3.1 Rationale

Localized drug delivery is an important alternative to systemic therapy owing to its fewer side effects upon chronic drug exposure. Intravitreal injection is the most common localized drug delivery route for treating retinal ailments as age-related macular degeneration (AMD), diabetic retinopathy, retinoblastoma and endophthalmitis [187,188].

Postoperative endophthalmitis remains as a most devastating complication of cataract surgery possessing significant vision threat. Moxifloxacin (Fig. 6), a fourth generation fluoroquinolone has shown a potent and rapid bactericidal activity against postoperative endophthalmitis pathogens. Reports have suggested safe and effective intracameral delivery of moxifloxacin in an animal endophthalmitis model [189]. Furthermore, efficacies intravitreal delivery of moxifloxacin for bacterial endophthalmitis has been reported clinically [189,190]. However, lowest vitreous half-life of moxifloxacin (1.76 h) among other fluoroquinolones (ofloxacin→5.6 h and ciprofloxacin→2.2 h) used for the treatment of bacterial endophthalmitis has been reported in the literature [190-192]. Typical order of fluoroquinolones lipophilicity (moxifloxacin > ciprofloxacin > ofloxacin) explains the faster vitreal elimination of highly lipophilic moxifloxacin [193]. Vitreal elimination of molecules largely depends on its physicochemical properties such as hydrophilicity, lipophilicity (log P), molecule size and diffusion across vitreous fluid. Moreover, substrate specificity of drug molecules for transporters expressed on retinal pigmented epithelium (RPE) or retinal blood capillaries may also have an effect on its vitreous half-life [193]. Therefore, in this report we aim to delineate interaction of moxifloxacin with monocarboxylate influx transporter present

on the RPE to evaluate its role in vitreous elimination of intravitreally administered moxifloxacin.

Monocarboxylates such as lactate, acetate, pyruvate and ketone bodies are known to be transported via H^+-coupled, Na^+-coupled or anionic-exchange carrier mediated process in a variety of cells and tissues [194]. Monocarboxylate transporter (MCT) is a family of proton-linked plasma membrane transporters which actively translocate monocarboxylates. The substrates recognized by MCT are in general weak monovalent organic acids with the carboxyl group attached to a relatively short side chain [195]. Various reports suggest that fluoroquinolones such as ciprofloxacin, levofloxacin and ofloxacin are known substrates of MCT [185,186]. This may be due to the presence of carboxyl group in the chemical structure of these fluoroquinolones acting as a MCT substrate recognition site (Fig. 6). Recently, functional and molecular localization of MCT has been reported on the apical membrane of retinal pigment epithelium cells (ARPE-19) [196]. Therefore, ARPE-19 can be used as a model retinal cell line to screen substrate specificity of potential drug candidates toward MCT expressed on RPE [196]. Here, we aim to evaluate the *in vitro* interaction of moxifloxacin with MCT using ARPE-19 cells. L-lactic acid, which has been widely used as a substrate for carrier-mediated monocarboxylate transport processes in various tissues/organs, was chosen as the model substrate along with other agents such as salicylic acid and ofloxacin [197-201]. In addition, pH dependency and competitive uptake inhibition studies were also performed to delineate the mechanism of moxifloxacin influx via MCT.

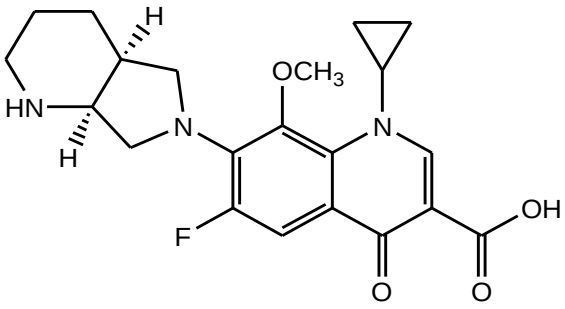

Moxifloxacin

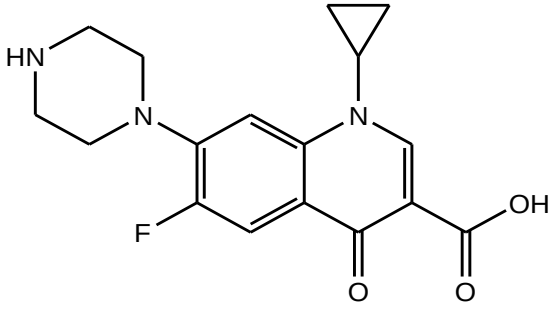

Ciprofloxacin

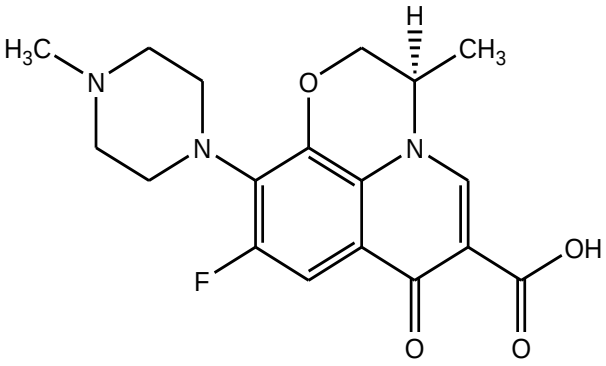

Levofloxacin

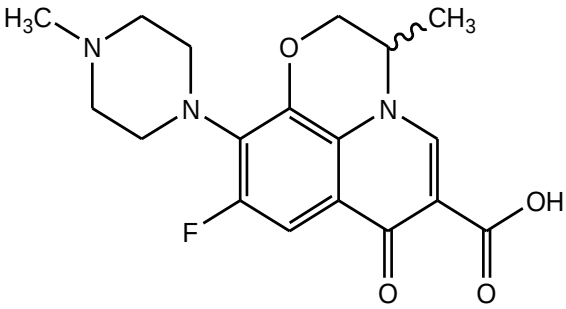

Ofloxacin

Figure 6. Chemical structures of fluoroquinolones.

3.2 Material and Methods

Materials

A retinal pigment epithelial (ARPE-19) cell line was purchased from American Type Culture Collections (ATCC; Manassas, VA, USA). Fetal bovine serum (FBS) was purchased from Atlanta Biologicals (Lawrenceville, GA, USA) and D-MEM/F-12 was obtained from Gibco (Invitrogen, Grand Island, NY, USA). Streptomycin, penicillin, sodium bicarbonate, HEPES, p-chloromercuribenzene sulfonate (pCMBS), quercetin, D,L-dithiothreitol (DTT), 4,4'-diisothiocyano-2,2'-stilbenedisulfonic acid (DIDS), 2,4-dinitrophenol (DNP), ouabain, and sodium azide were purchased from Sigma-Aldrich (St. Louis, MO, USA). Culture flasks (75 cm^2 growth area) and 12-well (3.8 cm^2 growth area per well) culture plates were obtained from Corning Costar Corp. (Cambridge, MA, USA). [^{14}C] L-lactic acid (specific activity : 131 mCi/mmol) was procured from Perkin-Elmer Inc. (Boston, MA, USA). Levofloxacin and moxifloxacin was acquired from TCI America (Sunnyvale, CA, USA) and China, respectively. Bradford protein assay reagent was purchased from Bio-Rad Laboratories (Hercules, CA, USA). All the solvents were of HPLC grade and obtained from Fisher Scientific (St. Louis, MO).

Cell Culture

ARPE-19 cells (passages 20-30) were cultured in D-MEM/F-12 (1:1) and incubated at 37 ^{0}C with 5% CO_2 and 90% relative humidity. The growth media was supplemented with 10% heat-inactivated FBS, 15 mM HEPES, 29 mM sodium biocarbonate, penicillin (100 U/mL), streptomycin (100 µg/mL). For uptake experiments, cells were seeded at a density of 3×10^6 cells per 12-well tissue culture plates. The medium was changed every alternate day and cells were allowed to grow for 26-28 days before conducting experiments.

Stock Solution and Sample Preparation

Different stocks were prepared for the calibration standards of moxifloxacin and other compounds. For moxifloxacin, the stock solutions were prepared in DMSO and diluted with the uptake buffer (for experiments) or mobile phase (for analysis). Stock solutions of various substrates and inhibitors such as quercetin, pCMBA, pCMBS, 2,4-DNP, DTT, DIDS, ouabain and sodium azide were also prepared in DMSO. Final concentration of DMSO in the uptake medium was adjusted to below 2% to avoid any damage to the ARPE-19 cells. For LC/MS analysis, samples were thawed at 37 ^{0}C and 20 µL (10 µg/mL) of levofloxacin (IS) was added and vortexed for 30 s. 900 µL of cold ethyl acetate (protein precipitating and extraction solvent) was added to the 200 µL of sample to promote protein precipitation. Samples were vortexed and centrifuged at 12,000 rpm for 5 min. The supernatants were subjected to vacuum drying at 40 ^{0}C for 2 h. Finally, the vacuum dried samples were reconstituted with 200 µL of mobile phase for analysis.

LC/MS–MS Conditions

All experiments were performed on an API 3200 triple quadrupole linear QTrap spectrometer (Applied Biosystem/MDS Sciex) Agilent LC pump and an auto-sampler. After sample preparation, 10 µL of the clear upper layer was injected on a Luna XTerra® C18 analytical column (50 × 2.1 mm, 5 µm) for chromatographic separation. The mobile phase (0.1 % trifluroacetic acid in distilled deionized water and acetonitrile (50:50)) flow rate was adjusted to 0.25 mL/min. The MDS Sciex API 3200 Triple Quadrupole linear QTrap mass spectrometry (Applied Biosystems/MDSSciex, Foster City, California) system was interfaced by turbo ion spray with positive ion source in Multiple Reaction Monitoring (MRM) mode was used for detection of positive ions (electrospray ionization). Levofloxacin was used as an

internal standard (IS) for analysis. With a scan width of 0.5 m/z and injection rate of 20 µL/min, following transitions were measured: 402.2→384.2 for moxifloxacin and 362.2→344.2 for levofloxacin (IS). Ion spray voltage, dwell time, and capillary temperature were set at 5200 V, 400 ms and 350 °C, respectively.

Concentration Dependence Uptake of Moxifloxacin on ARPE-19 Cells

Uptake of moxifloxacin was performed according to earlier published protocol with minor modifications [92]. Briefly, 28-30 days postseeding of ARPE-19 cells, the medium was removed and cells were washed twice with Dulbecco's phosphate buffered saline (DPBS, pH 5.0) containing 130 mM NaCl, 2.5 mM KCl, 7.5 mM Na_2HPO_4, 1.5 mM KH_2PO_4, 1 mM $CaCl_2$, 0.5 mM $MgSO_4$ and 5 mM glucose. Moxifloxacin solutions were prepared at different concentrations (0.5-250 µM) in DPBS (pH 5.0), and spiked with L-Lactic acid (10 mM). Uptake was initiated by incubating the cells with 1 mL of each solution for a predetermined time at 37 °C. Previously published experiments revealed that L-lactic acid uptake was linear for at least 60 s therefore, we kept constant incubation period of 60 s for moxifloxacin uptake [196]. Following incubation, the solution was removed and cells were washed twice with ice-cold stop solution (0.52 g/L HEPES and 15.64 g/L KCl) to stop cellular uptake of moxifloxacin. Cells were lysed by rapid freeze–thaw cycle (three times) and moxifloxacin was extracted following cold ethyl acetate extraction. Samples were further analyzed using the LC-MS/MS method as described previously. All the experiments were performed in quadruplicate and cellular accumulation was normalized using protein count measured by Bio-Rad protein assay.

pH Dependency and Competitive Inhibition Studies

The uptake experiment was performed as described previously. pH dependency of *in vitro* moxifloxacin uptake was determined using different pH buffer solutions (pH 5.0-7.4). Furthermore, interaction of moxifloxacin was evaluated using known MCT substrates such as salicylic acid (10 mM), ofloxacin (1 mM) and L-lactic acid (5 and 10 mM). Moxifloxacin (10 µM) and MCT substrates were simultaneously incubated for 60 s for *in vitro* uptake studies on ARPE-19 cells. Finally, effect of MCT inhibitors (Quercetin, pCMBA, and pCMBS), metabolic inhibitors (ouabain and sodium azide), protonophores (DNP), anion transporter inhibitors (DIDS), and sulfhydryl-group modifying agents (NEM and DTT) on moxifloxacin uptake was determined by pre-incubating ARPE-19 cells for 10 min with DPBS buffer (pH 7.4) (control) or above inhibitors. Uptake of moxifloxacin (10 µM) was then performed for 60 s and samples were analyzed using LC-MS/MS as described previously.

Data Treatment

Uptake data was fitted to the classical Michaelis-Menten equation represented in equation 1,

$$V = \frac{Vmax * C}{Km + C} \quad \text{……Eq. 1.}$$

when V is the total rate of uptake, V_{max} is the maximum uptake rate for the carrier-mediated process, K_m (Michaelis-Menten constant) is the concentration at half maximum velocity and C is the substrate concentration. Data were fitted to equation 1 with the aid of a nonlinear least squares regression analysis program (Kaleida Graph V3.09, Synergy Software).

Statistical Analysis

All experiments were conducted in quadruplicate and results are expressed as mean ± standard deviation (SD). Michaelis-Menten parameters Km and Vmax, are expressed as

mean ± SD. Statistical analysis between two groups were determined using Student's t test. A difference between mean values was considered statistically significant at $p < 0.05$.

3.3 Results

LC/MS-MS Method Moxifloxacin Detection

An LC/MS method was successfully developed for moxifloxacin with levofloxacin (IS) (Fig. 7). The method was developed over the linear ($r^2 > 0.99$) concentration range 30-1000 ng/mL for both moxifloxacin and levofloxacin. Lower limit of quantification (LLOQ) was found to be 5.0 and 7.8 ng/mL for moxifloxacin and levofloxacin, respectively.

Concentration Dependent Uptake of Moxifloxacin

Concentration dependency of moxifloxacin was determined by incubating ARPE-19 cells with L-lactic acid (10 mM) and various concentrations of moxifloxacin (0.5-250 μM). The concentration of moxifloxacin was determined by LC/MS-MS analysis following cold ethyl acetate extraction. Cellular accumulation of moxifloxacin display saturable kinetics (Fig. 8). Km and Vmax of moxifloxacin uptake on ARPE-19 cells were found to be 2.02 ± 0.04 μM and 14.51 ± 2.94 nmol/min/mg of protein, respectively.

Effect of MCT Substrates on Moxifloxacin Uptake

Moxifloxacin uptake was analyzed in presence of various MCT substrates on ARPE-19 cells. Significant ($p < 0.05$) reduction of moxifloxacin uptake was observed in presence of salicylic acid (~ 72%), ofloxacin (~ 56%) and L-lactic acid (~ 52% and ~ 64%) (Fig. 9).

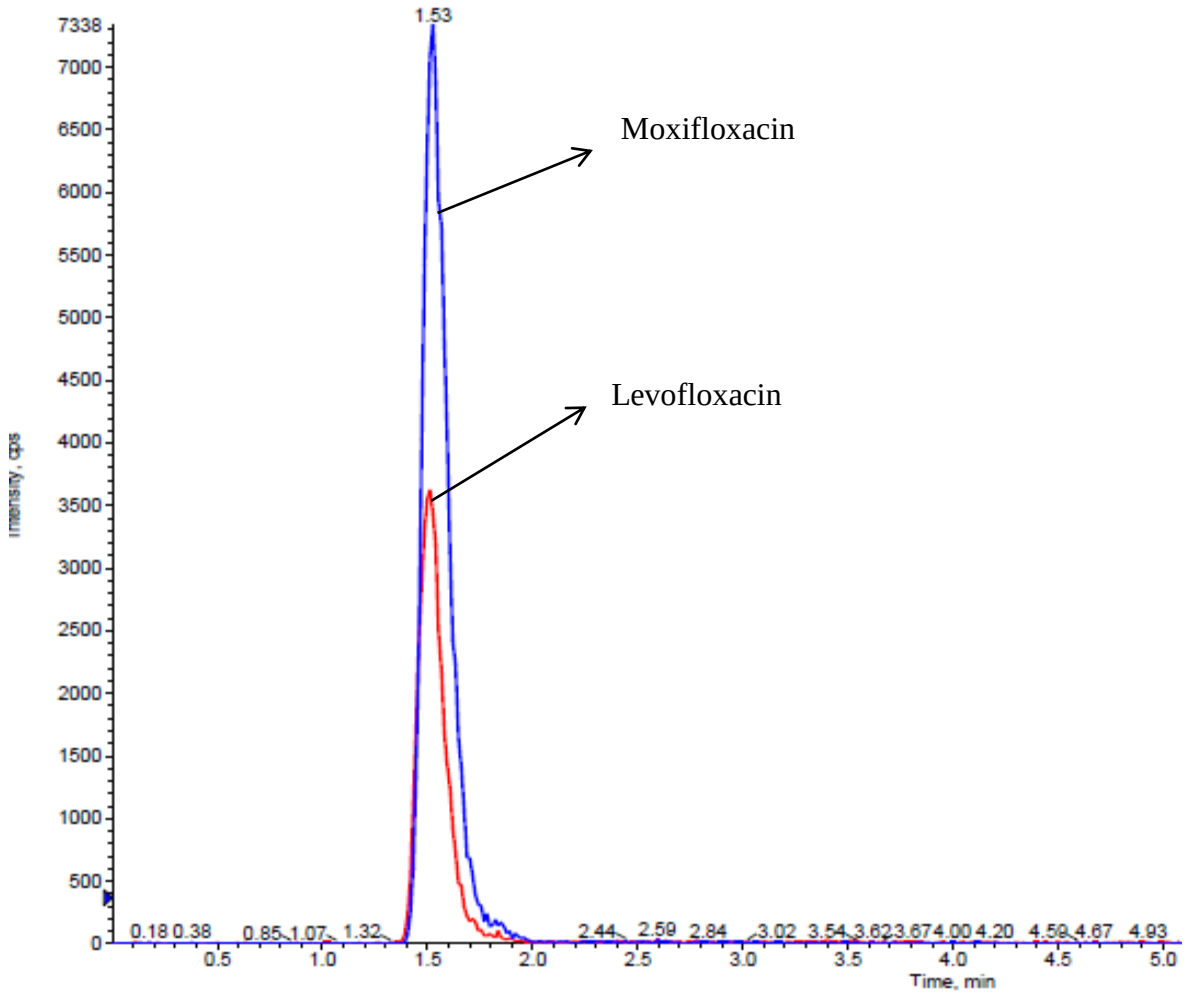

Figure 7. LC/MS mass spectrum of moxifloxacin (m/z 402.2→384.2) using levofloxacin (m/z 362.2→344.2) as an internal standard.

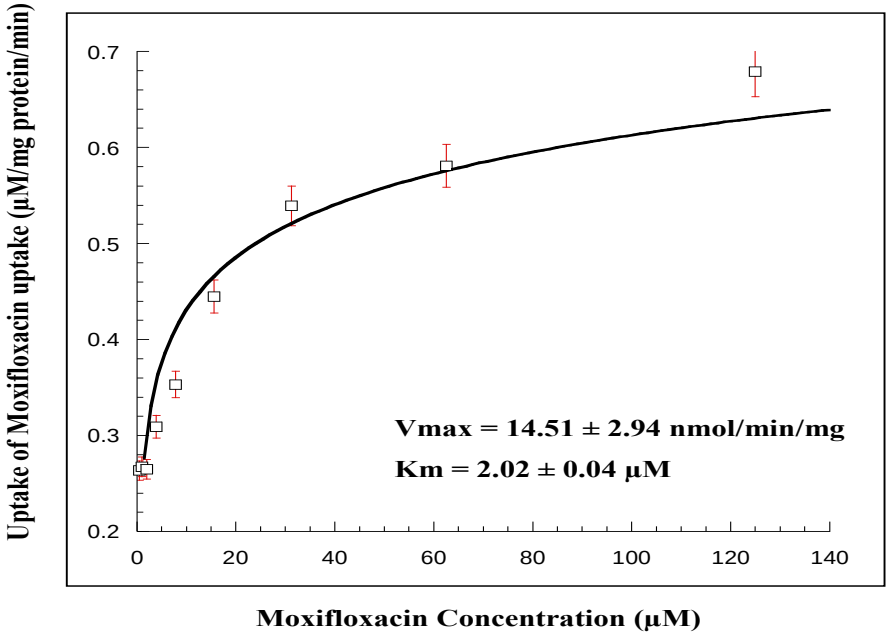

Figure 8. Concentration dependent uptake of moxifloxacin (0.5 - 250 µM) on ARPE-19 cells. Values are expressed as mean ± SD (n = 4).

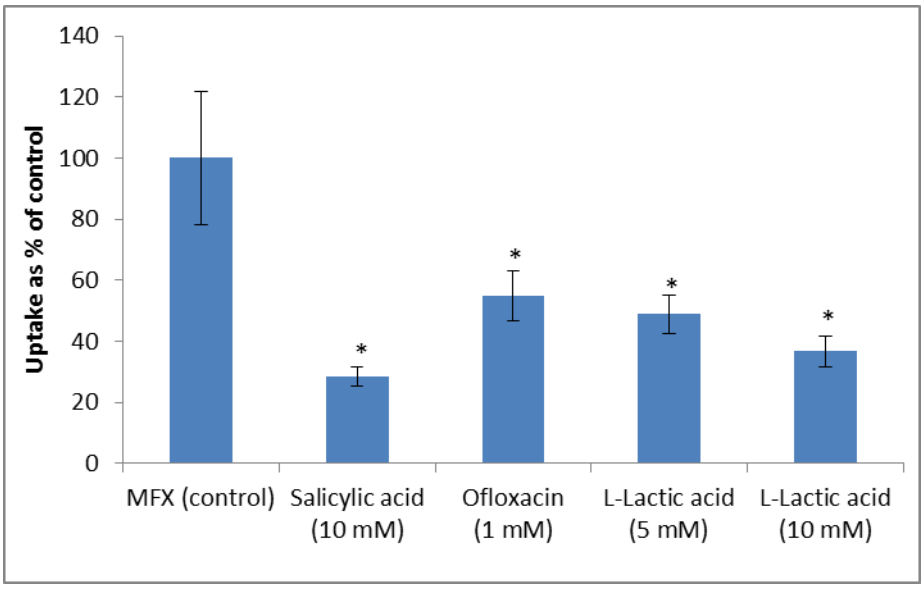

Figure 9. Cellular accumulation of moxifloxacin (MFX) alone and in presence of salisylic acid, ofloxacin and L-lactic acid across ARPE-19 cells. Values are expressed as mean ± SD (n = 4). *Data were considered statistically significant for $P \leq 0.05$.

Effect of MCT Inhibitors on Moxifloxacin Uptake

Effect of specific MCT inhibitors such as quercetin (100 and 200 µM), pCMBA (200 and 500 µM) and pCMBS (1, 10, 50 and 100 µM) on moxifloxacin (10 µM) uptake was studied on ARPE-19 cells. Significant ($p < 0.05$) reduction of moxifloxacin uptake was observed in response to MCT inhibitors. Moxifloxacin uptake was reduced to ~ 70% at 100 and 200 µM concentration of quercetin and ~ 40% at 200 and 500 µM concentration of pCMBA (Fig. 10). Furthermore, pCMBS (MCT1 inhibitor) also exhibited concentration dependent inhibition of moxifloxacin uptake by ~ 25-65% on ARPE-19 cells (Fig. 10).

Effect of Protonophore and Organic Anion Transporter Inhibitor on Moxifloxacin Uptake

Effect of protonophore (DNP) on moxifloxacin (10 µM) uptake was studied on ARPE-19 cells. Cellular accumulation of moxifloxacin was reduced to ~ 40% by DNP (500 µM) whereas, no significant change in moxifloxacin uptake was observed due to DIDS (organic anion transporter inhibitor) on ARPE-19 cells (Fig. 11).

Effect of Sulfhydryl-Modifying Agents on Moxifloxacin Uptake

Effect of sulfhydryl-modifying agents (NEM and DTT) on the uptake of moxifloxacin (10 µM) was determined on ARPE-19 cells. Cellular uptake of moxifloxacin was reduced to ~ 62% and ~ 51% by NEM (500 µM) and DTT (500 µM), respectively (Fig. 11).

Effect of pH and Metabolic Inhibitors on Moxifloxacin Uptake

Uptake of moxifloxacin (10 µM) was performed as a function of different buffer pH compositions. Cellular accumulation of moxifloxacin was observed ~ 2.3 and ~ 1.4 fold higher at pH 5.0 relative to pH 7.4 and pH 6.0, respectively (Fig. 12). Furthermore, effect of metabolic inhibitors such as ouabain (Na^+/K^+ ATPase inhibitor) and sodium azide (an uncoupler of oxidative phosphorylation) on moxifloxacin uptake was also determined on

ARPE-19 cells. Moxifloxacin uptake was reduced to 40% and 50% by sodium azide (1 and 10 mM) and 50% by ouabain (1 mM) (Fig. 13).

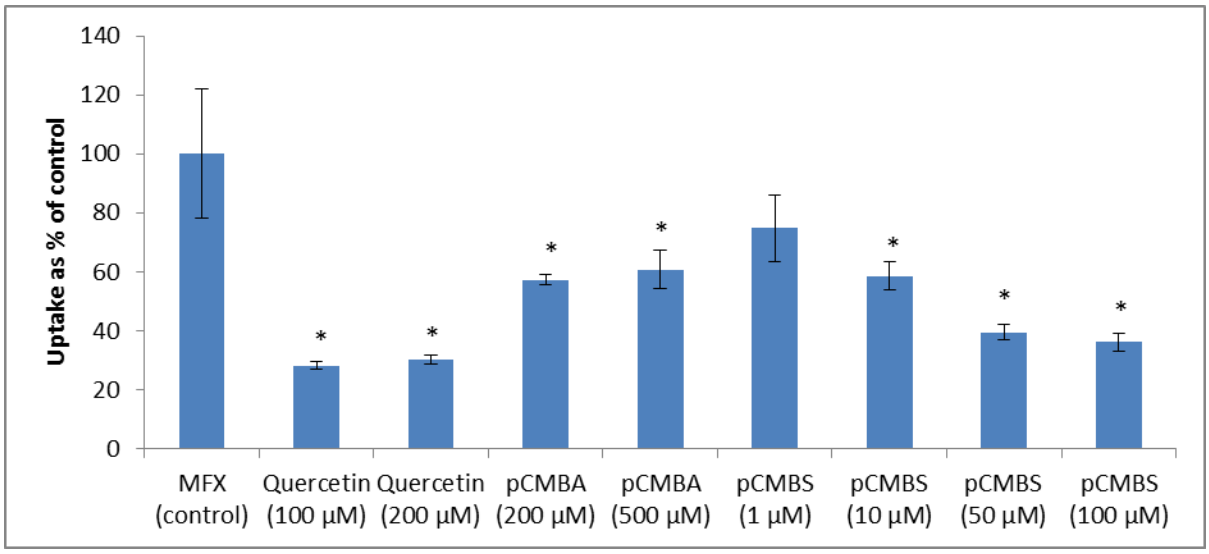

Figure 10. Inhibition of moxifloxacin (MFX) uptake by MCT inhibitors. Values are expressed as mean ± SD (n = 4). *Data were considered statistically significant for $P \leq 0.05$.

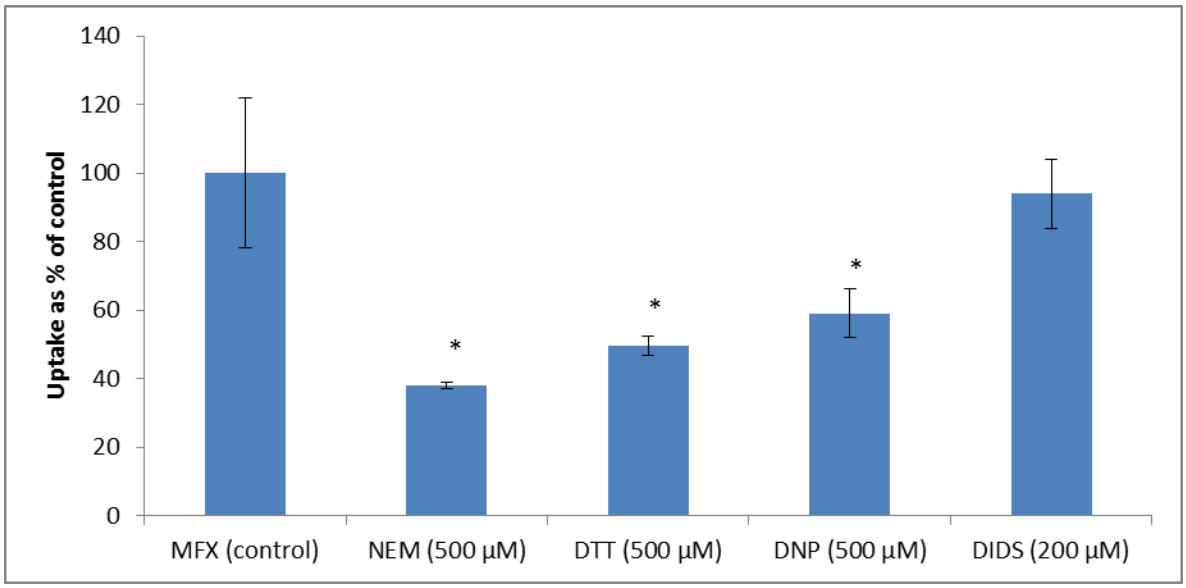

Figure 11. Inhibition of moxifloxacin (MFX) uptake by protonophore (DNP), organic anion transporter inhibitor (DIDS) and sulfhydryl-modifying agents (NEM and DTT). Values are expressed as mean ± SD (n = 4). *Data were considered statistically significant for $P \leq 0.05$.

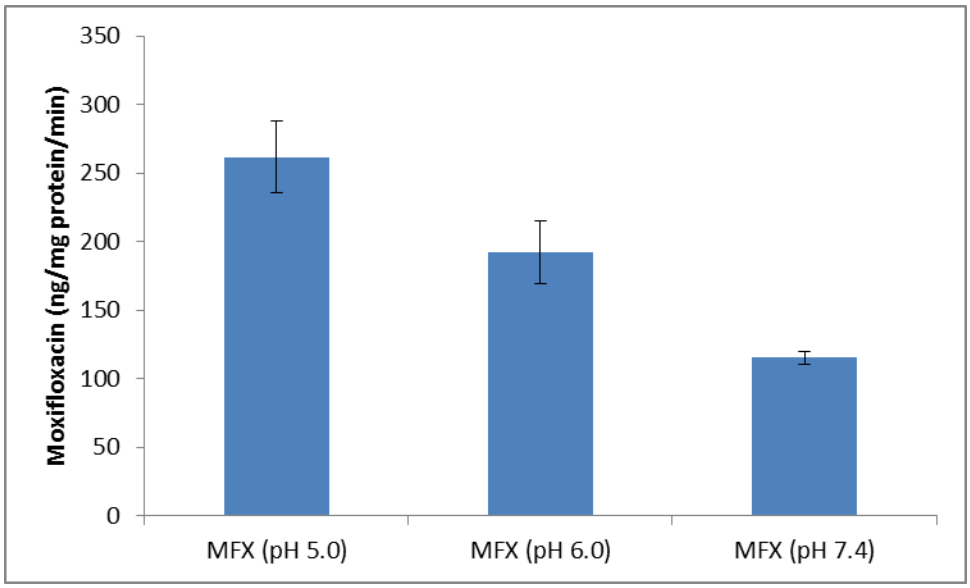

Figure 12. Effect of pH on cellular accumulation of moxifloxacin (MFX) across ARPE-19 cells. Values are expressed as mean ± SD (n = 4).

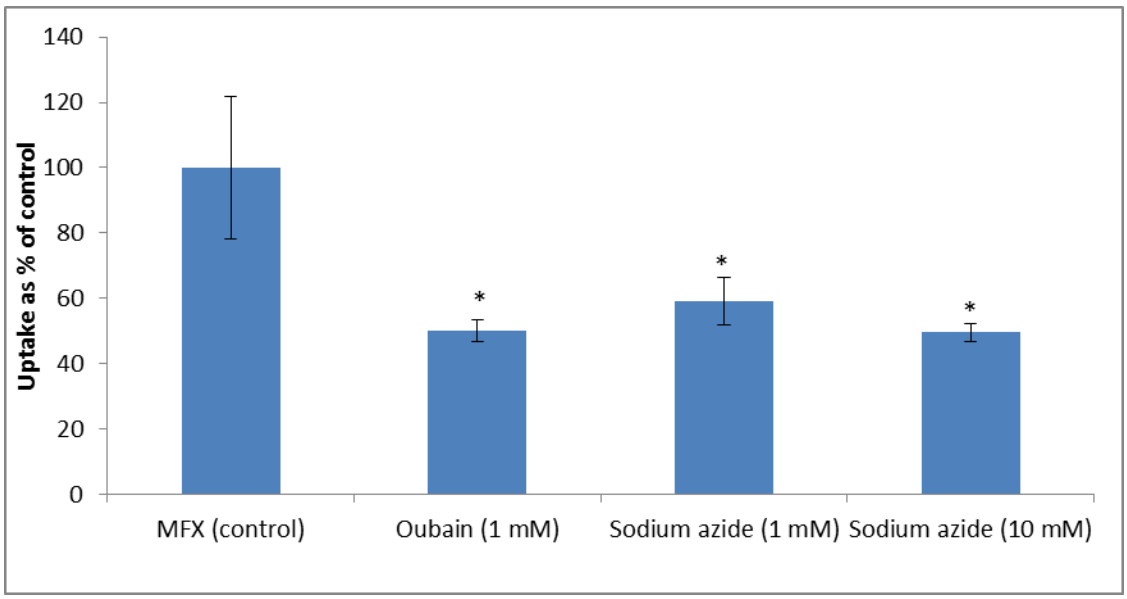

Figure 13. Inhibition of moxifloxacin (MFX) uptake by metabolic inhibitors (ouabain and sodium azide) across ARPE-19 cells. Values are expressed as mean ± SD (n = 4). *Data were considered statistically significant for $P \leq 0.05$.

3.4 Discussion:

Clinical endophthalmitis may affect the elimination half-life of a drug depending on its physiochemical properties (e.g. lipophilicity, size and structure) and elimination route (e.g. posterior route through passive or active transport across retina and anterior route through aqueous humor). Zwitterions such as ciprofloxacin and other fluoroquinolones are eliminated by posterior route and display shorter elimination half-lives relative to cationic compounds, which are primarily eliminated by passive transport through anterior chamber and aqueous humor [190]. However, *in vitro* MIC 90 value (minimum inhibitory concentration to inhibit 90% pathogens) of moxifloxacin for bacteria commonly encountered in postoperative and posttraumatic endophthalmitis are lowest (0.25 to 2.5 μg/mL) relative to other fluoroquinolones, making it promising candidate for treating ocular infections [202-204].

Moxifloxacin displays a low vitreous half-life compared to other fluoroquinolones indicating possibilities of its reorganization and translocation by active transport system present on the retina, which leads to rapid drug elimination from vitreous. Carrier-mediated (Na^+ and H^+) transport mechanism of monocarboxylic acid via MCT has been reported on retinal pigment epithelium cells (ARPE-19) [196]. A carrier mediated uptake of L-lactic acid (known MCT substrate) on ARPE-19 cells represents a potential mechanism by which monocarboxylic acid drugs eliminates from vitreous humor to retina.

The aim of present study was to evaluate moxifloxacin recognition by carrier-mediated MCT as a possible cause of its faster vitreous elimination. Significant reduction of moxifloxacin uptake in presence of competitive MCT substrates (L-lactic acid, ofloxacin and salisylic acid) on ARPE-19 cells suggests competitive inhibition of moxifloxacin uptake by

these monocarboxylates (Fig. 9). This study provides preliminary indication of possible moxifloxacin interaction with MCT. However, moxifloxacin uptake inhibition was not observed by di- and tri- carboxylic acids in ARPE-19 cells (data not shown) [205-208]. This observation further suggests that cellular accumulation of moxifloxacin is mediated by MCT influx transporter. Furthermore, significant reduction of moxifloxacin uptake by quercetin and pCMBA (classical inhibitors of MCT) [206,209,210] confirms active involvement of MCT during moxifloxacin uptake across ARPE-19 apical cell monolayer (Fig. 10). Reduction of moxifloxacin uptake by pCMBS (Fig. 10), a potent inhibitor of MCT1 but not MCT2 [196], states that MCT1 is involved in moxifloxacin uptake process.

The uptake of moxifloxacin on ARPE-19 cells was found saturable (Fig. 8). The kinetics determination of moxifloxacin uptake on ARPE-19 cells yielded Km of 2.02 ± 0.04 μM and Vmax of 14.51 ± 2.94 nmol/min/mg. Moreover, sulfhydryl group modifying agents (NEM and DTT) have demonstrated significant reduction of moxifloxacin uptake (Fig. 11) suggesting role of sulfhydryl groups and MCT1 in moxifloxacin translocation, which was consistent with the earlier report [211]. Since, presence of a protonophore (DNP) hinders MCT transporter activation by proton binding therefore, significantly reduced transcellular accumulation of moxifloxacin was observed (Fig. 11). Furthermore, translocation of moxifloxacin was found proton dependent (highest at pH 5.0) on ARPE-19 cells (Fig. 12).

This result provides direct evidence of proton-coupled mediated transport of moxifloxacin across ARPE-19 cells, which was found consistent with the previously published reports [194,196]. In addition, metabolic inhibitors such as sodium azide (uncoupler of oxidative phosphorylation) and ouabain (Na^+/K^+ ATPase inhibitor) significantly inhibited cellular accumulation of moxifloxacin on ARPE-19 cells (Fig. 13),

which was found consistent with the characteristics of Na^+/K^+ ATPase polarization on the apical membrane of ARPE-19cells [208].

3.5 Conclusion:

In conclusion, this is the first study attempted to demonstrate moxifloxacin interaction with Na^+ and H^+-coupled monocarbxylate transporter, most likely MCT1. Knowledge of elimination pharmacokinetics from vitreous humor is vital for designing dosage regime for posterior segment diseases. Therefore, interaction of moxifloxacin with MCT expressed on retina (a major elimination route for intravitreal drugs) may offer better understanding of its vitreous clearance. We anticipate that lowest vitreal half-life of intravitreally injected moxifloxacin compared to other fluoroquinolones may be due to its interaction with MCT influx transporter. Since, moxifloxacin is clinically delivered intravitreally for treating postoperative bacterial endophthalmitis, information about such interactions will be crucial in clinical settings and can further be explored to improve vitreous half-life and therapeutic efficacy of moxifloxacin.

CHAPTER 4

INTERACTION OF MOXIFLOXACIN WITH EFFLUX TRANSPORTERS

4.1 Rationale

Moxifloxacin is a promising fourth generation fluoroquinolone that exhibits broad spectrum of antimicrobial activity against both gram-positive as well as gram-negative microorganisms. Moxifloxacin generates bactericidal activity by binding to essential bacterial enzymes (topoisomerase II or DNA gyrase and topoisomerase IV) and thereby interferes with the bacterial DNA replication, transcription, and repair mechanism [202,212,213]. Fluoroquinolone moxifloxacin is approved for various respiratory tract (acute sinusitis, chronic bronchitis, and community-acquired pneumonia) and ocular (bacterial conjunctivitis) infections [213,214].

Mechanisms of resistance to the fluoroquinolones include: (i) mutations in DNA gyrase and/or topoisomerase genes, (ii) gene mutations that block drug entry, and (iii) presence of an efflux pump that reduces drug accumulation [175]. Since a majority of fluoroquinolones become ineffective due to bacterial as well as efflux pump mediated acquired resistance [87,215,216]. It is important to delineate the interaction of moxifloxacin with major efflux transporters. P-glycoprotein (MDR1) and multidrug resistance protein 2 (MRP2) belongs to the ATP-binding cassette transporter super family and act as energy-dependent efflux pumps. These efflux proteins hinder intracellular drug entry and reduce drug concentration inside the cells. This study investigates the interaction of moxifloxacin with major efflux transporters (MDR1 and MRP2). Model cell lines transfected with efflux transporters (MDCK-MDR1 and MDCK-MRP2) were used to perform uptake and bi-

directional transport experiments to screen the interaction of moxifloxacin with efflux transporters.

4.2 Material and Methods

Materials

Cell culture supplies, MDCK-WT (wild-type) cells and MDCK cells transfected with the human MDR1 (MDCK-MDR1) and MRP2 (MDCK-MRP2) genes were generously provided by Drs. Alfred H. Schinkel and Piet Borst (The Netherlands Cancer Institute, Amsterdam, Netherlands). Fetal bovine serum (FBS; heat inactivated and non-heat inactivated) was purchased from Atlanta Biologicals (Lawrenceville, GA, USA). Dulbecco's modified eagle medium (DMEM, for MDCK-WT, -MDR1 and -MRP2 cells) and non-essential amino acids (NEAA) were obtained from Gibco (Invitrogen, Grand Island, NY, USA). Streptomycin, penicillin, sodium bicarbonate, HEPES and all other chemicals were purchased from Sigma-Aldrich (St. Louis, MO, USA). Culture flasks (75 cm^2 growth area) and 12-well (3.8 cm^2 growth area per well) culture plates were obtained from Corning Costar Corp (Cambridge, MA, USA).

GF120198 was a generous gift from Glaxo SmithKline Ltd and MK571 was procured from Biomol International (Plymouth Meeting, PA, USA). [^{14}C]-erythromycin (specific activity: 53.8 mCi/nmol) was procured from Perkin Elmer Life Sciences (Boston, MA, USA). Levofloxacin and moxifloxacin was acquired from TCI America (Sunnyvale, CA, USA) and China, respectively. CellTiter 96® AQueousnon-radioactive cell proliferation assay kit was obtained from Promega Corporation (Madison, WI, USA). Bradford protein assay reagent was purchased from Bio-Rod Laboratories (Hercules, CA, USA). All the solvents were of HPLC grade and obtained from Fisher Scientific (St. Louis, MO).

Cell Culture

MDCK-WT, MDCK-MDR1 and MDCK-MRP2 cells (passages 5-15) were cultured in DMEM supplemented with 10% FBS (heat inactivated), 1% NEAA, penicillin (100 U/mL), streptomycin (100 µg/mL), 20 mM HEPES, 29 mM sodium bicarbonate and adjusted to pH 7.4. All the cell lines were grown and incubated at 37 ^{0}C with 5% CO_2 and 90% relative humidity. The medium was changed every alternate day and cells were passaged upon reaching 80%–90% confluency. For uptake experiments, cells were seeded at a density of 25000 per well in 2 mL of medium in 12-well tissue culture plates. For transport experiments, the collagen-coated Transwell® permeable inserts (Costar®) were plated at a density of 25000 cells per well in 12-well tissue culture plates. The apical (AP) and basolateral (BL) side of cells were treated with 0.5 mL and 1.5 mL of medium, respectively.

Moxifloxacin Cytotoxicity

Cytotoxicity of moxifloxacin was evaluated in MDCK-WT, MDCK-MDR1 and MDCK-MRP2 cells using CellTiter 96® AQueous nonradioactive cell proliferation assay kit according to the previously published protocol [92]. Briefly, a fixed number of MDCK-WT, MDCK–MDR1 and MDCK-MRP2 cells (10000 cells per well) were plated in 96-well plate for 24 h. After 24 h, culture medium was replaced with 100 µL of freshly prepared solutions of moxifloxacin in culture medium at different concentrations (1.0 µM-1.5 mM) and cells were incubated for 48 h (at 37 ^{0}C with 5% CO_2 and 90% relative humidity). Untreated and treated (5% of Triton X-100) cell culture media were used as a blank and positive control, respectively. After 48 h, the drug solution was replaced with MTT dye (3-[4,5-di-methylthiazolyl-2]-2, 5-diphenyl-tetrazolium bromide) and cells were further incubated for 2-

3 h. At the end of incubation, cell viability (n = 8) was calculated at 485 nm using 96-well microtiter plate reader (Spectra Fluor Plus, Tecan, Switzerland).

Cellular Accumulation of [^{14}C]-***Erythromycin***

Uptake studies were performed according to the previously published protocol [87,92]. Briefly, MDCK-MDR1 and MDCK-MRP2 cell monolayer was washed (3 × 10 min) with Dulbecco's Phosphate-Buffered Saline (DPBS) pH 7.4. The uptake of [^{14}C]-erythromycin (0.25 µCi/mL) was initiated alone or in presence of moxifloxacin (500 µM), GF120198 (2 µM) and MK571 (50 µM) in DPBS (pH 7.4) onto the cell monolayer at 37 ^{0}C. After 30 min incubation, the donor solution was removed and cells were immediately washed with ice-cold stop solution (200 mM KCl and 2 mM HEPES) three times. Cells were lysed with 1 mL lysis solution (0.1% w/v Triton X-100 in 0.3 N sodium hydroxide) and kept overnight at room temperature. The next day, 500 µL of cell lysate was transferred to scintillation vials containing 3 mL scintillation cocktail. Finally, samples were analyzed by Beckman Scintillation Counter (Model LS-6500, Beckman Instruments, Inc.). Uptake was normalized to the protein content of each well. Protein content of cell lysate was quantified using Bradford reagent. Uptake experiments were performed in quadruplicate (n = 4).

Following a similar procedure, the inhibitory potential of moxifloxacin against MDR1 and MRP2 mediated [^{14}C]-erythromycin efflux was determined. [^{14}C]-erythromycin (in DPBS pH 7.4, 0.25 µCi/mL) was spiked with increasing concentrations of moxifloxacin (0.1 µM - 1 mM) in MDCK-MDR1 and MDCK-MRP2 cells. Data was fitted to calculate the half maximal inhibitory concentration (IC_{50}) from the modified log [dose]-response curve.

Bi-directional Transport of [^{14}C]-***Erythromycin***

Bi-directional transport experiments of [^{14}C]-erythromycin were performed using Transwell® diffusion chamber system according to the previously published protocol [92]. MDCK-WT, MDCK-MDR1 and MDCK-MRP2 cell monolayers grown on the Transwell® inserts were rinsed and incubated with DPBS (pH 7.4) at 37 ^{0}C (2 × 10 min) for both AP and BL sides. AP to BL transport was initiated by adding 500 µL of [^{14}C]-erythromycin (in DPBS pH 7.4, 0.5 µCi/mL) alone and in presence of moxifloxacin (500 µM in DPBS pH 7.4), GF120918 (2.0 µM) or MK571 (50 µM) towards AP side of cells (donor chamber) where, receiver chamber (BL side) contains DPBS (pH 7.4). Similarly, BL to AP transport was initiated by adding 1500 µL of [^{14}C]-erythromycin alone and in presence of moxifloxacin, GF120918 or MK571 toward BL side of cells (donor chamber), where AP side of cells was treated as the receiver chamber. Cell monolayer integrity (around 250 Ωcm^2) was determined by transepithelial electrical resistance (TEER) measurement. Bi-directional transport was conducted for 3 h. Sampling (100 µL) from the receiver chamber was conducted at predetermined time intervals of 15, 30, 45, 60, 90, 120, 150, and 180 min. Fresh DPBS (pH 7.4) was replaced to maintain the sink conditions in the receiver chamber. Samples (n = 3) were analyzed by Beckman Scintillation Counter (Model LS-6500, Beckman Instruments, Inc.).

LC/MS-MS Method Development for Moxifloxacin

MDS Sciex API 3200 Triple Quadrupole linear QTrap mass spectrometry system (Applied Biosystems/MDS Sciex, Foster City, California) interfaced by turbo ion spray with positive ion source in Multiple Reaction Monitoring (MRM) mode was used for the analysis of moxifloxacin by LC-MS/MS. Mass-dependent parameters were tuned and optimized for

moxifloxacin and levofloxacin. Levofloxacin was used as an internal standard (IS) for analysis. Ultra high purity nitrogen was used for collisionally activated dissociation (CAD) at 4 psi and curtain gas at 20 psi. Nebulizer and turbo gas were optimized at 40 and 50 psi, respectively. The TIS temperature was maintained at 350 °C with source voltage and dwell time optimized at 5200 V and 400 ms, respectively. Parent and daughter ions obtained by direct infusion mode (20 µL/min) were injected with built-in infusion syringe pump. Initially, full scan mass spectra were acquired in positive ion mode for both the compounds. During the direct infusion experiment, the mass spectra for moxifloxacin and levofloxacin peaks at mass to charge ratio (m/z) were found to be 402.2 and 362.2, respectively, as the protonated molecular ions $[M + H]^+$. The most stable abundant fragment ions observed in each product tandem mass spectrometry (MS/MS) spectrum were at m/z of 384.2 and 344.2 for moxifloxacin and levofloxacin, respectively. Quantitative determination was performed in MRM scan positive ion mode using the mass transitions of 402.2→384.2 and 362.2→344.2 for moxifloxacin and levofloxacin, respectively. Method was developed over the linear ($r^2 >$ 0.99) concentration range 30–1000 ng/mL. Lower limit of quantification (LLOQ) was found to be 5.0 and 7.8 ng/mL for moxifloxacin and levofloxacin, respectively. The composition of mobile phase used was 0.1% trifluro acetic acid (TFA) and acetonitrile (50:50) at a flow rate of 0.25 mL/min.

Sample Preparation and Extraction

Frozen samples were thawed at room temperature and thoroughly vortexed for 1 min. 100 µL of sample was aliquoted using calibrated pipette into 1.5 mL polypropylene microcentrifuge tubes. 20 µL of 10.0 µg/mL freshly prepared IS working solution (levofloxacin) was added to the above aliquots (except for blank sample) and the mixture was

vortexed for 30 s. 900 µL of cold ethyl acetate was added to the above mixture and the drug was extracted by vortexing (2 min). The mixture was centrifuged at 5000 rpm (5 min) and the supernatant was evaporated in vacuum cetrifuge (Speed Vac®) at 40 ^{0}C for 2 h and reconstituted in 100 µL of mobile phase. 10 µL of resulting solution was injected into LC–MS/MS for analysis using XTerrs® MS C18 column (5 µm).

Bi-directional Transport of Moxifloxacin

Bi-directional transport of moxifloxacin was performed as described previously. AP to BL transport was initiated by adding 500 µL of moxifloxacin (in DPBS pH 7.4, 500 µM) alone and in presence of GF120918 (2.0 µM) or MK571 (50 µM) towards AP side of cells (donor chamber) where, receiver chamber (BL side) contains DPBS (pH 7.4). Similarly, BL to AP transport was initiated by adding 1500 µL of moxifloxacin (in DPBS pH 7.4, 500 µM) alone and in presence of GF120918 or MK571 toward BL side of cells (donor chamber), where AP side of cells were treated as a receiver chamber. Samples (n = 4) were analyzed by LC–MS/MS after cold ethyl acetate extraction. Extracted samples were evaporated in speed vacuum and reconstituted in optimized mobile phase.

Data Treatment

For dose–response studies, the effect of moxifloxacin on [^{14}C]-erythromycin efflux was calculated using a modified log [dose]-response curve method to fit the data in equation 1 in order to obtain IC_{50} values,

$$Y=[Min+\frac{max-min}{1+10^{(logIC50-x)*H}}]$$ .....Eq. 1.

where *x* denotes the log concentration of moxifloxacin, *Y* is the cellular accumulation of [^{14}C]-erythromycin, IC_{50} represents the inhibitor concentration where the efflux of [^{14}C]-erythromycin is inhibited by 50%, and *H* is the Hill constant. *Y* starts at a minimum (min)

value (at low inhibitor concentration) and then plateaus at a maximum (max) value (at high inhibitor concentration) resulting in a sigmoidal curve.

Cumulative amounts transported in bi-directional transport experiments across cell monolayers were plotted as a function of time. Linear regression of amounts transported as a function of time yielded the rate of transport across the cell monolayer (dM/dt). Rate divided by the cross-sectional area available for transport (A) generated steady state flux as shown in Eq. 2.

$$Flux=\left(\frac{dM}{dt}\right)/A \quad \text{.....Eq. 2.}$$

Slopes were obtained from the linear portion of the curve to calculate apparent permeability (Papp) through normalization of the steady-state flux to the donor concentration (Cd) according to Eq. 3.

$$Papp = \frac{dM/dt}{(Cd*A*60)} \quad \text{.....Eq. 3.}$$

When a dM/dt (mol/min) represents the rate of drug transport across the cell monolayer, A (cm^2) is the cross-sectional area available for transport, and Cd (µM) is the donor concentration. The net efflux ratio was assessed from Papp in BL to AP and AP to BL directions as shown in Eq. 4.

$$\text{Efflux Ratio} = (\text{Papp BL}\rightarrow\text{AP}) / (\text{Papp AP}\rightarrow\text{BL}) \quad \text{.....Eq. 4.}$$

Statistical Analysis

All the results are expressed as mean ± standard deviation (SD). The student t test was applied to determine statistical significance between two groups where, $p < 0.05$ being considered statistically significant.

4.3 Results

Moxifloxacin Cytotoxicity

Moxifloxacin (1.0 µM - 1.5 mM) cytotoxicity was evaluated on MDCK-WT, MDCK-MDR1 and MDCK-MRP2 cells. From MTT assay result it was observed that moxifloxacin is not cytotoxic up to 1.5 mM concentration in all the three cell lines (Fig. 14).

Cellular Accumulation of [^{14}C]-*Erythromycin*

Cellular accumulation of [^{14}C]-erythromycin was significantly elevated in the presence of GF120918 (193%) and MK571 (273%) relative to control on MDCK-MDR1 (Fig. 15) and MDCK-MRP2, respectively (Fig. 16). In the presence of moxifloxacin, cellular accumulation of [^{14}C]-erythromycin was increased by 150% and 220% on MDCK-MDR1 and MDCK-MRP2 cells, respectively (Fig. 15-16).

Dose-dependent inhibition of [^{14}C]-erythromycin efflux was observed in presence of increasing concentration of moxifloxacin on MDCK-MDR1 and MDCK-MRP-2 cells, respectively (Fig. 17-18). A modified log [dose]-response curve was applied to fit the data in order to obtain IC_{50} values. From the dose-response curve, moxifloxacin IC_{50} values against MDR1 and MRP2 mediated inhibition of [^{14}C]-erythromycin efflux was 217 and 187 mM, respectively.

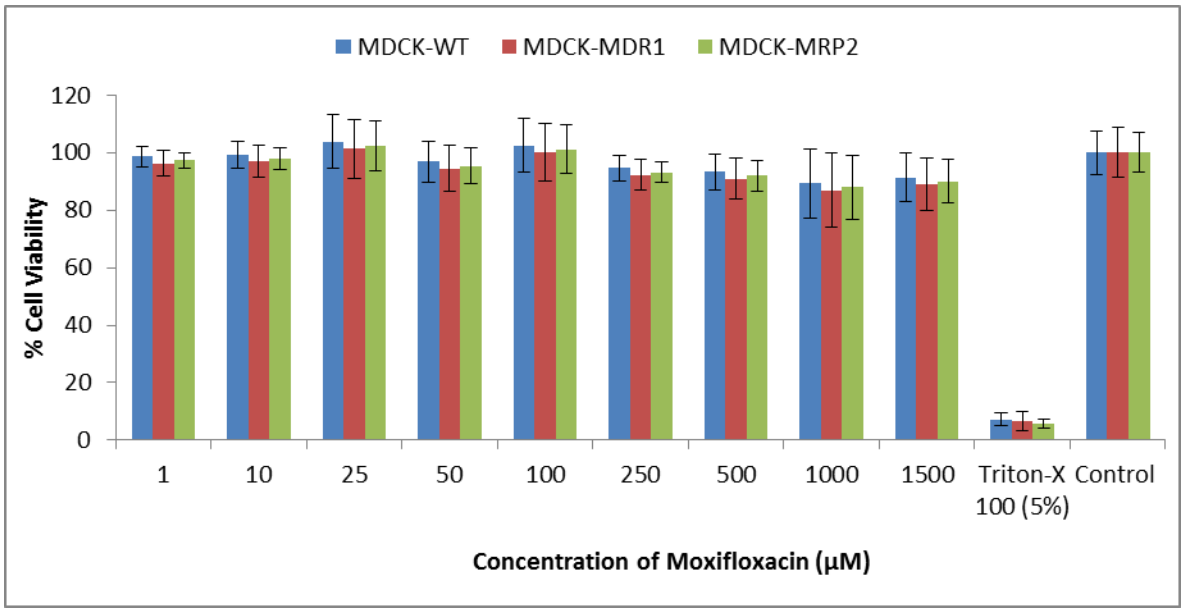

Figure 14. Cytotoxicity study (MTT assay) for moxifloxacin on MDCK-WT, MDCK-MDR1 and MDCK-MRP2. Values are expressed as mean ± SD (n = 6).

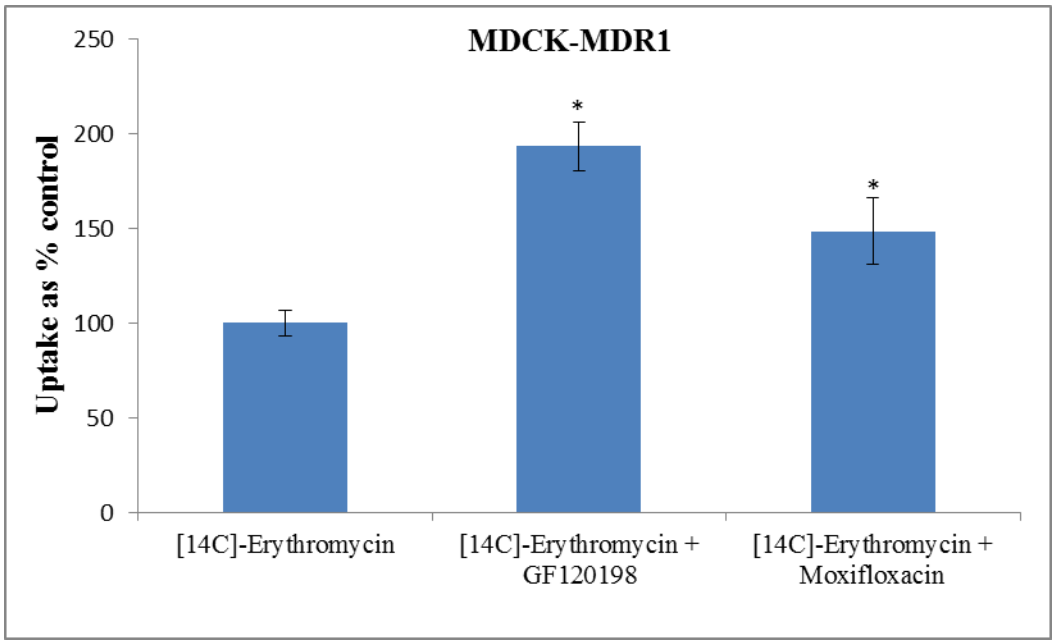

Figure 15. Accumulation of [^{14}C]-erythromycin (0.25 µCi/mL) alone and in presence of moxifloxacin (500 µM) and GF120198 (2 µM) across MDCK-MDR1 cells. Values are expressed as mean ± SD (n = 4). *Data were considered statistically significant for $P \leq 0.05$.

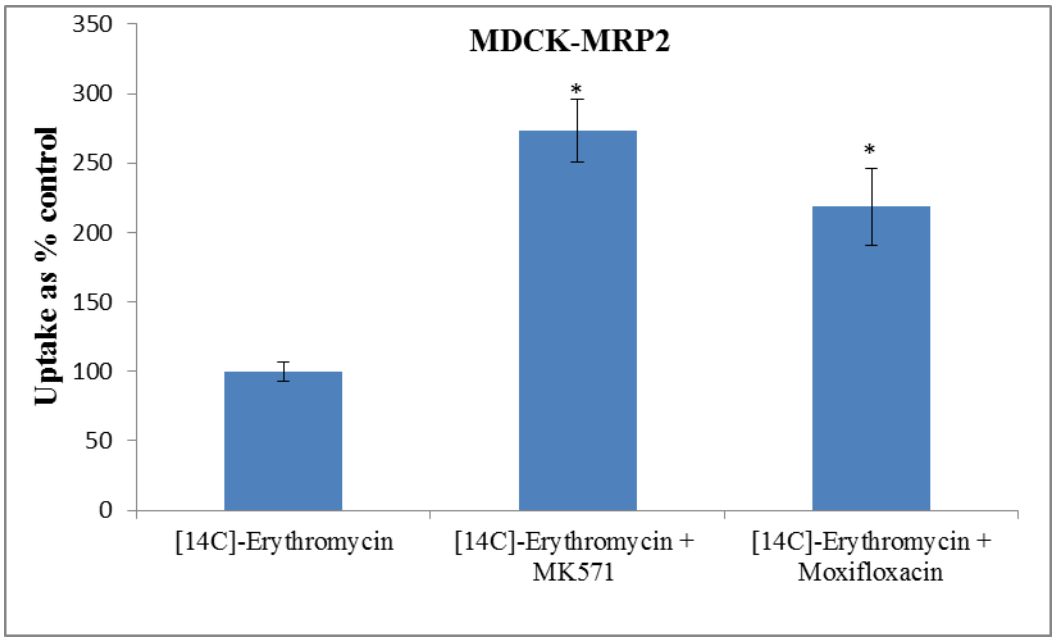

Figure 16. Accumulation of [^{14}C]-erythromycin (0.25 µCi/mL) alone and in presence of moxifloxacin (500 µM) and MK571 (50 µM) across MDCK-MRP2 cells. Values are expressed as mean ± SD (n = 4). *Data were considered statistically significant for $P \leq 0.05$.

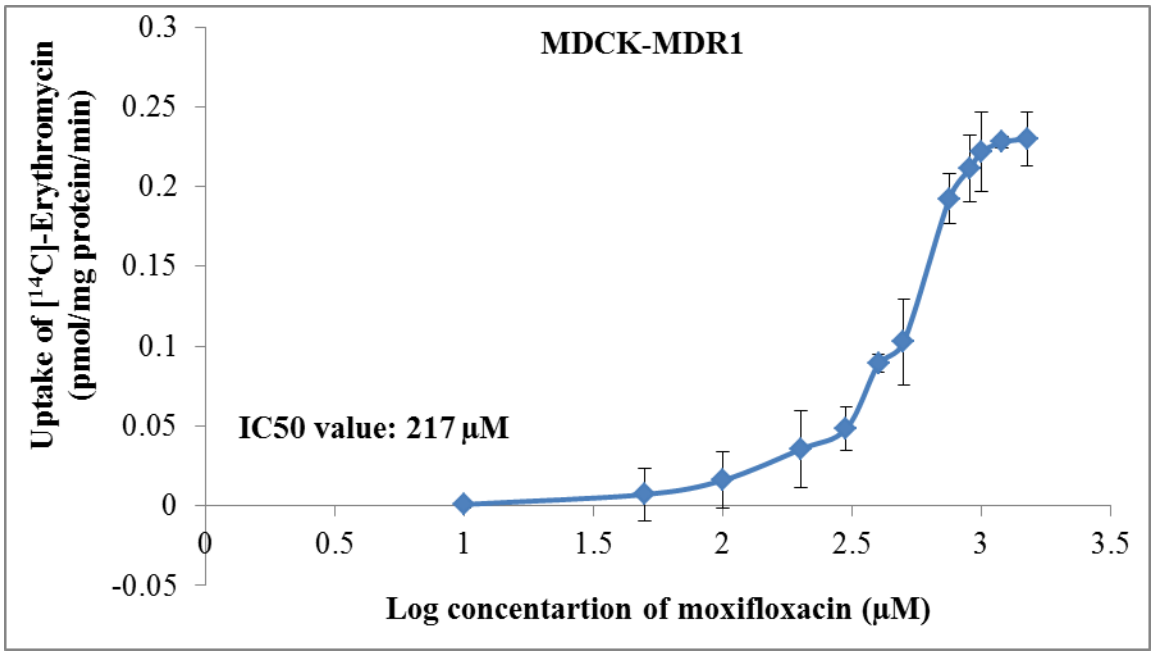

Figure 17. Moxifloxacin mediated inhibition of [^{14}C]-erythromycin (0.25 µCi/mL) efflux across MDCK-MDR1 cells. Values are expressed as mean ± SD (n = 4).

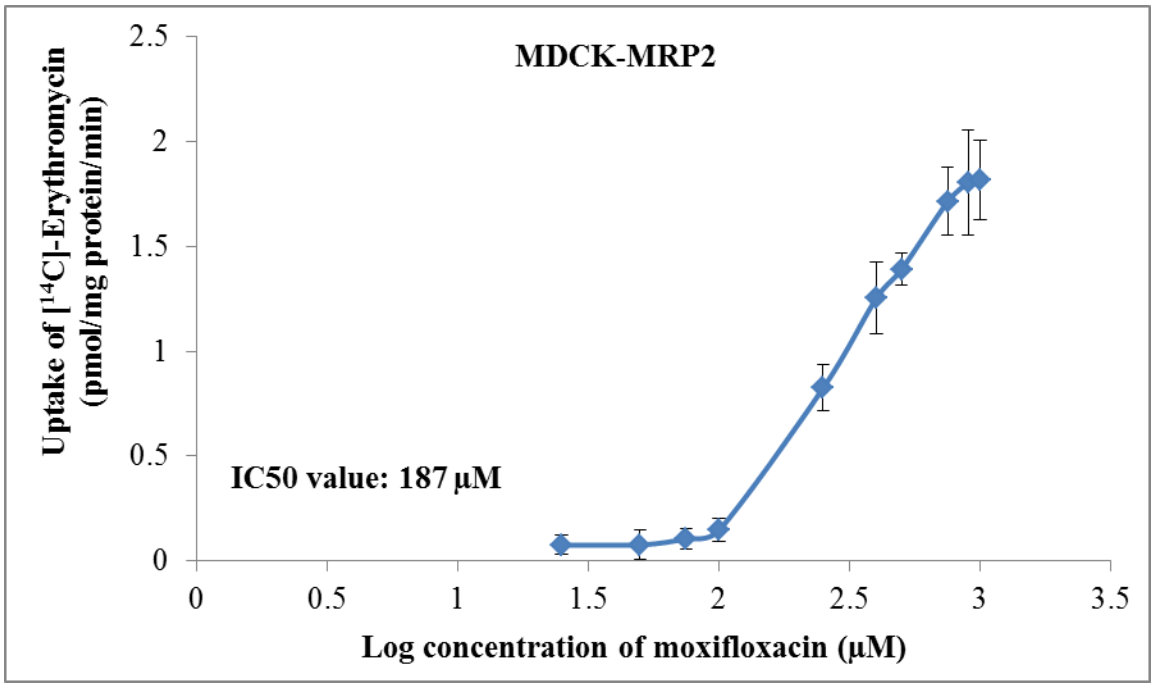

Figure 18. Moxifloxacin mediated inhibition of [^{14}C]-erythromycin (0.25 µCi/mL) efflux across MDCK-MRP2 cells. Values are expressed as mean ± SD (n = 4).

Bi-directional Transport of [^{14}C]-***Erythromycin***

The apparent permeability of [^{14}C]-erythromycin across MDCK cells overexpressing MDR1 and MRP2 proteins was significantly higher in the BL-AP direction relative to the AP-BL direction (Table 6) due to the expression of these transporters on the apical side of the cells. For MDCK-MDR1 cells, the BL-AP and AP-BL permeabilities of [^{14}C]-erythromycin were $18.83 \pm 1.05 \times 10^{-6}$ and $5.44 \pm 0.52 \times 10^{-6}$cm/s, respectively, leading to an efflux ratio of 3.46. Similarly, BL-AP and AP-BL permeabilities of [^{14}C]-erythromycin across MDCK-MRP2 cells were $2.70 \pm 0.18 \times 10^{-6}$ and $0.62 \pm 0.13 \times 10^{-6}$ cm/s, respectively, leading to an efflux ratio of 4.35. However, in the presence of moxifloxacin a significant reduction in the efflux ratio of [^{14}C]-erythromycin was observed across MDCK-MDR1 (1.71) and MDCK-MRP2 (1.92) cells due to the elevation of AP-BL permeabilities ($9.50 \pm 1.55 \times 10^{-6}$ and $1.34 \pm 0.17 \times 10^{-6}$) across both the cell lines, respectively (Table 6). Moreover, similar efflux ratio reduction (1.14 and 1.36) of [^{14}C]-erythromycin was also observed in the presence of known MDR1 (GF120918) and MRP2 (MK571) inhibitors across MDCK-MDR1 and MDCK-MRP2 cells, respectively (Table 6).

Bi-directional Transport of Moxifloxacin

Similar to [^{14}C]-erythromycin, the apparent permeability of moxifloxacin across MDCK-MDR1 and MDCK-MRP2 cells was significantly elevated in BL-AP direction relative to AP-BL direction (Table 7) suggesting moxifloxacin is a substrate for MDR1 and MRP2 efflux transporters. For MDCK-MDR1 cells, the BL-AP and AP-BL permeabilities of moxifloxacin were $20.46 \pm 2.26 \times 10^{-6}$ and $5.81 \pm 0.44 \times 10^{-6}$ cm/s, respectively, leading to an efflux ratio of 3.52. Similarly, BL-AP and AP-BL permeabilities of moxifloxacin across MDCK-MRP2 cells were $1.97 \pm 0.41 \times 10^{-6}$ and $0.78 \pm 0.13 \times 10^{-6}$ cm/s, respectively,

leading to an efflux ratio of 2.53. Moreover, reduction of moxifloxacin efflux ratio was observed in the presence of known MDR1 (1.25) and MRP2 (1.20) inhibitors across MDCK-MDR1 and MDCK-MRP2 cells, respectively (Table 7).

Table 6. Bi-directional transport of [^{14}C]-erythromycin (0.5 µCi/mL) alone and in presence of moxifloxacin (500 µM), GF120198 (2 µM) and MK571 (50 µM) across MDCK-MDR1, MDCK-MRP2 and MDCK-WT cells. Values are expressed as mean ± SD (n = 3).

Cell Line	Drug	Permeability ($\times 10^{-6}$) cm/s		Efflux Ratio
		AP-BL	BL-AP	
MDCK-MDR1	Erythromycin	5.44 ± 0.52	18.83 ± 1.05	3.46
	Erythromycin + Moxifloxacin	9.50 ± 1.55	16.23 ± 1.43	1.71
	Erythromycin + GF120918	14.13 ± 0.48	16.08 ± 3.24	1.14
MDCK-MRP2	Erythromycin	0.62 ± 0.13	2.70 ± 0.18	4.35
	Erythromycin + Moxifloxacin	1.34 ± 0.17	2.58 ± 0.34	1.92
	Erythromycin + MK571	1.98 ± 0.21	2.46 ± 0.28	1.36
MDCK-WT	Erythromycin	4.20 ± 0.76	8.05 ± 2.53	1.91
	Erythromycin + Moxifloxacin	5.68 ± 0.49	7.94 ± 1.69	1.40
	Erythromycin + GF120918	5.02 ± 1.19	7.63 ± 2.04	1.51

Table 7. Bi-directional transport of moxifloxacin (500 µM) alone and in presence of GF120198 (2 µM) and MK571 (50 µM) across MDCK-MDR1, MDCK-MRP2 and MDCK-WT cells. Values are expressed as mean ± SD (n = 4).

Cell Line	Drug	Permeability ($\times 10^{-6}$) cm/s		Efflux Ratio
		AP-BL	BL-AP	
MDCK-MDR1	Moxifloxacin	5.81 ± 0.44	20.46 ± 2.26	3.52
	Moxifloxacin + GF120918	16.29 ± 0.94	20.36 ± 1.81	1.25
MDCK-MRP2	Moxifloxacin	0.78 ± 0.13	1.97 ± 0.41	2.53
	Moxifloxacin + MK571	1.64 ± 0.17	1.86 ± 0.24	1.20
MDCK-WT	Moxifloxacin	5.70 ± 0.04	7.40 ± 0.14	1.29
	Moxifloxacin + GF120918	6.62 ± 0.09	7.82 ± 0.07	1.18

4.4 Discussion:

Moxifloxacin is a potent fluoroquinolone antibiotic used in the clinical settings for the treatment of respiratory and ocular infections [213,214]. It exhibits broad spectrum of activity against gram positive and gram negative pathogens by inhibiting bacterial DNA gyrase and topoisomerase IV enzymes. Besides bacterial drug resistance, MDR represents a major barrier to clinically successful fluoroquinolone therapy. Majority of fluoroquinolones are reported to be substrates of MDR efflux proteins which significantly reduces its intracellular accumulation and bioavailability [87]. Therefore, primary objective of this report was to evaluate interaction of moxifloxacin with major efflux transporters (MDR1 and MRP2) to delineate effect of MDR proteins on intracellular translocation of moxifloxacin.

Previous report indicates that erythromycin can be selected as a model substrate to study MDR1 and MRP2 mediated efflux [217]. Therefore, a preliminary interaction experiment was carried out by studying cellular accumulation of erythromycin in the presence of moxifloxacin in MDCK-MDR1 and MDCK-MRP2 cells. Cellular accumulation of [^{14}C]-erythromycin appears to be significantly higher in presence of GF120918 (known MDR1 inhibitor) and MK571 (known MRP2 inhibitor) relative to control in MDCK-MDR1 and MDCK-MRP2 cells, respectively (Fig. 15-16) confirming an excellent MDR1 and MRP2 substrate specificity of [^{14}C]-erythromycin [217]. Significantly higher cellular accumulation of [^{14}C]-erythromycin in presence of moxifloxacin across both the cell lines indicates moxifloxacin interacts with MDR1 and MRP2, suggesting moxifloxacin substrate specificity for both efflux transporters.

Furthermore, dose-dependent inhibitions of [^{14}C]-erythromycin efflux suggest high affinity of moxifloxacin towards MDR1 and MRP2 efflux transporters (Fig. 17-18). IC_{50}

values indicates higher affinity of moxifloxacin towards MRP2 (187 μM) relative to MDR1 (217 μM) efflux transporter. This observation suggests that inhibitory potential of moxifloxacin for MDR1 and MRP2 mediated [^{14}C]-erythromycin efflux was competitive in nature.

Apical localization of MDR1 and MRP2 efflux transporters on the MDCK-MDR1 and MDCK-MRP2 cells exhibited much higher [^{14}C]-erythromycin transport in BL-AP direction relative to AP-BL direction (Table 6). A significant elevation of AP-BL transport of [^{14}C]-erythromycin to 1.75 fold (MDCK-MDR1) and 2.16 fold (MDCK-MRP2) in presence of moxifloxacin confirms the substrate specificity of moxifloxacin towards MDR1 and MRP2. Similarly, AP-BL transport elevation of [^{14}C]-erythromycin was also observed in presence of GF120918 (2.59 fold) and MK571 (3.19 fold) across MDCK-MDR1 and MDCK-MRP2 cells, respectively.

Since, reduction of efflux ratio value to 1.0 leads to equivalent transport in both the direction. Significant reduction of [^{14}C]-erythromycin efflux ratio from 3.46 to 1.71 (MDCK-MDR1) and from 4.35 to 1.92 (MDCK-MRP2) was evident in presence of moxifloxacin confirming competitive inhibition of MDR1 and MRP2 functional activities. Furthermore, AP-BL permeability of moxifloxacin increased by 2.80 and 2.10 times in presence of GF120918 and MK571, respectively (Table 7). This permeability escalation has led to moxifloxacin efflux ratio reduction from 3.52 to 1.25 and 2.53 to 1.20 in MDCK-MDR1 and MDCK-MRP2 cells, respectively. This observation further confirms the substrate specificity of moxifloxacin towards MDR1 and MRP2 efflux transporters.

4.5 Conclusion:

In summary, above results provides direct evidence that moxifloxacin is a substrate of MDR1 and MRP2 efflux transporters. This overlapping substrate specificity of moxifloxacin for MDR1 and MRP2 may endure a synergistic efflux action and may develop resistance by lowering intracellular concentration and permeability of moxifloxacin. Therefore, it is suggested that attention must be given to the eventual consequences of moxifloxacin interaction with efflux transporters and strategies should be developed to circumvent MDR1 and MRP2 mediated moxifloxacin resistance. Furthermore, co-administration of moxifloxacin with therapeutic substrate of these efflux transporters such as erythromycin may inhibit efflux of later due to competitive inhibition of MDR1 and MRP2. This may ultimately improve the intracellular permeability of MDR1 and MRP2 substrates and may also lower the incidence of drug resistance. Therefore, the co-administration hypothesis must be further tested with moxifloxacin to explore its potential to overcome efflux-based drug resistance of other therapeutic substrates.

CHAPTER 5

INTERACTION OF MOXIFLOXACIN WITH ANTICANCER AGENTS FOR RETINOBLASTOMA MANAGMENT

5.1 Rationale

Retinoblastoma is a major vision threatening intraocular malignancy affecting 300 children per year in the USA [173]. About 80% of the children are diagnosed with retinoblastoma at less than 5 year of age. Overall, retinoblastoma makes 3% of all childhood cancers diagnosed within 15 years of age [218]. The histological event includes development of retinoblastoma from immature retinal cells followed by replacement of healthy retinal tissues. Retinoblastoma displays elevated rate of apoptotic and tumor turnover events which leads to ocular necrosis and dystrophic calcification [218]. The most common symptoms of retinoblastoma include leukocoria (white discoloration in pupil) and strabismus (ocular misalignment) [219,220].

Chemotherapy is the key retinoblastoma treatment to reduce tumor size and to facilitate local therapies (cryotherapy, laser photocoagulation or thermotherapy) for eradication of the remaining disease [218]. The commonly used chemotherapeutic agents include carboplatin, topotecan, etoposide, and vinblastine. These agents suffer from poor cell permeability and chemo-resistance due to major interaction with multidrug resistant (MDR) efflux proteins. Innate expression of several efflux proteins such as P-glycoprotein (P-gp/MDR1), multidrug resistant proteins (MRPs), and lung resistance protein are reported on the retinoblastoma tumor [97-99,221]. Over-expression of cell membrane-based efflux transporters play an important role in drug resistance by restricting intracellular entry of therapeutic drugs used in a clinical setting. Many scientists have utilized different efflux pump evasion strategies to overcome drug resistance for improving drug intracellular

permeability [92,222]. One of such strategies involves co-administration of MDR1/MRP inhibitors to increase intracellular accumulation of therapeutic substrates [223-225]. However, utilization of efflux pump inhibitors has its own limitations as (i) it is not clinically approved, (ii) causes undesirable clinical pharmacokinetic interactions including interaction with major drug metabolizing enzymes [226,227], and (iii) little or no additional improvement in the therapeutic activity of drug. In the present report, we intend to study drug interaction strategy to simultaneously overcome chemo-resistance and to improve anticancer activity for retinoblastoma tumor.

Moxifloxacin is a promising fourth generation fluoroquinolone that exhibits broad spectrum of antimicrobial activity against both gram-positive as well as gram-negative microorganisms. Ocular cells (corneal endothelial cells, primary human trabecular meshwork and retinal pigment epithelial cells) have shown good tolerability against clinically accepted moxifloxacin even at higher dose levels (concentration up to 500 µg/mL for 30 days) [174,228]. Besides bactericidal activity, moxifloxacin mediated anti-topoisomerase II activity in eukaryotic and tumor cells have been reported [179]. Moreover, moxifloxacin mediated enhanced anti-topoisomerase I and cytotoxic activity of chemotherapeutic agents in tumor derived cell lines have been observed [177,178]. Moxifloxacin has further shown inhibition of anticancer mediated release of pro-inflammatory mediators (IL-8, IL-1b and TNF-a) in THP-1 and Jurkat cells [178,181]. Immunomodulatory and protective effects of moxifloxacin against bacterial strains have proposed its potential for treating patients undergoing chemotherapy and immune suppression [182-184]. Anti-angiogenic effects of moxifloxacin in combination with anticancer agent following spontaneous or drug induced release of pro-angiogenic cytokines have further suggested it potential for treating cancerous diseases [180].

Based on the above literature findings which suggest a potential role of moxifloxacin in modulating activity of cytotoxic agents, it would be interesting to study its interaction with anticancer agents for the management of retinoblastoma. In this report, we present the interaction of moxifloxacin with anticancer agents (topotecan, etoposide, vinblastine) currently used for the treatment of retinoblastoma. Anticancer topotecan, etoposide and vinblastine are known substrate of MDR1 and MRP2 efflux transporters (Fig. 19). We hypothesized that in such interactions, moxifloxacin will not only modulate the permeability of anticancer agent across retinoblastoma cells expressing efflux proteins (due to competitive inhibition at efflux sites) but it will also enhance the cytotoxic activity of chemotherapeutics.

Series of experiments have been performed to investigate above hypothesis. Model cell lines transfected with efflux transporters (MDCK-MDR1 and MDCK-MRP2) were used to perform *in vitro* uptake and bi-directional transport experiments to screen the interaction of moxifloxacin with anticancer agents. Time dependent *in vitro* uptake and bi-directional transport of anticancer agents in presence of moxifloxacin were performed to evaluate modulation of anticancer permeability across model cell lines. Anticancer agent mediated retinoblastoma (Y-79) cell cytotoxicity (MTT assay), apoptosis (caspase-3 and annexin V apoptosis assay), and release of pro-inflammatory mediators (ELISA assay) were evaluated in the presence of moxifloxacin.

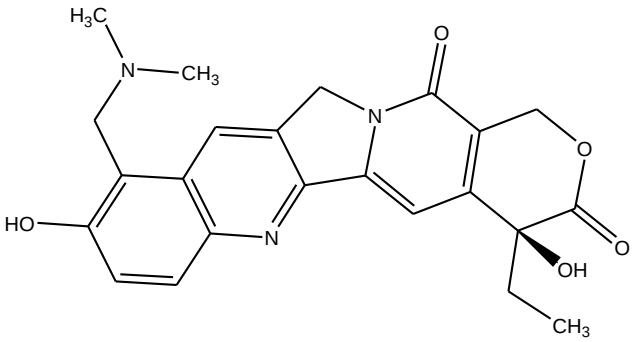

Topotecan

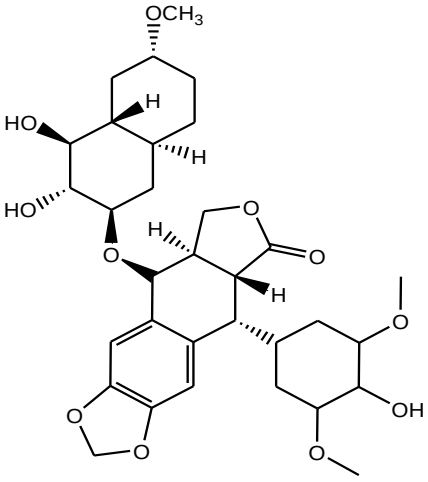

Etoposide

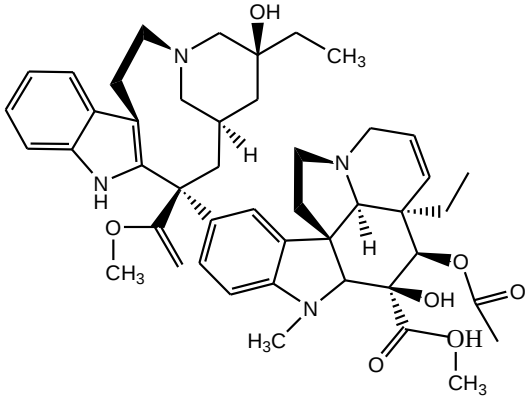

Vinblastine

Figure 19. Anticancer substrates of MDR1 and MRP2 efflux transporters.

5.2 Materials and Methods

Materials

Cell culture supplies, MDCK-WT (wild-type) cells and MDCK cells transfected with the human MDR1 (MDCK-MDR1) and MRP2 (MDCK-MRP2) genes were generously provided by Drs. Alfred H. Schinkel and Piet Borst (The Netherlands Cancer Institute, Amsterdam, Netherlands) and human retinoblastoma (Y-79) and retinal pigment epithelial (ARPE-19) cells were obtained from American Type Culture Collections (ATCC; Manassas, VA, USA). Fetal bovine serum (FBS; heat inactivated and non-heat inactivated) was purchased from Atlanta Biologicals (Lawrenceville, GA, USA). Dulbecco's modified eagle medium (DMEM, for MDCK-WT, -MDR1 and -MRP2 cells), D-MEM/F-12 (for ARPE-19 cells), RPMI 1640 (for Y-79 cells) and non-essential amino acids (NEAA) were obtained from Gibco (Invitrogen, Grand Island, NY, USA). Streptomycin, penicillin, sodium bicarbonate, HEPES, etoposide, vinblastine sulfate, topotecan hydrochloride, lipopolysaccharide (LPS) and dithiothreitol (DTT) and all other chemicals were purchased from Sigma-Aldrich (St. Louis, MO, USA). Culture flasks (75 cm^2 growth area), 12-well (3.8 cm^2 growth area per well) and 96-well (0.32 cm^2 growth area per well) culture plates were obtained from Corning Costar Corp (Cambridge, MA, USA).

GF120198 was a generous gift from Glaxo SmithKline Ltd and MK571 was procured from Biomol International (Plymouth Meeting, PA, USA). [^{3}H]-etoposide (specific activity: 480 mCi/mmol), [^{3}H]-topotecan (specific activity: 1.9 Ci/mmol) and [^{3}H]-vinblastine (specific activity: 1 Ci/mmol) were purchased from Moravek Biochemicals, Inc. (Brea, CA, USA). Moxifloxacin was acquired from China. CellTiter 96®Aqueous non-radioactive cell proliferation assay kit was obtained from Promega Corporation (Madison, WI, USA).

Bradford protein assay reagent and Annexin V/propidium iodide (PI) apoptosis detection kit was purchased from Bio-Rod Laboratories (Hercules, CA, USA) and BD Pharmingen (San Diego, CA, USA), respectively.

Cell Culture

MDCK-WT, MDCK-MDR1 and MDCK-MRP2 cells (passages 5-15) were cultured in DMEM supplemented with 10% FBS (heat inactivated), 1% NEAA, penicillin (100 U/mL), streptomycin (100 µg/mL), 20 mM HEPES, 29 mM sodium bicarbonate and adjusted to pH 7.4. Human retinoblastoma cells (Y-79) were incubated in 75 cm^2 tissue culture flasks as a suspension in RPMI 1640 medium supplemented with 15% non-heat inactivated FBS, 1 mM glutamine, penicillin (100 units/mL) and streptomycin (100 µg/mL). Human retinal pigment epithelium (ARPE-19) cells (passages 20-30) were cultured in D-MEM/F-12 supplemented with 10% heat-inactivated FBS, 15 mM HEPES, 29 mM sodium biocarbonate, penicillin (100 units/mL), and streptomycin (100 µg/mL).

All cell lines were grown and incubated at 37 ^{0}C with 5% CO_2 and 90% relative humidity. The medium was changed every alternate day and cells were passaged upon reaching 80%-90% confluency. For uptake experiments, cells were seeded at a density of 25000 per well in 2 mL of medium in 12-well tissue culture plates. For transport experiments, the collagen-coated Transwell® permeable inserts (Costar®) were plated at a density of 25000 cells per well in 12-well tissue culture plates. The apical (AP) and basolateral (BL) side of cells were treated with 0.5 mL and 1.5 mL of medium, respectively.

Cellular Accumulation of Anticancer Agents

Uptake studies were performed according to the previously published protocol [87,92]. Briefly, MDCK-MDR1 and MDCK-MRP2 cell monolayer was washed (3 × 10 min)

with DPBS (pH 7.4). The uptake of [^{3}H]-etoposide, [^{3}H]-topotecan and [^{3}H]-vinblastine (each 0.25 µCi/mL) was initiated alone or in presence of moxifloxacin (500 µM) in DPBS pH 7.4 (for etoposide and vinblastine) or pH 5.5 (for topotecan) onto the cell monolayer. The uptake was performed at different time point (15, 30 and 60 min) at 37 ^{0}C. Following incubation, the donor solution was removed and cells were immediately washed with ice-cold stop solution for 3 times. Cells were lysed with 1 mL lysis solution and kept overnight at room temperature. The next day, 500 µL of cell lysate was transferred in to scintillation vials containing 3 mL scintillation cocktail. Finally, samples were analyzed by Beckman Scintillation Counter (Model LS-6500, Beckman Instruments, Inc.). Uptake was normalized to the protein content of each well. Protein content of cell lysate was quantified using Bradford reagent. Uptake experiment was performed in quadruplicate (n = 4).

Bidirectional Transport of Anticancer Agents

Bi-directional transport of [^{3}H]-etoposide, [^{3}H]-topotecan and [^{3}H]-vinblastine was performed using Transwell® diffusion chamber system according to the previously published protocol [92]. MDCK-MDR1 and MDCK-MRP2 cell monolayers grown on the Transwell® inserts were rinsed and incubated with DPBS (pH 7.4) at 37 ^{0}C (2 × 10 min) for both AP and BL sides.

AP to BL transport was initiated by adding 500 µL (0.5 µCi/mL) of [^{3}H]-etoposide (in DPBS pH 7.4), [^{3}H]-vinblastin (in DPBS pH 7.4) and [^{3}H]-topotecan (in DPBS pH 5.5) alone and in presence of moxifloxacin (500 µM), GF120918 (2.0 µM) or MK571 (50 µM) towards AP side of cells (donor chamber) where, receiver chamber (BL side) contains DPBS (pH 7.4). Similarly, BL to AP transport was initiated by adding 1500 µL (0.5 µCi/mL) of [^{3}H]-etoposide, [^{3}H]-vinblastin and [^{3}H]-topotecan alone and in presence of moxifloxacin,

GF120918 or MK571 toward BL side of cells (donor chamber), where AP side of cells were treated as a receiver chamber. Cell monolayer integrity (around 250 Ωcm^2) was determined by TEER measurement. Bi-directional transport was conducted for 3 h. Sampling (100 µL) from the receiver chamber was carried out at predetermined time intervals of 15, 30, 45, 60, 90, 120, 150, and 180 min. Fresh DPBS (pH 7.4) was replaced to maintain the sink conditions in the receiver chamber. Samples (n = 3) were analyzed by Beckman Scintillation Counter (Model LS-6500, Beckman Instruments, Inc.).

Anti-proliferative Activity

Previously published protocol was followed with modification [229]. Y-79 cells (5×10^5) were seeded in 1 mL of culture medium/well in a 24-well plate. Y-79 cells were treated with various concentrations of etoposide (1-40 µM), vinblastine (1-40 nm) and topotecan (1-40 µM) alone and in presence of moxifloxacin (500 µM) for different time points (48 and 72 h at 37 ^{0}C with 5% CO_2 and 90% relative humidity). Following incubation, 100 µL MTT (5 mg/mL in PBS) per 1 mL medium was added to the cells and further incubated for 2-3 h. Cells were centrifuged at 5000 rpm and cell pellets were dissolved in 100 µL of DMSO. The optical density of cell suspension (n = 6) was measured at 485 nm using 96-well microtiter plate reader (SpectraFluor Plus, Tecan, Switzerland). Cells suspended in culture medium were treated as a control. IC_{50} values of anticancer agents were calculated from nonlinear regression analysis using GraphPad Prism Software version 5.0 (GraphPad Software Inc., San Diego, CA). Data were plotted as percentage viable cells against anticancer drug concentrations.

Caspase-3 Assay

Caspase-3 release was measured according to the previously published protocol with modification [178]. Briefly, Y-79 cells were incubated (24 h) with different concentrations (1, 5 and 10 µM) of anticancer agent (etoposide, topotecan and vinblastine) alone and in presence of moxifloxacin (500 µM). Following incubation, cells were washed and re-suspended in 50 mM HEPES (pH 7.4), 0.1% Triton X-100, DTT (5 mM), EDTA (0.1 mM) and incubated on ice for 15 min. Cells were lysed by three successive freeze–thaw cycles (dry ice/37 ^{0}C). The cell lysates were centrifuged at 12000 rpm (15 min, 4 ^{0}C) and the supernatants were stored at -80 ^{0}C until further analysis. The protein concentration of each sample was estimated using Bradford Bio-Rad protein assay. To determine caspase-3 activity, 25 mg protein was incubated in dark (37^{0}C, 60 min) with 30 mM Ac-DEVD-AMC (caspase-3 substrate with Km = 9.7 µM; Anaspec, San Jose, CA). Ac-DEVD is a caspase-specific peptide that is conjugated to the fluorescent reporter molecule 7-amino-4-methyl coumarin (AMC). Caspase mediated cleavage of peptide releases fluorochrome (AMC) which was measured at 360 nm (excitation) and 460 nm (emission) wavelengths.

Apoptosis Assay

Y-79 cell apoptosis was measured by flow cytometry after concurrent staining with annexin-V FITC and propidium iodide (PI) [178,230]. Briefly, Y-79 cells were incubated with anticancer agent alone or in presence of moxifloxacin for 24 h. Following incubation, cells were washed with cold PBS and resuspended in annexin V-PI binding buffer (10 mM HEPES pH 7.4, 140 mM NaCl, 2.5 mM $CaCl_2$). An aliquot of 100 µL was mixed with 4 mL of annexin-V FITC and PI. The mixture was incubated for 15 min at room temperature in the

dark. Finally, cells were washed and resuspended in binding buffer and subjected to flow cytometric analysis on FACScan (Becton Dickinson, Franklin Lakes, NJ, USA).

Pro-inflammatory Cytokines Assay

Anticancer mediated release of IL-6 and IL-8 from ARPE-19 cells were quantified according to the previously published protocol with modification [231]. Briefly, ARPE-19 cells suspended in DMEM/F12 medium were placed in 24-well culture plates at a concentration of 1×10^6 cells per mL. Cells were incubated (48 h) with two different concentrations (0.5 and 1.0 µg/mL) of anticancer agent (etoposide, topotecan and vinblastine) alone and in presence of moxifloxacin (500 µM). Following drug exposure, cell-free supernatants were recovered and cytokines concentrations were determined using Legend Max® human IL-6 and IL-8 sandwich ELISA kit (BioLegend®, San Diego, CA) according to the manufacturer protocol. IL-6 and 8 standard controls (100 pg/mL - 3.125 pg/mL), negative control (cell culture medium), positive control (lipopolysaccharide (LPS) and phorbol myristate acetate (PMA)) were also quantified simultaneously. Absorbance was measured at 450 nm (excitation) and 570 nm (emission) wavelengths.

Data Treatment

For dose–response studies, the effect of moxifloxacin on [^{14}C]-erythromycin efflux was calculated using a modified log [dose]-response curve method to fit the data in equation 1 in order to obtain IC_{50} values.

$$Y=[Min+\frac{max-min}{1+10^{(logIC50-x)*H}}]$$ .....Eq. 1.

Where, x denotes the log concentration of moxifloxacin, *Y* is the cellular accumulation of [^{14}C] erythromycin, IC_{50} represents the inhibitor concentration where the efflux of [^{14}C]-erythromycin is inhibited by 50%, and *H* is the Hill constant. *Y* starts at a minimum (min)

value (at low inhibitor concentration) and then plateaus at a maximum (max) value (at high inhibitor concentration) resulting in a sigmoidal curve.

The IC50 the anticancer agents was determined by plotting a graph of log (concentration of anticancer agent) vs % cell viability. Data were plotted using equation 1 in order to obtain the IC50 values. Where, x denotes the log concentration of anticancer agents, *Y* is the % cell viability and *H* is the Hill constant. *Y* starts at a maximum (max) % cell viability value (at low anticancer concentration) and then plateaus at a minimum (min) % cell viability value (at high anticancer concentration) resulting in a sigmoidal curve.

Cumulative amounts transported in bi-directional transport experiments across cell monolayers were plotted as a function of time. Linear regression of amounts transported as a function of time yielded the rate of transport across the cell monolayer (dM/dt). The rate divided by the cross-sectional area available for transport (A) generated steady state flux as shown in Eq. 2.

$$\text{Flux}=\left(\frac{dM}{dt}\right)/A \qquad \text{Eq. 2.}$$

Slopes were obtained from the linear portion of the curve to calculate apparent permeability (Papp) through normalization of the steady-state flux to the donor concentration (Cd) according to Eq. 3.

$$\text{Papp} = \frac{dM/dt}{(Cd*A*60)} \qquad \text{Eq. 3.}$$

Where dM/dt (mol/min) represents the rate of drug transport across the cell monolayer, A (cm^2) is the cross-sectional area available for transport, and Cd (µM) is the donor concentration. The net efflux ratio was assessed from Papp in BL to AP and AP to BL directions as shown in Eq. 4.

$$\text{Efflux Ratio} = (\text{Papp BL}\rightarrow\text{AP}) / (\text{Papp AP}\rightarrow\text{BL}) \qquad \text{Eq. 4.}$$

Statistical Analysis

All the results are expressed as mean ± standard deviation (SD). The student t test was applied to determine statistical significance between two groups where, $p < 0.05$ being considered to be statistically significant.

5.3 Results

Cellular Accumulation of Anticancer Agents

Time and concentration dependent increased cellular accumulation of anticancer agents were observed in presence of moxifloxacin. Highest cellular accumulation of [^{3}H]-etoposide, [^{3}H]-vinblastine and [^{3}H]-topotecan was observed at 60 min in presence of moxifloxacin (500 µM) across MDCK-MDR1 (189%, 210% and 199%) and MDCK-MRP2 (264%, 190% and 212%) cells, respectively (Fig. 20,21,22).

Bidirectional Transport of Anticancer Agents

Apparent permeabilities of all three anticancer agents were significantly higher in BL-AP direction in presence of moxifloxacin across MDCK-MDR1 and MDCK-MRP2 cells (Table 8-9). The efflux ratio of [^{3}H]-etoposide was 3.25 (Papp AP→BL = 3.57 (± 0.65) × 10^{-6} cm/s) and 5.46 (Papp AP→BL = 37.82 (± 2.70) × 10^{-6} cm/s) across MDCK-MDR1 and MDCK-MRP2 cells, respectively. Significant reduction of [^{3}H]-etoposide efflux ratio was observed due to the elevation of AP-BL permeability in presence of moxifloxacin across MDCK-MDR1 (1.62, Papp AP→BL = 7.92 (± 1.78) × 10^{-6} cm/s) and MDCK-MRP2 (2.17, AP→BL = 89.34 (± 1.75) × 10^{-6} cm/s) cells. Moreover, [^{3}H]-etoposide efflux ratio reduction (1.03 and 1.08) was also observed in presence of known MDR1 (GF120918) and MRP2 (MK571) inhibitors across MDCK-MDR1 and MDCK-MRP2 cells, respectively (Tables 8-9).

Similarly, efflux ratio of [^{3}H]-vinblastine was 6.59 (Papp AP→BL = 1.55 (± 0.03) × 10^{-6} cm/s) and 5.46 (Papp AP→BL = 13.50 (± 3.24) × 10^{-6} cm/s) across MDCK-MDR1 and MDCK-MRP2 cells, respectively. Significant reduction of [^{3}H]-vinblastine efflux ratio was observed due to the elevation of AP-BL permeability in presence of moxifloxacin across MDCK-MDR1 (2.26, AP→BL = 3.95 (± 0.46) × 10^{-6} cm/s) and MDCK-MRP2 (2.48, AP→BL = 19.72 (± 2.56) × 10^{-6} cm/s) cells. Furthermore, [^{3}H]-vinblastine efflux ratio reduction was also observed in presence of GF120198 (1.33) and MK571 (1.39) across MDCK-MDR1 and MDCK-MRP2 cells, respectively (Tables 8-9).

The efflux ratio of [^{3}H]-topotecan was 4.63 (Papp AP→BL = 0.75 ± 0.03 × 10^{-6} cm/s) and 3.07 (Papp AP→BL = 8.06 ± 0.66 × 10^{-6} cm/s) across MDCK-MDR1 and MDCK-MRP2 cells, respectively. Significant reduction of [^{3}H]-topotecan efflux ratio was observed in presence of moxifloxacin across MDCK-MDR1 (2.16, Papp AP→BL = 1.56 ± 0.03 × 10^{-6} cm/s) and MDCK-MRP2 (1.80, Papp AP→BL = 12.67 ± 2.67 × 10^{-6} cm/s) cells. Likewise, [^{3}H]-topotecan efflux ratio reduction was also observed in presence of GF120198 (1.38) and MK571 (1.13) across MDCK-MDR1 and MDCK-MRP2 cells, respectively (Tables 8-9).

Anti-proliferative Activity

Cytotoxicity of anticancer agents against retinoblastoma cells (Y-79) was measured alone and in presence of moxifloxacin for different time points using the MTT assay. Significant reduction in % cell viability was observed upon co-exposure of anticancer drug and moxifloxacin relative to treatment of anticancer drug alone (Fig. 23). Based on cytotoxicity results, IC_{50} value of anticancer agents were calculated alone and in presence of moxifloxacin. The IC_{50} value of etoposide (27.07 µM), topotecan (27.89 µM) and vinblastine

(51.90 nm) against retinoblastoma cells were significantly reduced to 2.11 µM, 2.89 µM and 22.92 nm, respectively in presence of moxifloxacin (Table 10).

Caspase-3 Assay

Concentration dependant caspase-3 release was observed in response to anticancer drug treatment which was further increased up to 1.6 (etoposide), 2.9 (topotecan) and 6.6 (vinblastine) fold in presence of moxifloxacin (Fig. 24, 25, 26).

Apoptosis Assay

Anticancer concentrations equivalent to IC_{50} values (calculated from cytotoxicity studies) in presence or absence of moxifloxacin were exposed to Y-79 cells for 24 h. Live and dead cell discrimination was measure by flow cytometry analysis using Annexin-V FITC-PI dual staining.

The % cell population in early apoptotic (Annexin-V positive and PI negative) and necrosis/late apoptotic (Annexin-V positive and PI positive) stages were nearly similar when Y-79 cells were treated with equivalent concentration of etoposide (27 or 2.1 µM) (Fig. 27), topotecan (28 or 2.8 µM) (Fig. 28) and vinblastine (50 or 23 nm) (Fig. 29) alone or in combination with moxifloxacin, respectively.

Pro-inflammatory Cytokine Assay

Dose-dependent anticancer mediated cytokine release (IL-6 and IL-8) was observed in retinal cells (ARPE 19). After 48 h exposure of etoposide (0.5 and 1.0 µg) on Y-79 cells, release of IL-6 (105.2 ± 3.9, 151.4 ± 10.0 pg mL^{-1}) and IL-8 (191.9 ± 9.1, 286.6 ± 16.6 pg mL^{-1}) was reduced by 1.3, 1.4 (for IL-6) and 1.60, 1.28 (for IL-8) fold in presence of moxifloxacin, respectively (Figs. 30-31). Similarly, vinblastine (0.5 and 1.0 µg) mediated release of IL-6 (52.9 ± 4.3, 73.6 ± 2.3 pg mL^{-1}) and IL-8 (140.2 ± 14.4, 284.9 ± 18.0 pg mL^{-}

^{1}) was reduced by 1.11, 1.42 (for IL-6) and 1.40, 1.08 (for IL-8) fold in presence of moxifloxacin, respectively (Figs. 30-31). In case of topotecan (0.5 and 1.0 µg), release of IL-6 (156.9 ± 2.7, 157.5 ± 8.8 pg mL^{-1}) and IL-8 (157.7 ± 12.6, 239.2 ± 13.9 pg mL^{-1}) was reduced by 1.3 and 1.2 (for IL-6) and 1.48, 1.30 (for IL-8) fold in presence of moxifloxacin, respectively (Figs. 30-31).

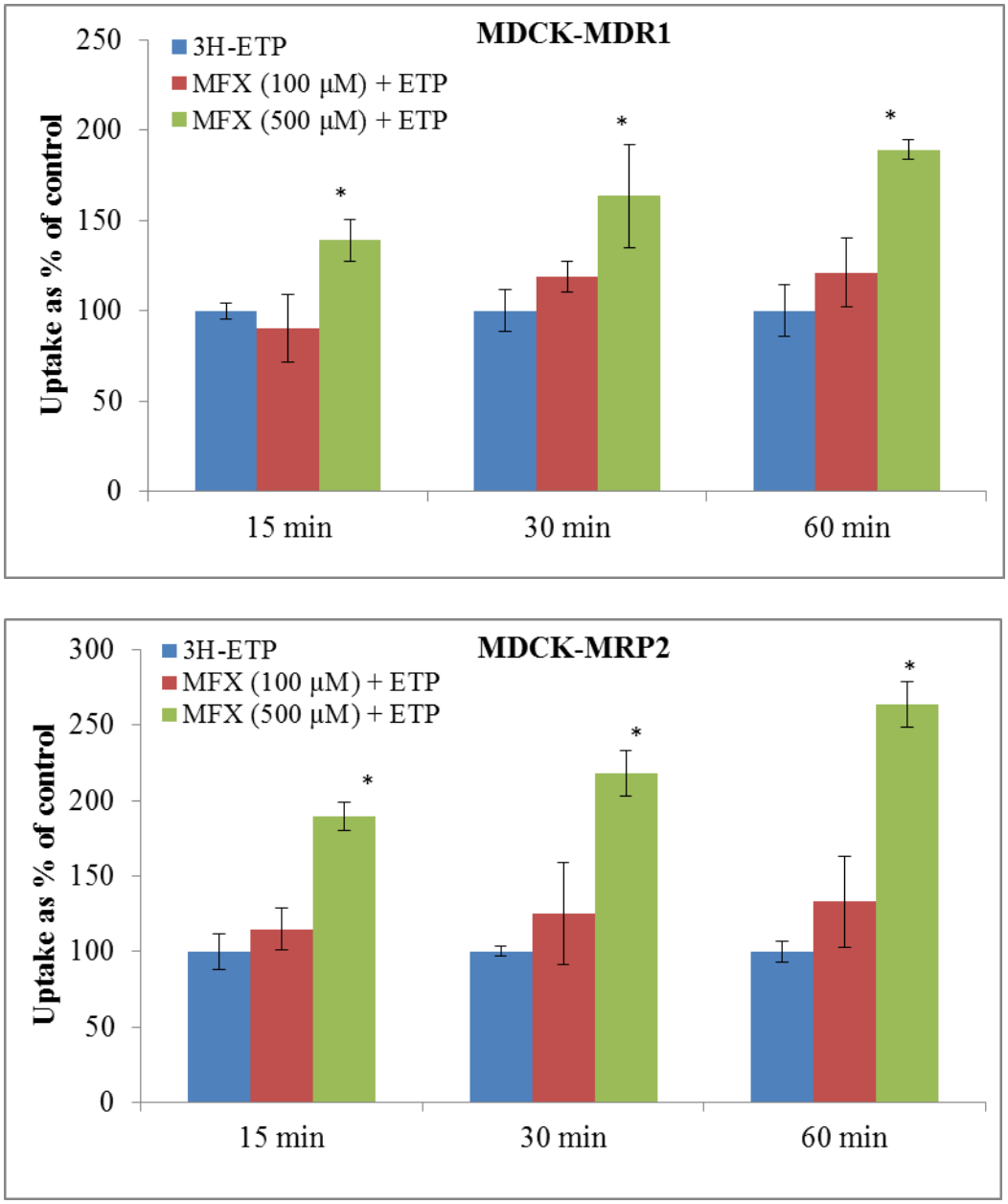

Figure 20. Cellular accumulation of [^{3}H]-etoposide (ETP) alone and in presence of moxifloxacin (MFX) across MDCK-MDR1 and MDCK-MRP2 cells. Values are expressed as mean ± SD (n = 4). *Data were considered statistically significant for $P \leq 0.05$.

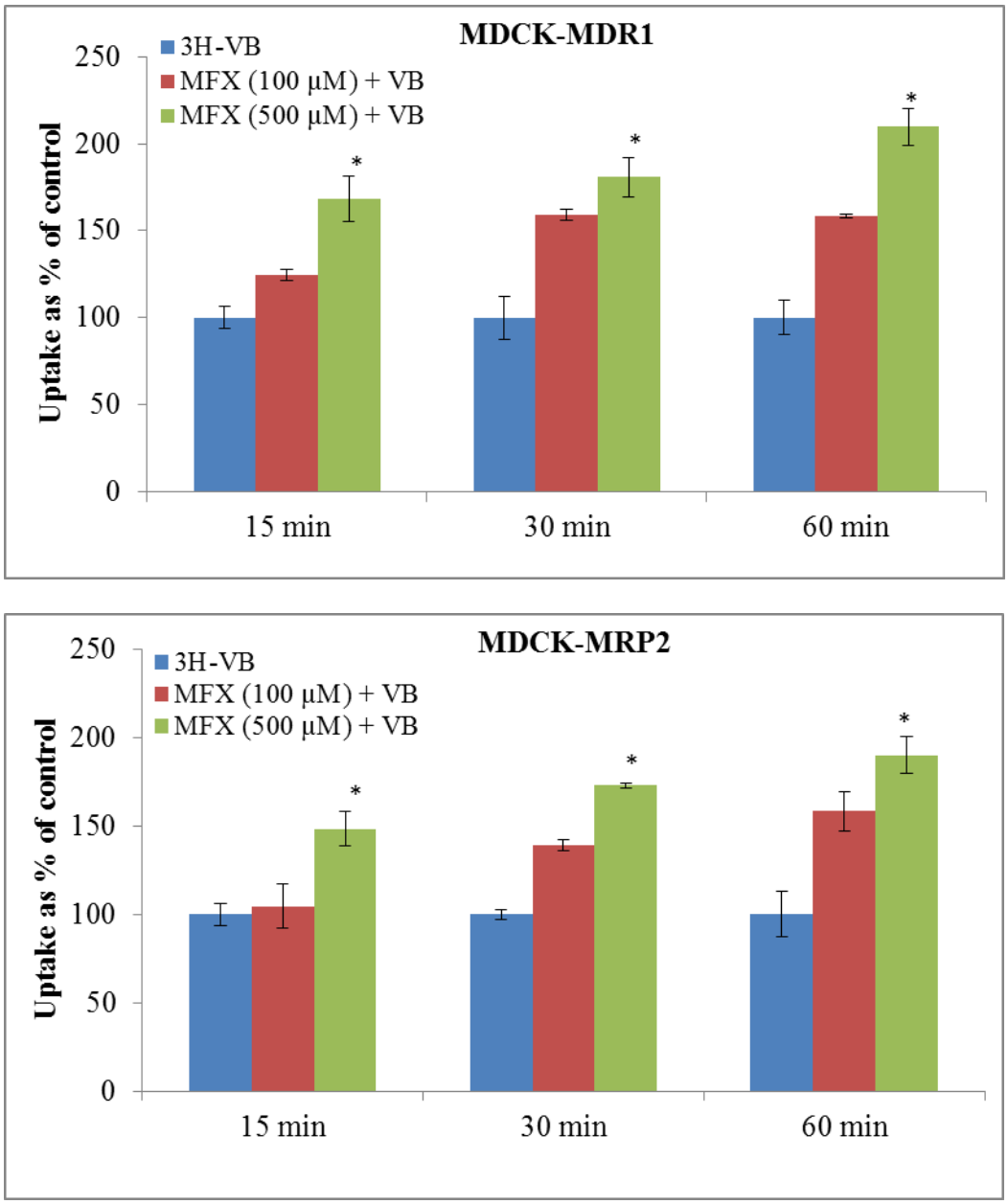

Figure 21. Cellular accumulation of [^{3}H]-vinblastine (VB) alone and in presence of moxifloxacin (MFX) across MDCK-MDR1 and MDCK-MRP2 cells. Values are expressed as mean ± SD (n = 4). *Data were considered statistically significant for $P \leq 0.05$.

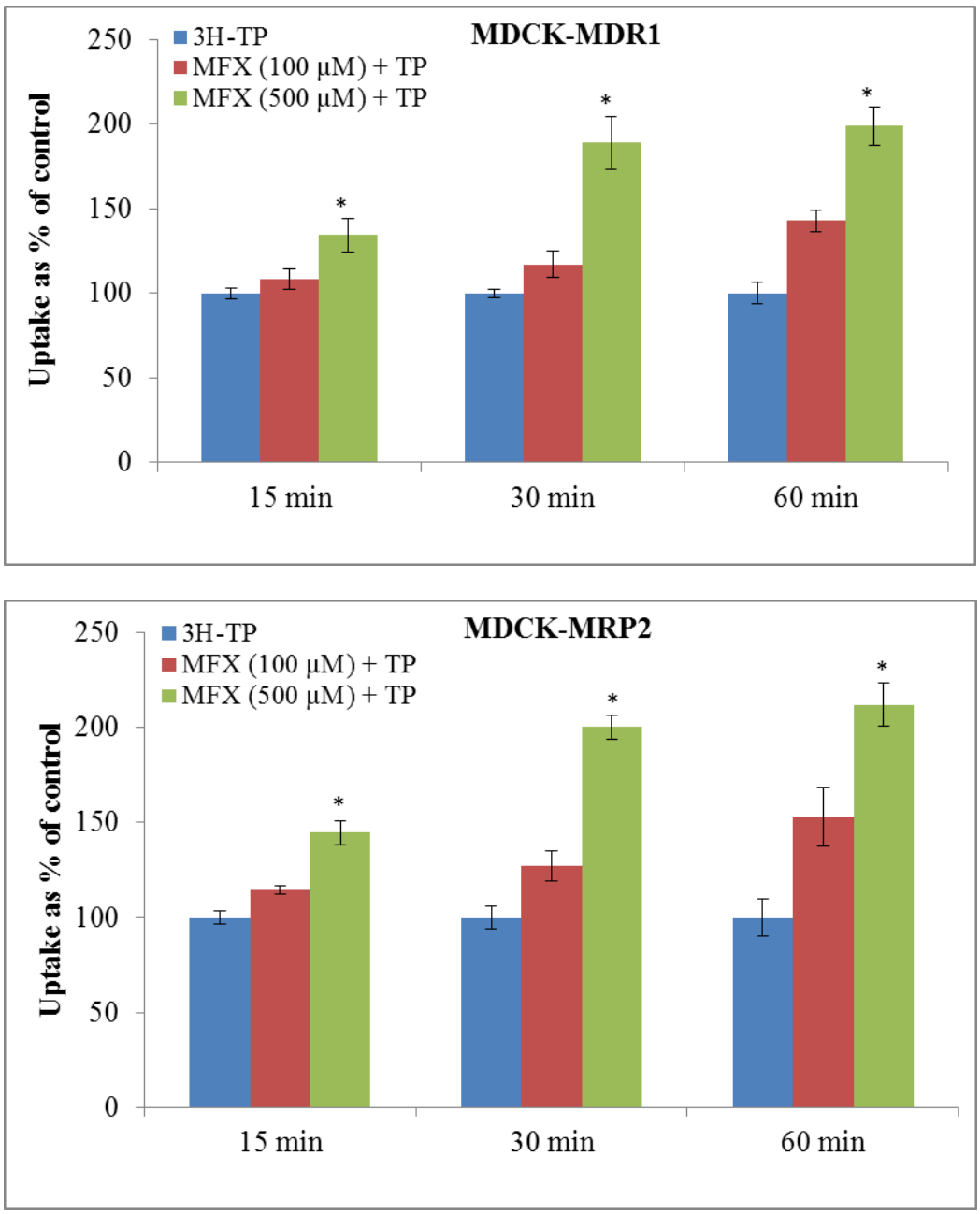

Figure 22. Cellular accumulation of [^{3}H]-topotecan (TP) alone and in presence of moxifloxacin (MFX) across MDCK-MDR1 and MDCK-MRP2 cells. Values are expressed as mean ± SD (n = 4). *Data were considered statistically significant for $P \leq 0.05$.

Table 8. Bi-directional transport of [^{3}H]-etoposide, [^{3}H]-topotecan and [^{3}H]-vinblastine alone and in presence of moxifloxacin (500 µM) and GF120198 (2 µM) across MDCK-MDR1. Values are expressed as mean ± SD (n = 3).

Cell Line	Drug	Permeability ($\times 10^{-6}$) cm/s		Efflux Ratio
		AP-BL	BL-AP	
MDCK-MDR1	Etoposide	3.57 ± 0.65	11.60 ± 1.78	3.25
	Etoposide + Moxifloxacin	7.92 ± 1.78	12.84 ± 2.08	1.62
	Etoposide + GF120918	10.71 ± 0.52	11.02 ± 1.45	1.03
	Vinblastine	1.55 ± 0.03	10.22 ± 0.47	6.59
	Vinblastine + Moxifloxacin	3.95 ± 0.46	8.92 ± 1.91	2.26
	Vinblastine + GF120918	5.35 ± 0.40	7.14 ± 1.47	1.33
	Topotecan	0.75 ± 0.03	3.50 ± 0.28	4.63
	Topotecan + Moxifloxacin	1.56 ± 0.03	3.38 ± 0.16	2.16
	Topotecan + GF120918	2.27 ± 0.18	3.14 ± 0.20	1.38

Table 9. Bi-directional transport of [^{3}H]-etoposide, [^{3}H]-topotecan and [^{3}H]-vinblastine alone and in presence of moxifloxacin (500 µM) and MK571 (50 µM) across MDCK-MRP2. Values are expressed as mean ± SD (n = 3).

Cell Line	Drug	Permeability ($\times 10^{-6}$) cm/s		Efflux Ratio
		AP-BL	BL-AP	
MDCK-MRP2	Etoposide	37.82 ± 2.70	206.76 ± 17.45	5.46
	Etoposide + Moxifloxacin	89.34 ± 1.75	194.29 ± 12.58	2.17
	Etoposide + MK571	175.62 ± 7.47	189.47 ± 20.42	1.08
	Vinblastine	13.50 ± 3.24	73.75 ± 8.16	5.46
	Vinblastine + Moxifloxacin	19.72 ± 2.56	48.90 ± 6.70	2.48
	Vinblastine + MK571	25.60 ± 4.42	35.58 ± 9.72	1.39
	Topotecan	8.06 ± 0.66	24.78 ± 2.44	3.07
	Topotecan + Moxifloxacin	12.67 ± 2.67	22.89 ± 3.54	1.80
	Topotecan + MK571	19.51 ± 1.31	22.08 ± 2.79	1.13

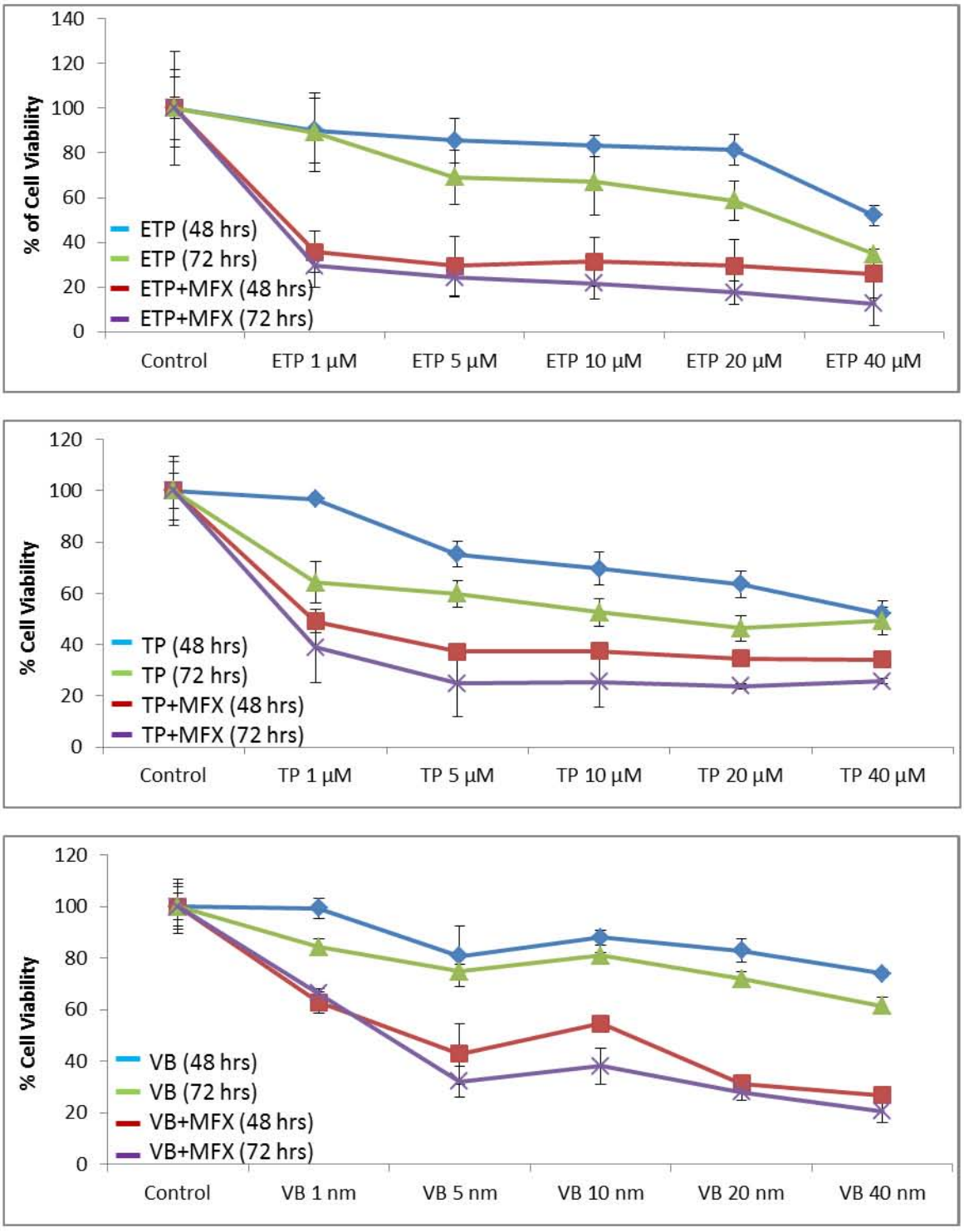

Figure 23. Modulation of anticancer cytotoxicity on Y-79 cells by moxifloxacin (MFX). Values are expressed as mean ± SD (n = 6). Etoposide (ETP); Topotecan (TP); Vinblastine (VB).

Table 10. IC_{50} values of anticancer agents alone and in presence of moxifloxacin.

Drug	IC_{50}
Etoposide	27.07 µM
Etoposide + Moxifloxacin	2.11 µM
Topotecan	27.89 µM
Topotecan + Moxifloxacin	2.89 µM
Vinblastine	51.90 nm
Vinblastine + Moxifloxacin	22.92 nm

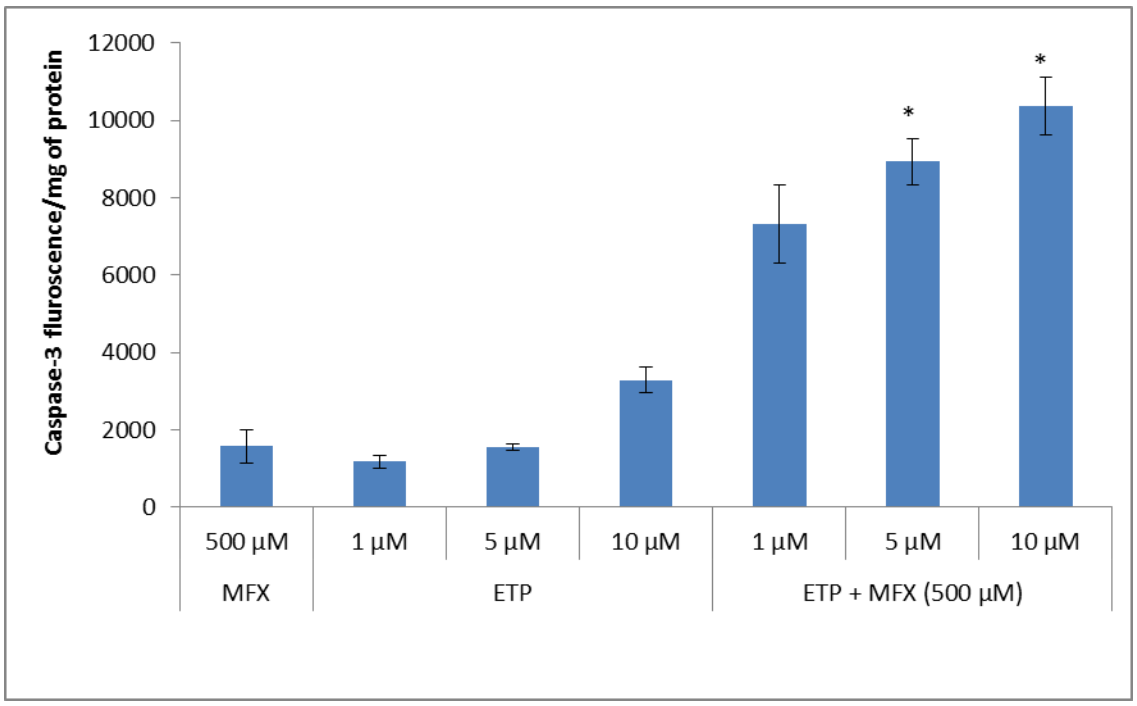

Figure 24. Modulation of etoposide (ETP) mediated caspase-3 activity on Y-79 cells by moxifloxacin (MFX). Values are expressed as mean ± SD (n = 3).

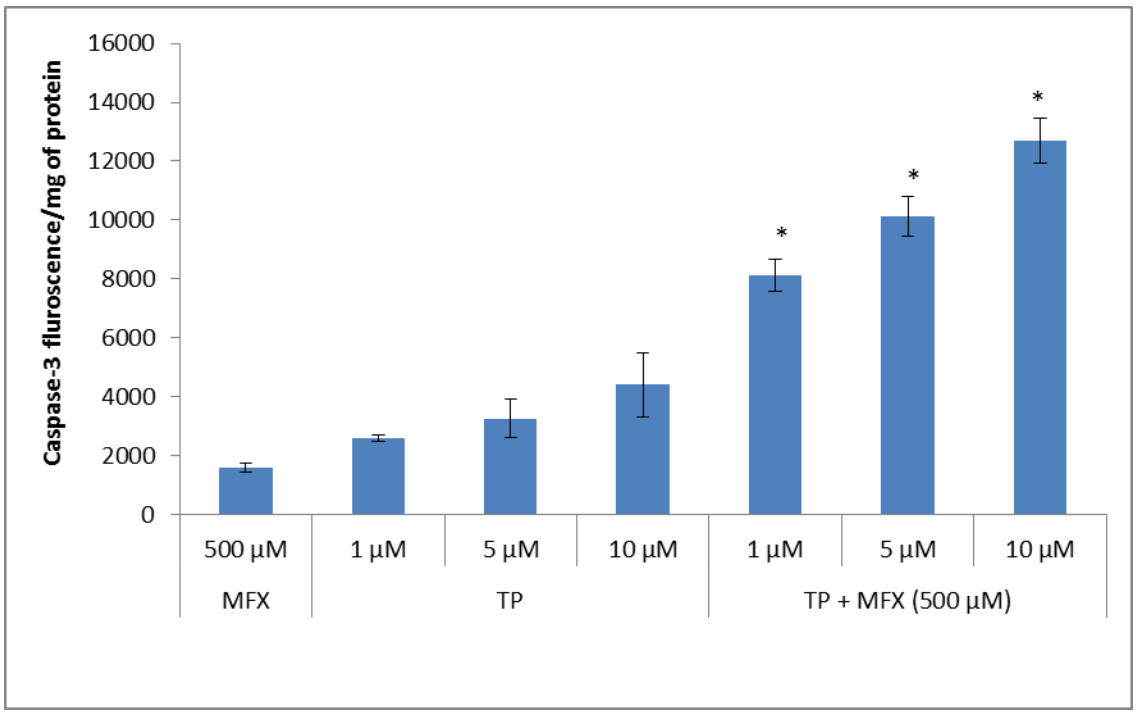

Figure 25. Modulation of topotecan (TP) mediated caspase-3 activity on Y-79 cells by moxifloxacin (MFX). Values are expressed as mean ± SD (n = 3).

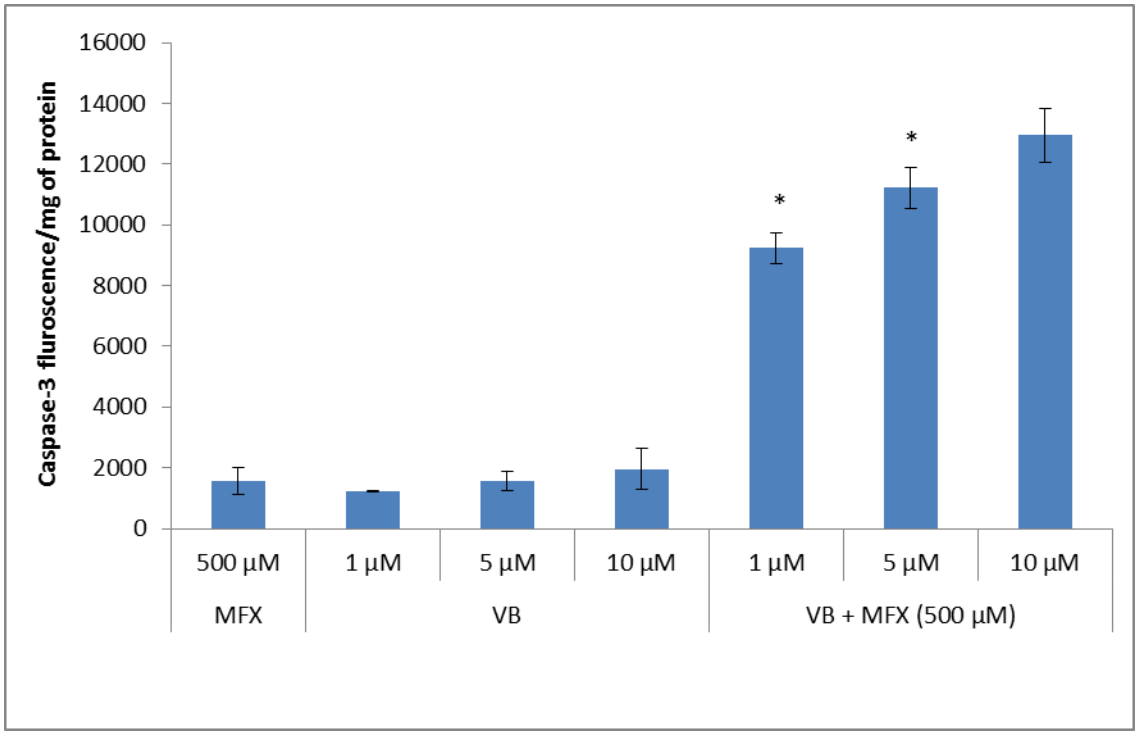

Figure 26. Modulation of vinblastine (VB) mediated caspase-3 activity on Y-79 cells by moxifloxacin (MFX). Values are expressed as mean ± SD (n = 3).

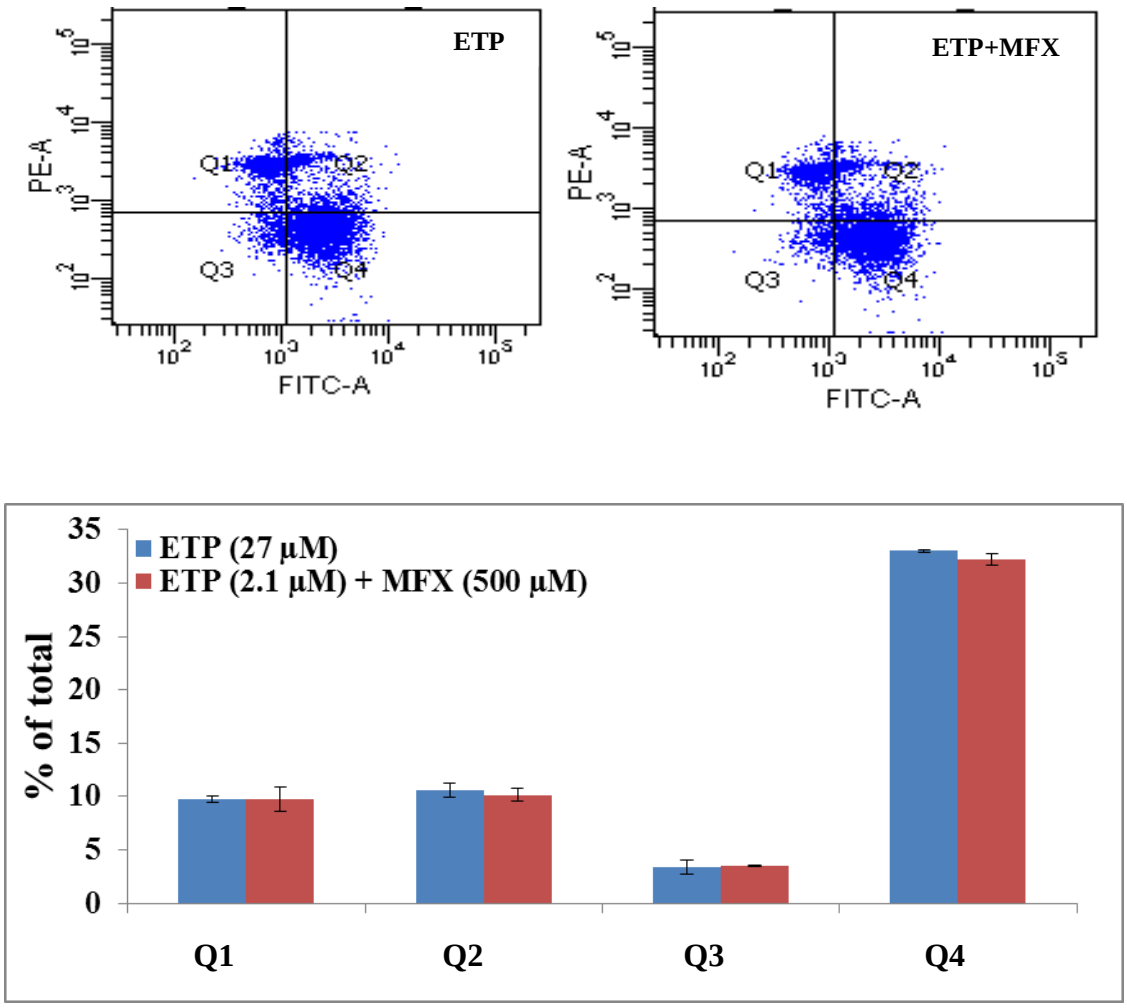

Figure 27. Flow cytometry analysis using Annexin V (AV) and propidium iodide (PI) staining illustrating modulation of etoposide (ETP) mediated Y-79 cell apoptosis by moxifloxacin (MFX). Q1= PI positive cells (AV^-PI^+); Q2 = Late apoptotic (dead) cells (AV^+PI^+); Q3 = Un-stained (non-apoptotic healthy) cells (AV^-PI^-); Q4 = Early apoptotic (but viable) cells (AV^+ PI^-).

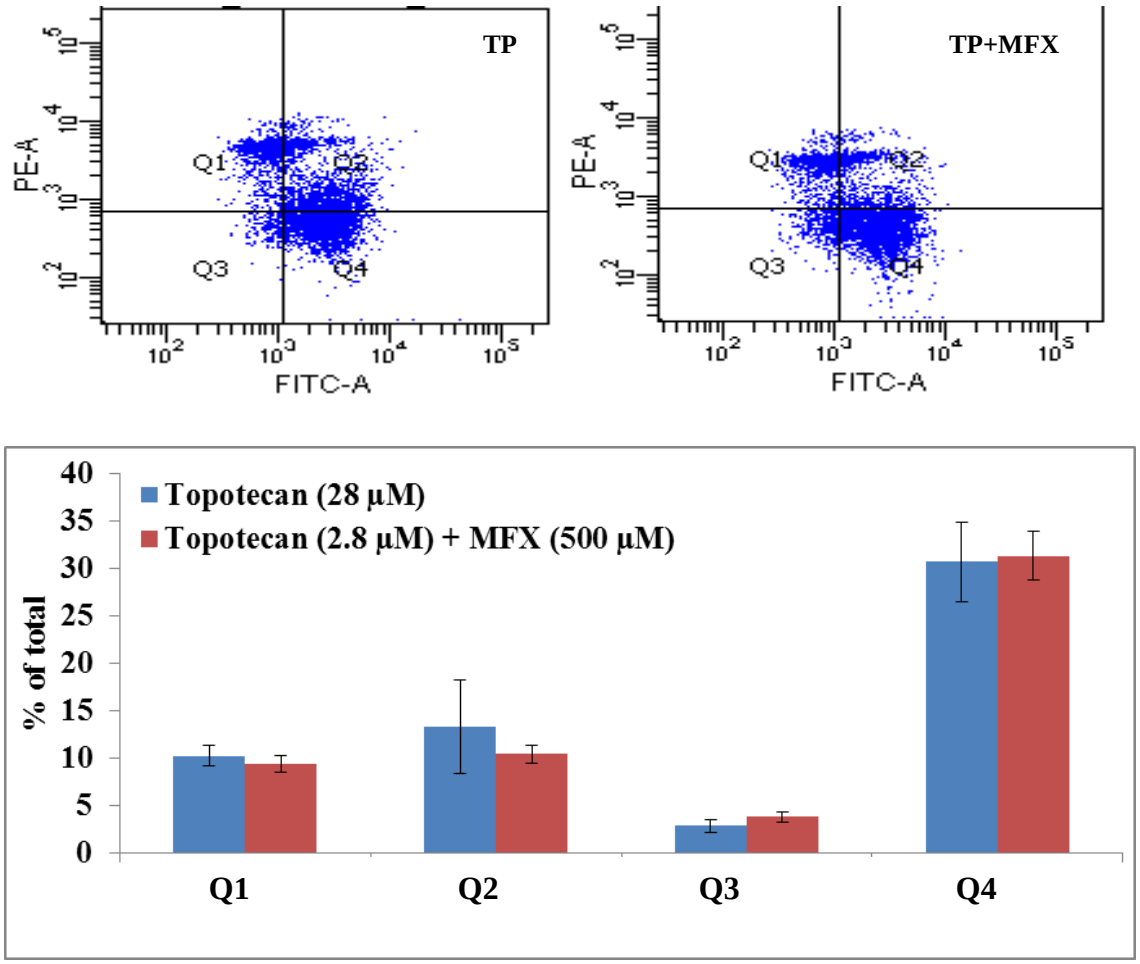

Figure 28. Flow cytometry analysis using Annexin V (AV) and propidium iodide (PI) staining illustrating modulation of topotecan (TP) mediated Y-79 cell apoptosis by moxifloxacin (MFX). Q1= PI positive cells (AV^-PI^+); Q2 = Late apoptotic (dead) cells (AV^+PI^+); Q3 = Un-stained (non-apoptotic healthy) cells (AV^-PI^-); Q4 = Early apoptotic (but viable) cells (AV^+ PI^-).

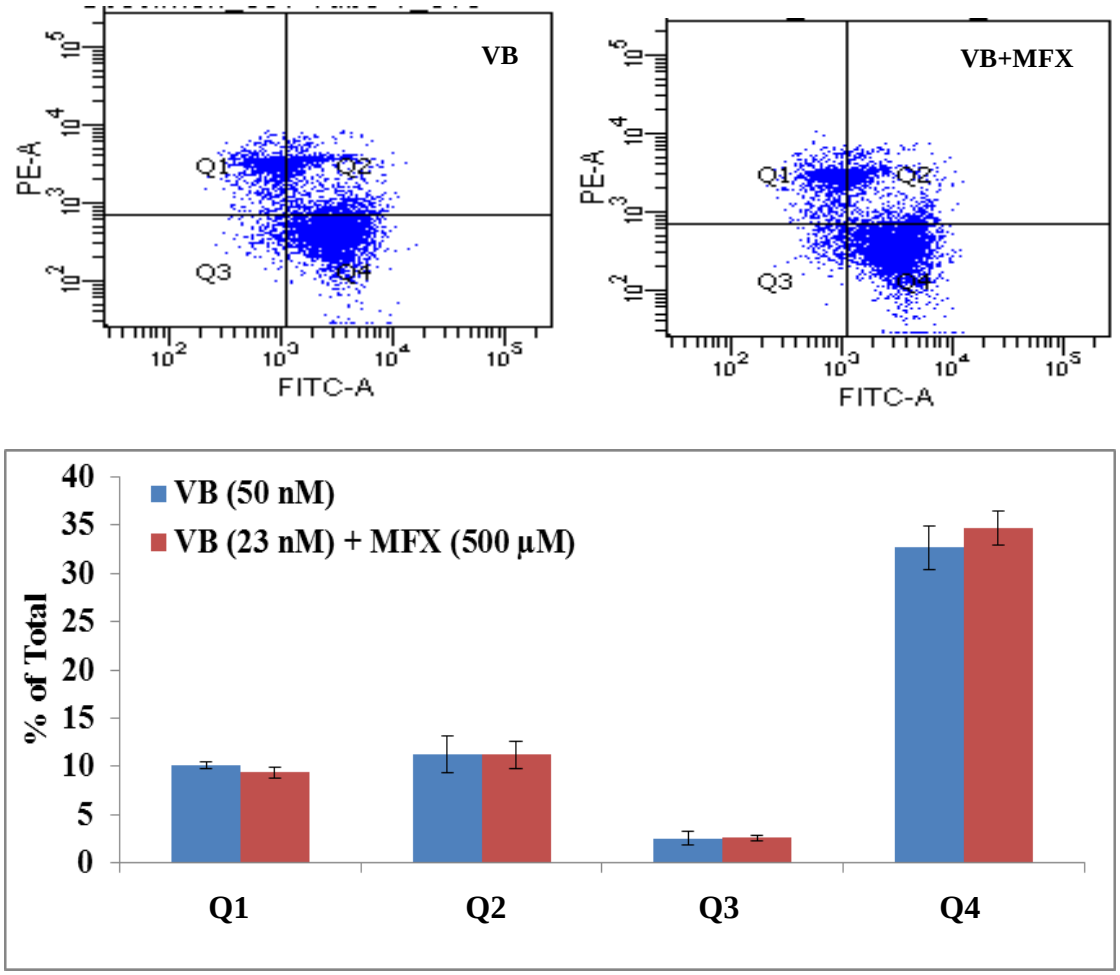

Figure 29. Flow cytometry analysis using Annexin V (AV) and propidium iodide (PI) staining illustrating modulation of vinblastine (VB) mediated Y-79 cell apoptosis by moxifloxacin (MFX). Q1= PI positive cells (AV^-PI^+); Q2 = Late apoptotic (dead) cells (AV^+PI^+); Q3 = Un-stained (non-apoptotic healthy) cells (AV^-PI^-); Q4 = Early apoptotic (but viable) cells (AV^+ PI^-).

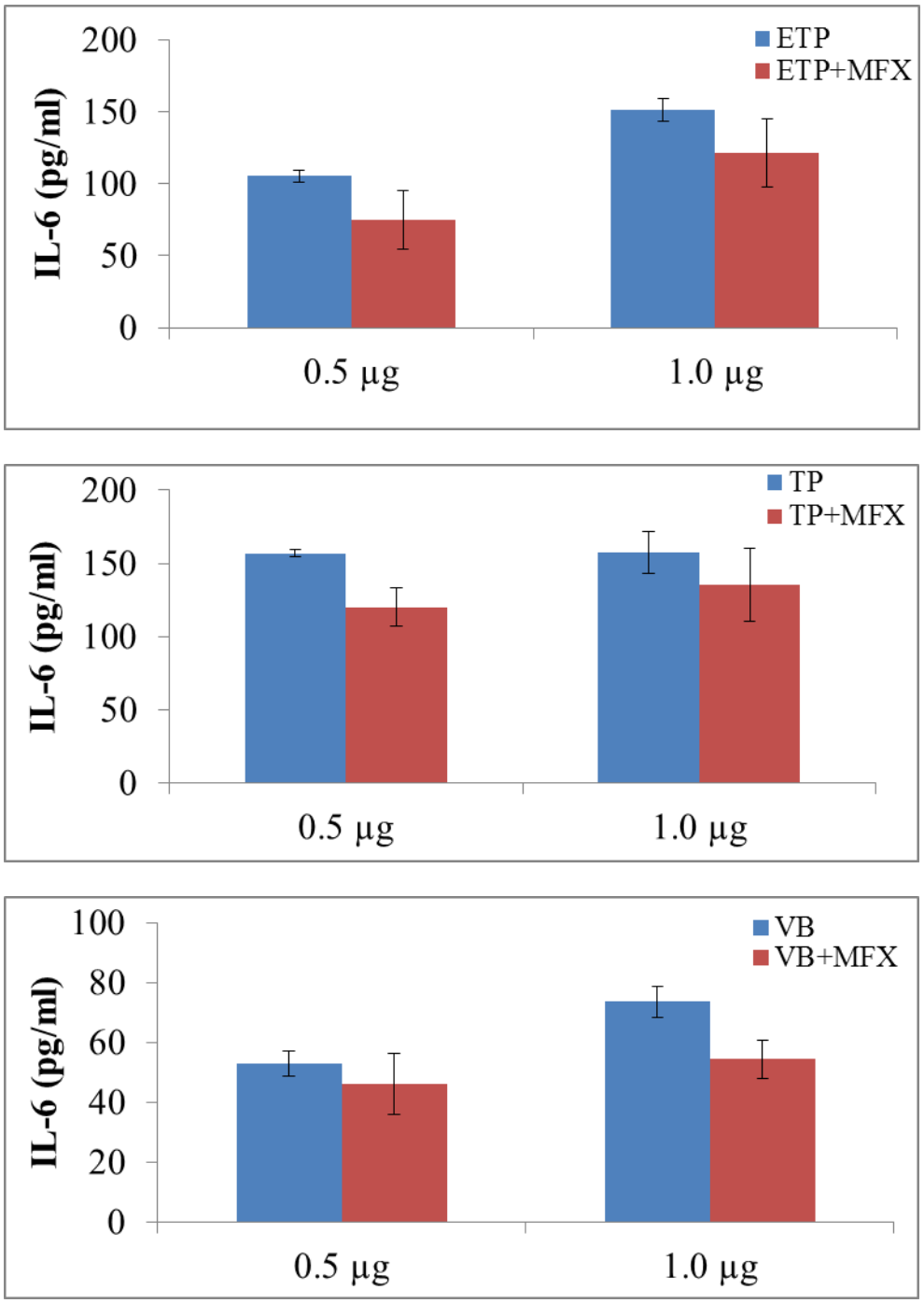

Figure 30. Modulation of anticancer induced IL-6 release by moxifloxacin (MFX) across ARPE19 cells. Values are expressed as mean ± SD (n = 4). Etoposide (ETP); Topotecan (TP); Vinblastine (VB).

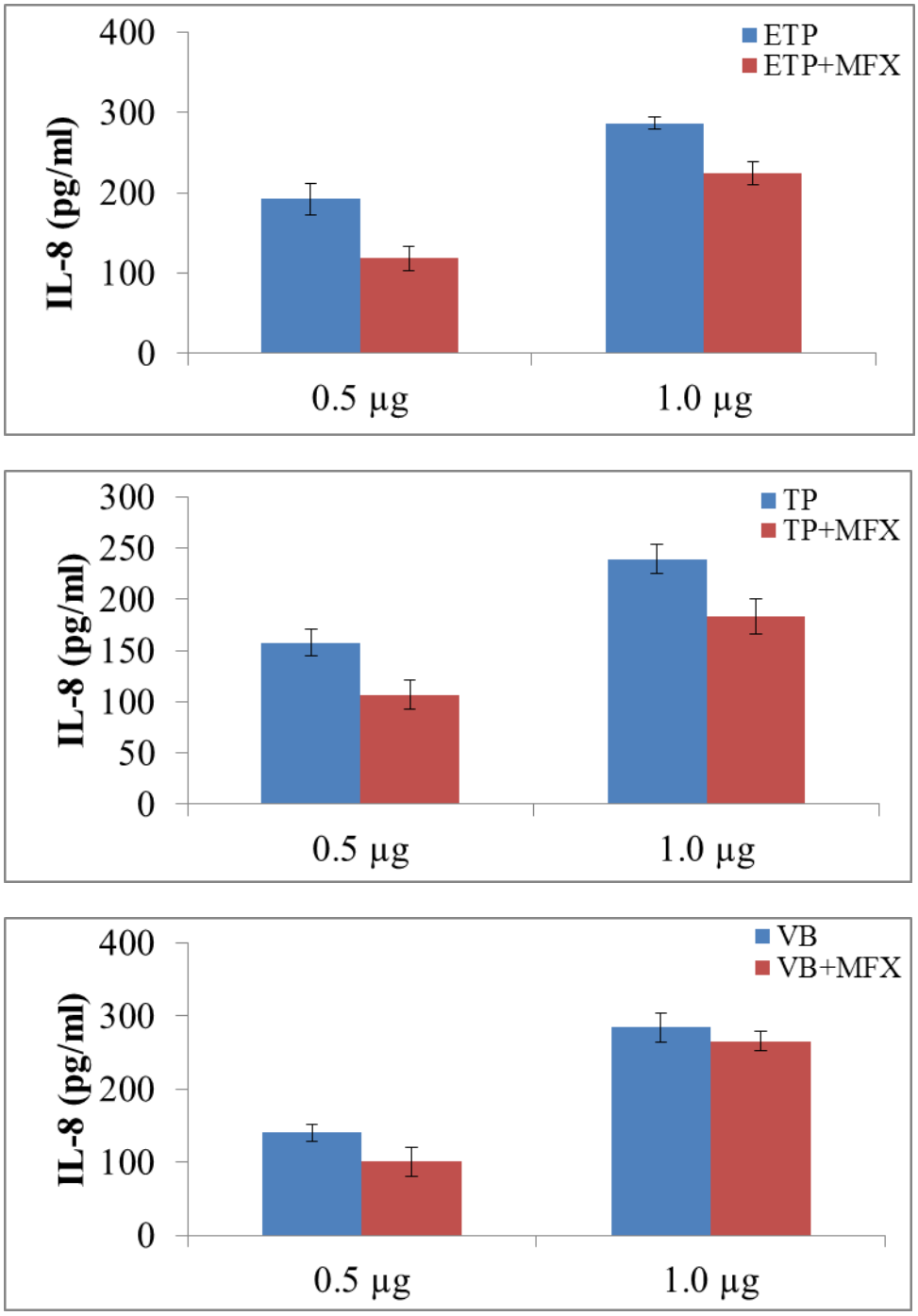

Figure 31. Modulation of anticancer induced IL-8 release by moxifloxacin (MFX) across ARPE19 cells. Values are expressed as mean ± SD (n = 4). Etoposide (ETP); Topotecan (TP); Vinblastine (VB).

5.4 Discussion:

It is evident that co-administration of drugs is a viable strategy to overcome MDR [217]. Therefore, we have tested moxifloxacin potential to overcome efflux based drug resistance to anticancer agents (etoposide, topotecan and vinblastine) that are also substrates of MDR1 and MRP2 and currently used for retinoblastoma therapy. Retinoblastoma is the malignant tumors in the retinal cell layer of the eye. MDR mediated chemo-resistance due to interaction of anticancer agents with efflux proteins (MDR1 and MRP2) over-expressed on retinoblastoma tumors is the major cause of treatment failure [97,98,221]. We hypothesized that moxifloxacin being dual substrate of MDR1 and MRP2 efflux transporters may modulate the intracellular accumulation and permeability of anticancer agents due to competitive inhibition at efflux sites. This strategy might not only result in anticancer efflux modulation or inhibition, but might also result in a synergistic pharmacological effect because antimicrobial moxifloxacin has also displayed anticancer activity in eukaryotic and tumor cells [177-180]. Hence, *in vitro* experiments were carried out to test this strategy by studying cellular accumulation and bi-directional transport of anticancer agents in combination with moxifloxacin. Since, moxifloxacin and anticancer agents are overlapping substrate of MDR1 and MRP2 therefore *in vitro* uptake and transport experiments were simultaneously studied on both MDCK-MDR1 and MDCK-MRP2 cells.

Increased cellular accumulation of etoposide, topotecan and vinblastine in presence of moxifloxacin suggest competitive inhibition of MDR1 and MRP2 mediated anticancer efflux (Fig. 20, 21, 22). Furthermore, moxifloxacin inhibited the anticancer efflux in a dose-dependent and time-dependent manner. Since, the maximum anticancer efflux inhibition was observed at a 500 μM concentration of moxifloxacin (a non-toxic and tolerable dose),

remaining studies were performed using this concentration. Elevation of AP-BL permeability of [^{3}H]-etoposide (2.22 and 2.36 fold), [^{3}H]-topotecan (2.08 and 1.57 fold) and [^{3}H]-vinblastine (2.55 and 1.46 fold) across MDCK-MDR1 (Table 8) and MDCK-MRP2 (Table 9) cells further confirms moxifloxacin mediated inhibition of anticancer efflux. Significant reduction of anticancer efflux ratio by moxifloxacin strongly supports co-administration of overlapping substrates as a viable strategy to overcome MDR. Overall, *in vitro* uptake and bi-directional transport studies suggest that moxifloxacin modulates the intracellular accumulation and permeability of anticancer agents.

Since, moxifloxacin mediated anti-tumor activity was reported in several tumor cells, the cytotoxicity of anticancer agents against retinoblastoma cells (Y-79) was measured alone and in presence of moxifloxacin using the MTT assay. Cytotoxicity was conducted with increasing concentration of anticancer agent (1-40 μM) at two different time points. A significant reduction of % cell viability was observed when anticancer agents and moxifloxacin were used in combination (Fig. 23). This result may be associated with the reported anti-proliferative activity of moxifloxacin [177]. Another possible explanation for moxifloxacin mediated modulation of anticancer cytotoxicity may be due to improved intracellular accumulation and permeability of anticancer agents (as demonstrated in *in vitro* anticancer uptake and transport studies). However, the significant reduction of etoposide (13 fold), topotecan (10 fold) and vinblastine (2 fold) IC_{50} values in the presence of moxifloxacin suggest that moxifloxacin is not only modulating the intracellular anticancer accumulation but is also elevating the cytotoxicity of the chemotherapeutic agents (Table 10). Furthermore, a larger reduction in IC_{50} values for etoposide and topotecan in combination with moxifloxacin support the previous observation that moxifloxacin alone slightly inhibits

human topoisomerase II activity. In contrast, a combination of moxifloxacin with a topoisomerase II inhibitor (etoposide) exhibited significantly high inhibitory effect on topoisomerase II activity [178].

Using flow cytometric analysis, the potency of calculated IC_{50} values of anticancer agents (with or without moxifloxacin) were validated. We observed a similar pattern of apoptotic events at reduced IC_{50} values of anticancer drug in presence of moxifloxacin (Figs. 27, 28, 29). These results showed that moxifloxacin potentiated the apoptotic effect of the anticancer agents and a similar effect can be achieved at reduced anticancer dose. This finding was further supported by measuring caspase-3 levels in Y-79 cells. Caspase-3 is the key enzyme activated during the apoptosis process and is also required for the execution of apoptotic events. The results showed that moxifloxacin alone slightly elevated caspase-3 activity, however it led to significantly high anticancer induced caspase-3 activation in dose-dependent manner (Figs. 24, 25, 26).

We show in the present study that treatment of ARPE-19 cells with anticancer agents induced the release of the proinflammatory cytokines IL-6 (Fig. 30) and IL-8 (Fig. 31). Recent studies have shown that IL-8 is a proangiogenic cytokine regulating tumorigenesis in DLD-1 colon cancer cells [232], and also serves *in vitro* as an autocrine growth factor in human colon carcinoma cells [233]. These effects should be looked at as undesired side effects of the drug. Our results showed that moxifloxacin significantly inhibited the drug induced IL-8 and IL-6 release in ARPE-19 cells. This may suggest that moxifloxacin may also modulate the anticancer mediated release of proinflammatory cytokines.

Overall, the drug interactions study for the treatment of retinoblastoma shows triple benefit in terms of overcoming chemoresistance, enhancing cytotoxic activity and inhibiting

proinflammatory cytokines release. Knowing that moxifloxacin is a clinically approved drug and exhibits tolerability in ocular cells at higher dose levels and cytochrome P450 metabolizing enzyme system is not involved in its metabolism, future implications of above research findings are very promising. There is a need to further explore this finding to confirm its clinical feasibility; if proven, these results will aid in the reduction of chemotherapeutic doses and associated dose-limiting toxicities.

5.5 Conclusion

The strategy of utilizing efflux pump inhibitors (yet not clinically approved) has its limitations, however, ocular cells have shown good tolerability against moxifloxacin, a clinically accepted drug even at higher dose level. Our findings suggest that moxifloxacin may be a valuable new addition to chemotherapeutic strategies, concurrently improving cytotoxic activity while evading MDR mediated chemoresistance of various anticancer agents currently used for retinoblastoma management. These novel drug interactions may ultimately help reduce chemotherapeutic dosing which eventually reduces the probability of dose-limiting toxicity.

CHAPTER 6

MITOCHONDRIAL LOCALIZATION OF TRANSPORTERS

6.1 Overview

Mitochondria are an attractive target for drug-delivery because of their role in cellular energy metabolism, programmed (apoptotic) cell death, and cell signaling. Moreover, mitochondria are a vital intracellular organelle in ocular cell function and survival. This organelle is an attractive target for drug-delivery because of the association between mitochondrial dysfunction and a number of ocular diseases such as age-related macular degeneration, diabetic retinopathy, and glaucoma [234]. Investigations have unveiled mitochondrial genomic instability as one of the contributing factors for age-related ocular pathophysiology. The susceptibility of neural retina and retinal pigment epithelium (RPE) mitochondria to oxidative damage with age appears to be a major factor in retinal degeneration. It thus appears that the mitochondrion is a weak link in the antioxidant defenses of retinal cells. In addition, failure of mtDNA repair pathways can also specifically contribute to the pathogenesis of AMD. Mitochondrial based drug targeting to diminish oxidative stress or promote repair of mtDNA damage may offer potential alternatives for the treatment of various retinal degenerative diseases.

Several reports have indicated localization and the activity of MDR1 efflux protein within the mitochondria. Reports have suggested that an inward onrientation of mitochondrial MDR1 can offer higher drug accumulation inside the organelle and can protect the nucleus by preventing therapeutic drug entry into nuclear targets [235]. However, an outward orientation of mitochondrial MDR1 facilitates therapeutic drug efflux from the organelle and is likely to protect mitochondrial DNA from cytotoxic damage [236].

MDR associated transporter proteins such as P-glycoprotein (MDR1), breast cancer resistance protein (BCRP) and multidrug resistance protein 1 (MRP1) are expressed on the corneal cell membrane to prevent intracellular accumulation of toxins and drugs [237,238]. Nevertheless these proteins could be expressed in subcellular compartments and may actively sequester drugs and traffic them away from their cellular targets.

This part of dissertation deals with functional localization of efflux (MDR1) and influx (PepT-1) transporters on the mitochondria of cultured rabbit primary corneal epithelial cells (rPCECs).

6.2 Statement of the Problem

Since most drug targets are contained within specific intracellular compartments the mitochonrion or the nucleus, the ability of a drug to accumulate these sites is a critical determinant in the observed drug response. The mitochondrion is an attractive target for drug-delivery because of growing support of the association between mitochondrial dysfunction and a number of ocular diseases (glaucoma, diabetic retinopathy, retinoblastoma, and age-related macular degeneration). Thus, substantial effort should be devoted to developing strategies for the targeting of therapeutic molecules to the mitochondria. A range of possibilities exist for the selective drug delivery to the mitochondria including a transporter targeted strategy. Localization of various influx and efflux transporters is generally considered to be restricted to the cell surface level. However, several cellular compartments (mitochondria or nucleus) may also be potential sites for these transporters. Based on the potential role of mitochondrial dysfunction in pathogenesis of various ocular diseases, we hypothesized that various influx and efflux transporters useful in drug targeting may also localize on the surface of mitochondria and can be utilized for the intracellular

delivery of therapeutic molecules across the cornea to enhance drug absorption at subcellular target sites.

6.3 Objectives

The objectives of this project are:

a) to isolate and purify mitochondria from cultured rabbit primary corneal epithelial cells (rPCECs) using cell fractionation and differential centrifugation.

b) to evaluate and confirm the integrity and purity of isolated mitochondria.

c) to study efflux activity of MDR1 by performing *in vitro* uptake of Rhodamine (Rho) 123 on isolated mitochondria in the presence or absence of MDR1 inhibitors (quinidine and cyclosporine A) using fluorimetry and flow cytometry analysis.

d) to study functional activity of peptide transporter by performing *in vitro* uptake of [^{3}H]-Gly-Sar on isolated mitochondria in the presence or absence of a peptide transporter substrate (Val-Val).

e) to confirm MDR1 and peptide transporter localization on mitochondria of rPCECs using western blot and confocal analysis.

CHAPTER 7

MITOCHONDRIAL LOCALIZATION OF P-GLYCOPROTEIN AND PEPTIDE TRANSPORTERS IN CORNEAL EPITHELIAL CELLS – NOVEL STRATEGIES FOR INTRACELLULAR DRUG TARGETING

7.1 Rationale

Multidrug resistance (MDR) is the major complication of cancer chemotherapy. It is a situation in which cancer cells become simultaneously resistant to structurally unrelated drugs with different mechanisms of action [239]. Alterations in common drug targets, increased drug detoxification, drug efflux, DNA repair, and apoptosis defects have all been implicated as MDR mechanisms [239-245]. Besides cancer chemotherapy, MDR also represents a major barrier to the success of ocular drug delivery. Since most drug targets are located within specific intracellular compartments, drug accumulation into these sites is a critical determinant of therapeutic response [246]. Drug resistance phenotypes showing altered intracellular distribution of drugs have been observed in MDR cancer cell lines relative to drug sensitive lines [247,248]. Such intracellular redistribution proceedings may decrease the opportunity for a drug molecule to invade a drug targeting compartment and thus limit its therapeutic effectiveness [246].

MDR associated transporter proteins such as P-glycoprotein (P-gp/MDR1), breast cancer resistance protein (BCRP) and multidrug resistance protein 1 (MRP1) are also expressed at the corneal cell membrane level for reducing intracellular accumulation of toxins and drugs [87,237,238]. Nevertheless these proteins could be expressed in subcellular compartments and may actively sequester drugs and traffic away from their sub-cellular targets [235,246,249-252].

Mitochondria represent a vital intracellular organelle for ocular cell function and survival. It is an attractive target for drug-delivery because there is growing confirmation to support an association between mitochondrial dysfunction and a number of ocular diseases (such as age-related macular degeneration, diabetic retinopathy and glaucoma) [234]. Several reports have indicated the mitochondrial localization and activity of MDR1 efflux protein. Munteanu *et al*. have shown presence and functional activity of mitochondrial MDR1 in MDR resistant human myeloid leukemia cells (K562). These authors have observed a reversed orientation of mitochondrial MDR1 relative to its outward localization on cell surface. This finding suggested that inwardly oriented mitochondrial MDR1 could offer higher drug accumulation inside the organelle and extracellular antibodies cannot affect such accumulations since they cannot reach the mitochondrial binding site. However, a mitochondrial membrane permeable to small molecule inhibitors could reduce intra-organelle drug concentrations. Therefore, inward orientation of mitochondrial MDR1 in MDR cells could protect the nucleus and prevent the therapeutic drug entry in its nuclear targets [235]. Another study reported the functional localization of MDR1 in the mitochondrial membrane of MDR resistant hepatocellular carcinoma (HCC) cells. This finding suggested that mitochondrial membrane localized MDR1 can work like a pump to efflux cytotoxic agents from mitochondria into the cytosol. Therefore, the outward orientation of mitochondrial MDR1 is likely to protect mitochondrial DNA from cytotoxic damage [236]. Furthermore, Ling *et al*. have shown that overexpression and localization of MDR1 on mitochondrial membrane of mitochondrial DNA depleted human hepatoma cells (SK-Hep1) confers resistance to chemotoxic drug-induced apoptosis [253]. Recently, another study has reported mitochondrial localization of MDR1 only on doxorubicin-resistant human breast cancer cells

(MCF-7) but not in the parent cell line [254]. Overall, the above two findings further support the hypothesis that mitochondrial membrane localized MDR1 possess an efflux function and facilitate MDR at the intracellular site by pumping chemotoxic drugs from mitochondria to protect mitochondrial functioning.

Expression of MDR1 efflux and peptide influx transporters have been previously identified by our laboratory on the corneal epithelial cell surface [255,256]. Therefore, the aim of this study was to elucidate the expression, localization, and functional activity of MDR1 efflux and peptide (PepT-1) influx transporters in the mitochondria of cultured rabbit primary corneal epithelial cells (rPCECs). In this study, *in vitro* efflux activity of MDR1 was measured by a model fluorescent MDR1 substrate Rho-123 and two specific inhibitors of MDR1 (quinidine and cyclosporine A, CsA). In addition, two peptide transporter substrates [^{3}H] Glycylsarcosine (Gly-Sar) and Val-Val were selected to examine the *in vitro* function of the PepT-1 transporter. All *in vitro* uptake experiments were performed in isolated mitochondria from rPCECs. Furthermore, localization and protein expression of both the transporters were confirmed by confocal microscopy and western blot analysis.

7.2 Material and Methods

Materials

Cell culture materials including minimum essential medium (MEM), TripLE Express® solution and non-essential amino acids were obtained from Invitrogen (Carlsbad, CA). Fetal bovine serum (FBS) was procured from Atlanta Biological (Lawrenceville, GA). Cell culture flasks (150 cm^2 area) were purchased from Fisher Scientific (Houston, TX). Rho-123, CsA and quinidine were procured from Sigma-Aldrich (St. Louis, MO). [^{3}H]-Gly-Sar (specific radioactivity, 4 Ci/mmol) was obtained from Moravek Biochemicals (Brea, CA, USA).

Cell Culture

rPCECs were cultured according to our published procedure [256]**.** Briefly, cells were grown with culture medium containing MEM, 10% FBS, HEPES, sodium bicarbonate, penicillin, streptomycin sulphate and 1% (v/v) non-essential amino acids, adjusted to pH 7.4. Cells were grown in 150 cm^2 culture flasks and maintained at 37 °C, in a humidified atmosphere of 5% CO_2 and 90% relative humidity. The culture medium was replaced every other day.

Mitochondria Isolation

The isolation of mitochondria from the corneal cells was performed based on the principle of cell fractionation and differential centrifugation [235,257,258]. Briefly, confluent rPCECs grown in 150 cm^2 flask were harvested by trypsinization, washed twice with ice-cold phosphate buffered saline (PBS) and pelletized at 4^0C (1000 × g) for 10 min. The resulting pellet was re-suspended in 500 µL of ice-cold homogenization buffer (0.25 M sucrose, 1 mM EDTA, 10 mM HEPES; pH 7.4) and incubated on ice for 10 min. Following incubation, cells were homogenized with a pre-chilled Dounce homogenizer (40-50 strokes) and cell lysis was ensured using the LDH assay. The resulting homogenate was transferred into 10 mL centrifuge tube and made up to 5 mL volume with homogenization buffer and centrifuged at low speed (1000 × g, 10 min, 4 ^{0}C) to remove nuclei and unlysed cells. The resulting supernatant was again centrifuged at high speed (16,000 × g, 40 min, 4 ^{0}C) in order to remove lysosomal or peroxisomal contamination. The formed pellet (‘‘crude mitochondria’’) was resuspended in homogenization buffer containing 0.25 M sucrose and centrifuged at 16,000 × g for 30 min at 4 ^{0}C. The resulting mitochondrial pellet was re-suspended in

mitochondrial suspension buffer (pH 7.0) containing sucrose (250 mmol/L), tris (10 mmol/L) and protease inhibitors for further studies.

Mitochondrial Membrane Integrity Evaluation by JC-1 Uptake

Mitochondrial membrane integrity was assessed by measuring the potential gradient ($\Delta\psi$) across the membrane using the lipophilic, cationic JC-1 fluorescent dye as per the manufacturer's instructions (Sigma). Generally in healthy cells with high mitochondrial $\Delta\psi$, JC-1 concentrates in the mitochondrial matrix and forms red fluorescent aggregates (J-aggregates). Any incident that disperses the mitochondrial membrane potential also averts accumulation of the JC-1 dye in the mitochondria. As an outcome the dye is dispersed all over the cytoplasm leading to a shift from red (J-aggregates) to green fluorescence (JC-1 monomers) [259]. Valinomycin is an antibiotic agent that permeabilizes the mitochondrial membrane and therefore dissipates the mitochondrial potential gradient. In this experiment, valinomycin (1 µL) was used as a control that prevents JC-1 aggregation. Fluorescence of JC-1 stained mitochondrial aggregates was measured by fluorimeter at 490 nm (excitation) and 590 nm (emission) wavelengths, respectively.

Mitochondrial Preparation for Transmission Electron Microscopy (TEM)

For morphological characterization, 100 µL of mitochondrial suspension was centrifuged at 7000 × g for 10 min. The resulting pellet was fixed with glutaraldehyde (2.5%) in cacodylate buffer, post fixed with osmium tetroxide (2%) and dehydrated in ethanol. The fixed pellet was processed for thin sectioning using routine procedure. Ultrathin sections (0.2 µM) were examined by TEM.

Uptake Experiments on Isolated Mitochondria

In vitro efflux activity of MDR1 was measured on isolated mitochondria with modifications. Briefly, isolated rPCECs mitochondria were washed with Dulbecco's modified phosphate-buffered saline (DPBS) at 37 °C. Rho 123 solution was prepared at a concentration of 5 µM in DPBS and was added to isolated mitochondria (0.5 mg/mL) for incubation in microfuge tube containing 1 mL of DPBS for 30 min at 37 °C for control experiments or with 1 mL solution of appropriate MDR1 inhibitor (quinidine, 75 µM and 100 µM) in DPBS. During incubation period tubes were rotated constantly. At the end of an experiment, samples were centrifuged at 2000 × g for 5 min at 4 ^{o}C. The resulting mitochondrial pellets were washed three times with ice cold stop solution (210 mM KCl, 2 mM HEPES) to arrest mitochondrial uptake. Mitochondria were then solubilized in 1 mL of lysis solution (0.3 M NaOH, 0.1% Triton X-100). The lysates were transferred to a 96-well plate and were assayed using a 96-well fluorescent microplate reader. Rho 123 fluorescence was measured at 485 nm (excitation) and 535 nm (emission) wavelengths, and quantified against a standard curve of Rho-123. The fluorescence of the mitochondrial lysates was corrected for auto-fluorescence of untreated mitochondria. The uptake was normalized to the protein content of mitochondria. Protein content of the mitochondrial samples was measured using BioRad protein estimation kit (BioRad, Hercules, CA). The results were calculated as the total Rho 123 uptake/milligram of protein. Nonspecific binding was deducted from the total uptake values obtained.

For identification of peptide transporter, uptake was initiated by adding 1 mL of solution containing 0.5 µCi/mL [^{3}H]-Gly-Sar in DPBS to isolated mitochondria (0.5 mg/mL) in the presence or absence of competing substrate (Val-Val, 2.5 mM and 5.0 mM). Uptake

was then performed as described previously for Rho-123. For analysis, aliquots of 500 µL was withdrawn from each sample containing lysed mitochondria and transferred to scintillation vials containing 3 mL scintillation cocktail. Samples were then analyzed using Beckman Scintillation Counter (Model LS-6500, Beckman Instruments, Inc.). Uptake was normalized to the protein content of each sample and the amount of protein in the mitochondrial lysate was quantified as described previously.

Efflux Assays for Mitochondrial MDR1 by Flow Cytometry

Mitochondrial fractions, prepared as previously described, were suspended in PBS and kept on ice. A direct functional assay for the MDR1 efflux pump on mitochondrial suspension in PBS was performed using flow cytometry analysis. Whole isolated mitochondria from rPCECs were divided in test tubes to evaluate mitochondrial auto-fluorescence as well as the accumulation of Rho 123 (500 nm) in the presence or absence of CsA (10 µM) after 30 min. Fluorescence measurements of individual samples were performed using flowcytometer (Becton-Dickinson FACScanto II) equipped with an ultraviolet argon laser (excitation at 488 nm, emission at 530/30 band-pass filters). Analysis was gated to include single mitochondria on the basis of forward and side light-scattering and was based on an acquisition of data from total events. Log fluorescence was collected and displayed as a single parameter histograms.

Further, isolated samples of mitochondria were equally divided into test tubes to conduct the uptake of Rho 123 (500 nm) at 37 ^{0}C for 60 min. Following mitochondrial accumulation of Rho 123, samples were centrifuged at 200 × *g* for 5 min. The mitochondrial pellets were re-suspended in PBS (pH 7.4) for 30 min in the presence or absence of CsA (10 µM). Subsequently, the mitochondrial suspensions were centrifuged at 5000 rpm for 5 min

and washed with PBS (pH 7.4). The mitochondrial accumulation of Rho 123 was determined using flow cytometry analysis as described previously.

Western Blot Analysis

Detection and analysis of MDR1 and PepT-1 protein expressions from mitochondrial fractions of rPCECs were performed by immunoblotting. Preparation of mitochondrial protein lysate was performed similar to previously published protocol for whole cell protein lysate [256]. Two concentrations (75 and 100 μg/μL) of mitochondrial protein were suspended in a denaturing buffer (Tris–HCl 10 mM, pH 8 containing 5% glycerol, 2.5% SDS, 5% β-mercaptoethanol and 0.005% bromophenol blue). Proteins from mitochondria were resolved by SDS-PAGE gel electrophoresis at 120 V and electroblotted at 15 V for 90 min onto polyvinylidene fluoride (PVDF) membrane (Immobilon-P, Millipore, IPVH00010). The blot was blocked for 2 h with constant shaking in 2.5 % non-fat dry milk and 0.25 % BSA prepared in TBST (Tris-buffered saline + 0.1% Tween 20, pH 7.4). The resulting membrane was incubated with Mdr-1 goat polyclonal primary antibody (1:300 dilution, Santacruz Biotechnology, Catalog no. SC-1517) overnight at 4 ^{0}C. After five washes (4 min each) in TBST, the membranes were probed with secondary antibody in TBST (1:3000 HRP-conjugated goat anti-rabbit IgG antibody, Santacruz Biotechnology, Catalog No. SC-2030) for 2 h. The blots were finally washed three times (15 min each) with TBST. SuperSignal West Pico Chemiluminescence Substrate (Thermo Scientific, Catalog No. 34077) was used to develop the blot, according to the manufacturer's protocol. Peptide transporter expression was measured by similar method using PepT-1 rabbit polyclonal primary antibody (1:3000 dilution, Santacruz Biotechnology, Catalog no. SC

20653) and HRP-conjugated goat anti-rabbit IgG secondary antibody (1:3000 dilution, Santacruz Biotechnology, Catalog No. SC-2030), respectively.

Confocal Immunofluorescence and Correlation Analysis

rPCECs grown on glass coverslips were incubated for 30 min at 37 ^{0}C with 5 nm of MitoTracker® Red (molecular probe, Invitrogen), a cell-permeable mitochondria-selective dye. The cells were then rinsed with PBS three times and fixed in freshly prepared cold 4% paraformaldehyde in PBS for 30 min at 4 °C. Cells were rinsed with cold PBS four times and incubated with a solution of 1% BSA and 4% non-fat dry milk in PBS for non-specific binding for 2 h at room temperature (RT). Cells were rinsed with PBS again, and incubated with mdr-1 mouse monoclonal and PepT-1 rabbit polyclonal antibodies (Santa Cruz) for MDR1 and PepT-1 (diluted 1:500 as per manufacture's instruction) separately for 2 h at 37 °C. The cells were washed with PBST three times (15 min each) at RT and exposed to Alexa Fluor® 488 goat anti-mouse (for MDR1, 1:50 as per Invitrogen's instruction) and FITC labeled goat anti-rabbit monoclonal IgG (for PepT-1, 1:10,000 as per Sigma's instruction) separately for 1 hour at 37 °C. The cells were washed with PBST four times (15 min each) at RT. Glass coverslips were then placed on the glass slides, and covered with mounting medium. Slides were observed under a confocal laser fluorescence microscope. A sequence of images was acquired in the z-series (0.2 µM) with Olympus FV300 confocal laser scanning unit coupled to an Olympus BX61 upright microscope. Finally, images were processed using ImageJ colocalization Plugin Software (NIH) to determine the Pearson's correlation coefficient (R_r) and overlap coefficient (R).

7.3 Result

Integrity of the Isolated Mitochondria

To confirm the integrity of the isolated mitochondria, we measured the mitochondrial membrane potential with JC-1 dye that can selectively enter into the mitochondria. Relative fluorescence intensity of JC-1 staining in the mitochondrial fractions was assessed by a fluorescence microplate assay. A 30-fold higher accumulation of JC-1 (fluorescent units) into the isolated mitochondria fraction over that obtained with the valinomycin treated control mitochondria has confirmed the presence of mitochondria-enriched fractions (Fig. 32).

TEM Analysis of Isolated Mitochondria

TEM analysis of an isolated mitochondrion from the prepared pellet (Fig. 33) has displayed a pure fraction of the mitochondria. These images have further confirmed the condensed conformation of the isolated mitochondria showing easily visible cristae of the inner membrane along with the preserved outer mitochondrial membrane.

Uptake Experiments

Accumulation of Rho 123 and [^{3}H]-Gly-Sar was individually investigated to explore the possibility of MDR1 efflux pump and PepT-1 influx transporter on the mitochondrial fractions of rPCECs. Rho 123 (5 µM) uptake across isolated mitochondrial fraction of rPCECs was investigated at 30 min in the presence of 75 and 100 µM quinidine (Fig. 34). An increase in Rho 123 uptake was observed after 30 min in the presence of quinidine. Control uptake of Rho 123 in mitochondrial fraction of rPCEC was found to be 72.4 ± 8.4 pmole/mg protein in 30 min. However, uptake was significantly higher (1.4 and 2.1 times, $p < 0.05$) in the presence of 75 and 100 µM quinidine, respectively, thereby suggesting that MDR1 is significantly inhibited by 100 µM quinidine (Fig. 34).

Uptake of [^{3}H]-Gly-Sar in the presence of 2.5 and 5.0 mM Val-Val was also investigated at 30 min across isolated mitochondrial fraction of rPCECs. The dipeptide Val-Val significantly inhibited ($p < 0.05$) the uptake of [^{3}H]-Gly-Sar in a competitive manner (Fig. 35).

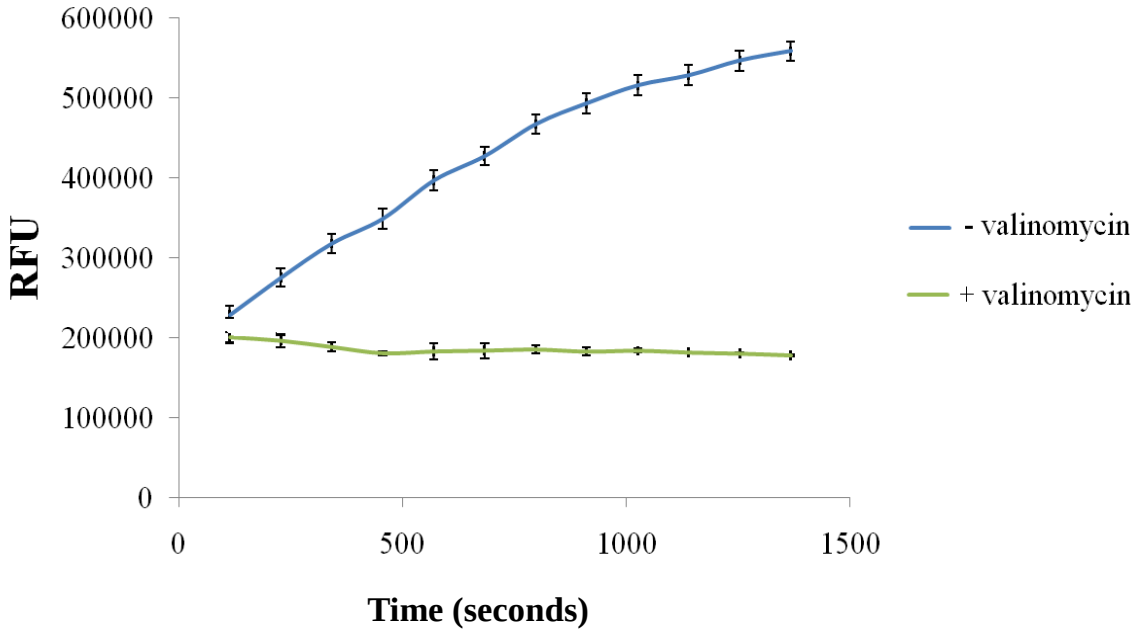

Figure 32. Mitochondria staining using JC-1 stain in a multiwell plate format. Mitochondria were isolated from rPCECs using the cell fractionation method and stained in a multiwell plate using the Isolated Mitochondria Staining Kit® (Sigma). The upper line represents the JC-1 dye uptake of an intact mitochondrial sample. The lower line represents the dye uptake of the valinomycin treated mitochondrial control sample. RFU – Relative Fluorescence units.

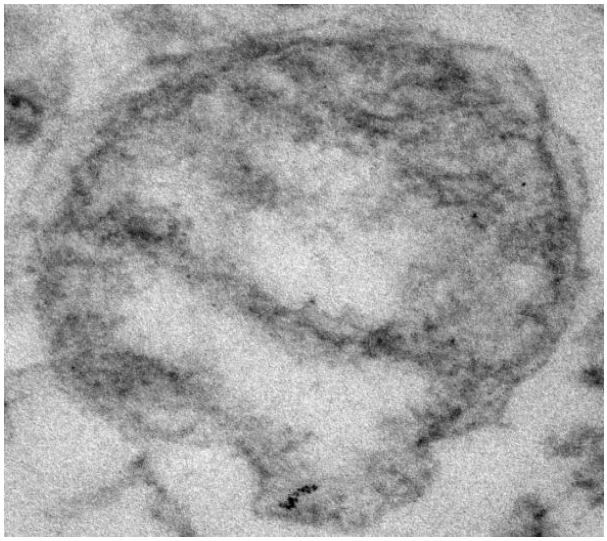

Figure 33. Transmission electron micrograph of a mitochondrion isolated from rPCECs showing visible cristae of the inner membrane along with the preserved outer mitochondrial membrane.

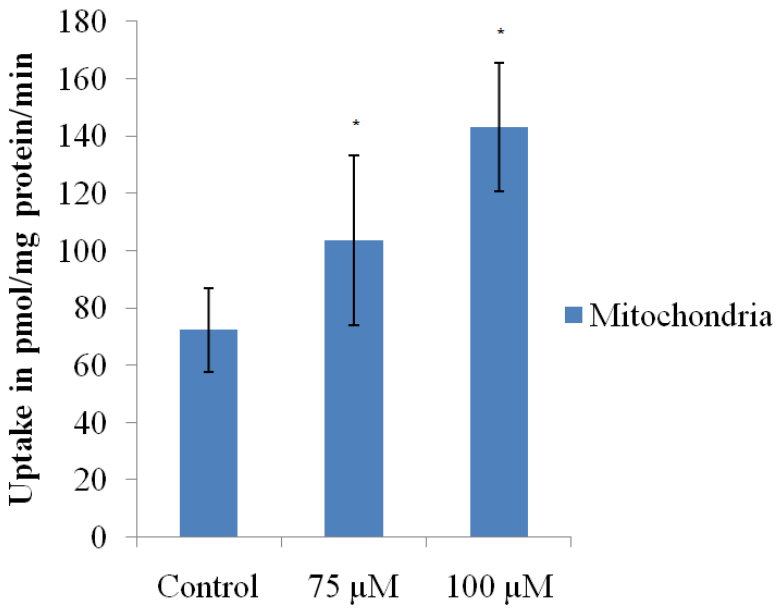

Figure 34. Accumulation of Rho 123 (5 µM) alone and in the presence of quinidine (75 and 100 µM) in the isolated mitochondria fraction from rPCECs. Values are expressed as mean ± SD (n = 3). *Data were considered statistically significant for $P \leq 0.05$.

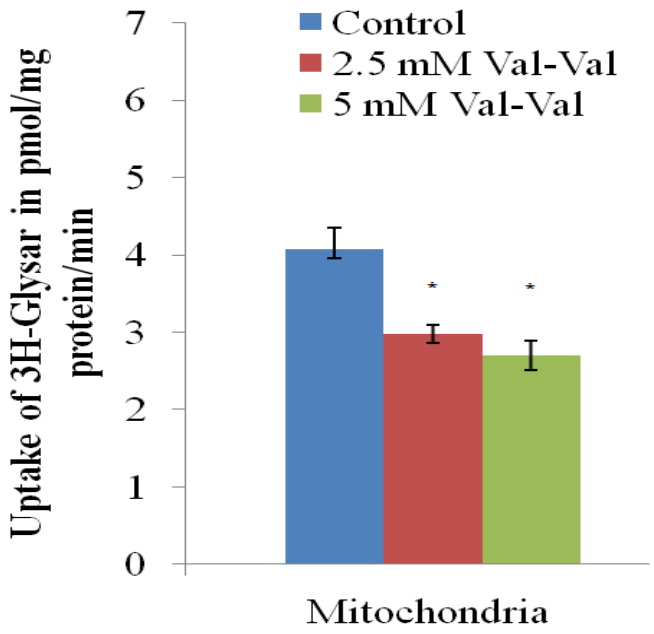

Figure 35. Accumulation of [^{3}H]-Gly-Sar alone and in the presence of Val-Val (2.5 and 5.0 mM) in the isolated mitochondria fraction from rPCECs. Values are expressed as mean ± SD (n = 3). *Data were considered statistically significant for $P \leq 0.05$.

Efflux Assays for Mitochondrial MDR1 by Flow Cytometry

An accumulation and efflux of Rho 123 was evaluated in isolated mitochondria of rPCECs. Flow cytometry observations suggested that Rho 123 accumulation in the isolated mitochondria was higher in the presence of CsA (Fig. 36B) but not in the absence of CsA (Fig. 36C). Figure 36A shows auto-fluorescence of untreated mitochondria. Reduction of Rho 123 fluorescence in CsA untreated mitochondria sample after 30 min (Fig. 36C) was probably due to MDR1 mediated efflux of Rho 123. Above observation has been further confirmed by determining efflux of accumulated Rho 123 upon subsequent treatment with or without CsA (10 μM). The efflux of Rho 123 was significantly reduced ($p \leq 0.05$) only upon subsequent treatment with CsA (Fig. 36E) whereas higher Rho 123 efflux has been observed in the absence of CsA treatment (Fig. 36F). These results strongly suggested the presence of MDR1 on the mitochondrial membrane of rPCECs. Quantitative accumulation of Rho 123 following above experiments has been listed in Table 11 and 12, respectively. Table 11 displays higher accumulation of Rho 123 in the mitochondria of rPCECs in the presence of CsA relative to untreated control samples whereas, Table 12 shows lesser efflux of Rho 123 in the mitochondria subsequently treated with CsA compared to CsA untreated mitochondria.

7.3.5 Western Blot Analysis

To confirm the localization of MDR1 and PepT-1 transporters, fractions of mitochondria isolated from rPCECs were studied to determine MDR1 and PepT-1 protein expression of respective transporters by Western blot analysis (Fig. 37). Results clearly show the expression of MDR1 and PepT-1 transporters on the mitochondrial fraction of rPCECs, as identified by a dark band at 170 kDa (Fig. 37A) and 85 kDa (Fig. 37B), respectively.

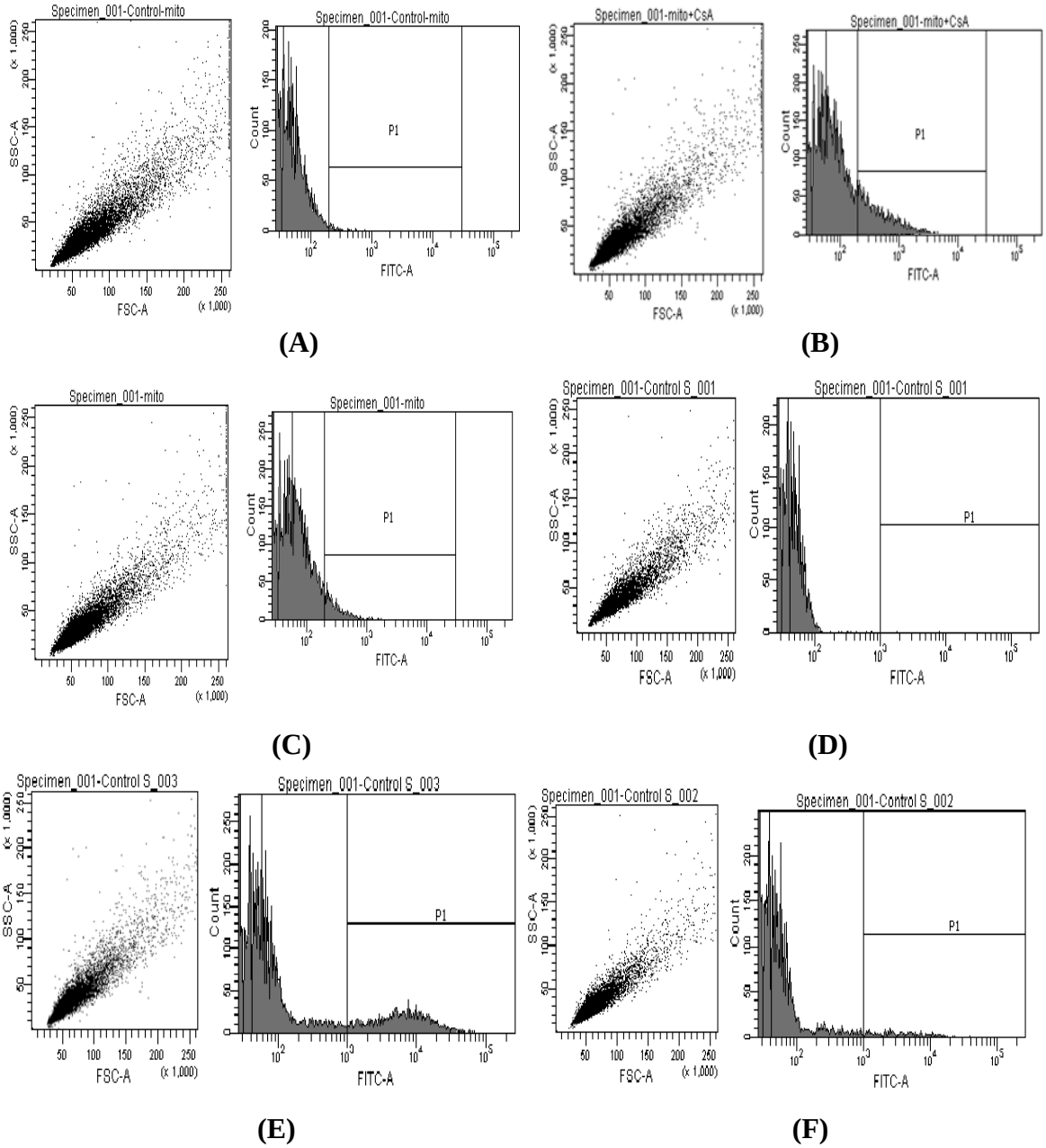

Figure 36. Functional assay for the MDR1 efflux pump on mitochondria by flow cytometry analysis. Untreated control mitochondria (A,D) Rho 123 accumulation in the isolated mitochondria of rPCECs with (B) and without (C) CsA treatment. The remaining amount of Rho 123 following subsequent treatment with (E) or without CsA (F).

Table 11. Functional analysis of MDR1 in mitochondria isolated from rPCECs by flow cytometry. The analyses were performed with isolated mitochondria to evaluate the accumulation of Rho 123 alone and in presence of CsA. Mean fluorescence of Rho 123 (accumulation) was determined by flow cytometry after 30 min and was expressed as percentages of the mean fluorescence of the control mitochondria. The results are reported as a mean ± SD of three independent analyses.

Sample	Rho 123 accumulation (mean fluorescence in percent of control)
(A) Untreated mitochondria	-
(B) Rho 123 alone (control)	100
(C) Rho 123 + CsA (10 µM)	146.9 ± 3.5

Table 12. Functional analysis of MDR1 in mitochondria isolated from rPCECs by flow cytometry. The analyses were performed with isolated mitochondria to evaluate the remaining amount of Rho 123 after subsequent treatment with or without CsA.

Sample	% of Rho 123 remaining
(A) Untreated mitochondrial	0.0
(B) Rho 123 without CsA treatment	2.6
(C) Rho 123 after CsA treatment (10 μM)	14.6

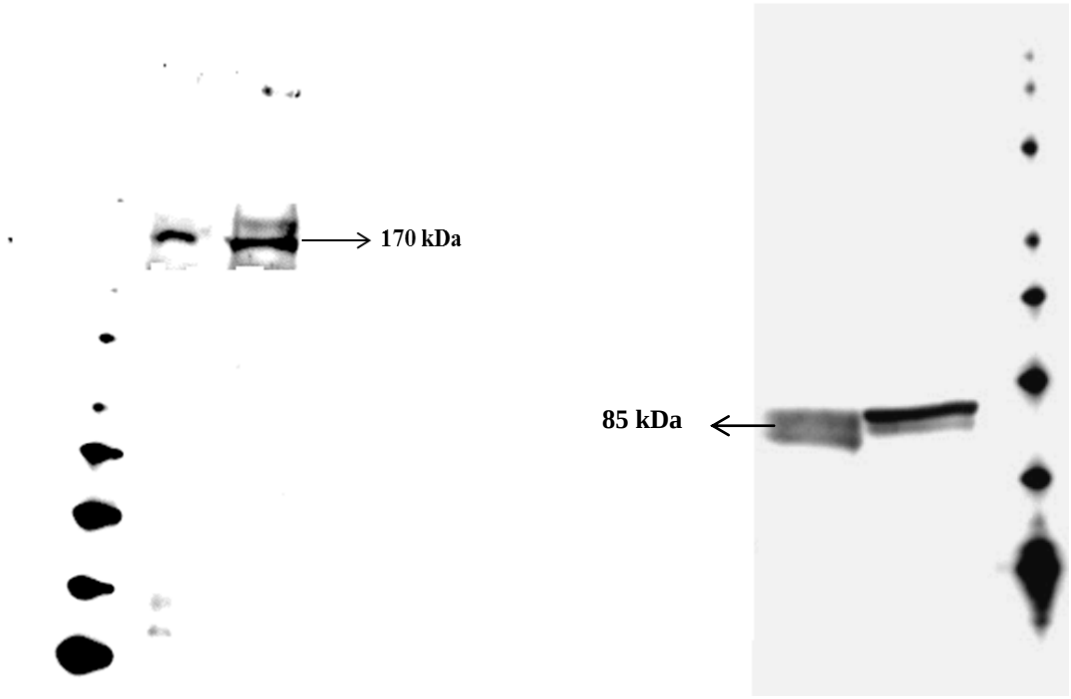

Figure 37. Western blot analysis of MDR1 (A) and PepT-1 (B) expression in the mitochondrial fraction of rPCECs. (A) The proteins were stained with MDR-1 goat polyclonal antibodies. Lanes 1 (left) and 2 (right): 75 and 100 μg/μL mitochondrial protein fractions from rPCECs, respectively. (B) Proteins stained with PepT-1 rabbit polyclonal antibodies. Lanes 1 (left) and 2 (right): 25 and 50 μg/μL mitochondrial protein fractions from rPCECs, respectively.

Confocal Immunofluorescence and Correlation Analysis

To determine the mitochondrial localization of MDR1, rPCECs were stained with mdr-1 mouse monoclonal antibody for MDR1 (Fig. 38A, green fluorescence) and MitoTracker (Fig. 38B, red fluorescence), a specific fluorescent probe for mitochondria, and analyzed by confocal microscopy. As shown in Fig. 38C, the superimposition of the red mitochondria and the green MDR1 labels shows the co-localization between the two signals (yellow).

Expression of PepT-1 was also studied in rPCECs by confocal microscopy with rabbit polyclonal antibody for PepT-1 (Fig. 39A, green fluorescence) and MitoTracker®Red (Fig. 39B, red fluorescence) for mitochondrial staining. Co-localization between PepT-1 and mitochondria is indicated by yellow fluorescence (Fig. 39C). Following confocal analysis, co-localization coefficients (Rr and R) were determined using ImageJ colocalization Plugin Software (NIH) for two independent experiments. Rr and R values greater than 0.5 and 0.6 were considered as a good colocalization, respectively [260]. For MDR1 and mitochondria, the calculated value of mean Rr and R was 0.58 and 0.99, respectively. Whereas, for PepT-1 and mitochondria, the calculated value of mean Rr and R was 0.69 and 0.99, respectively.

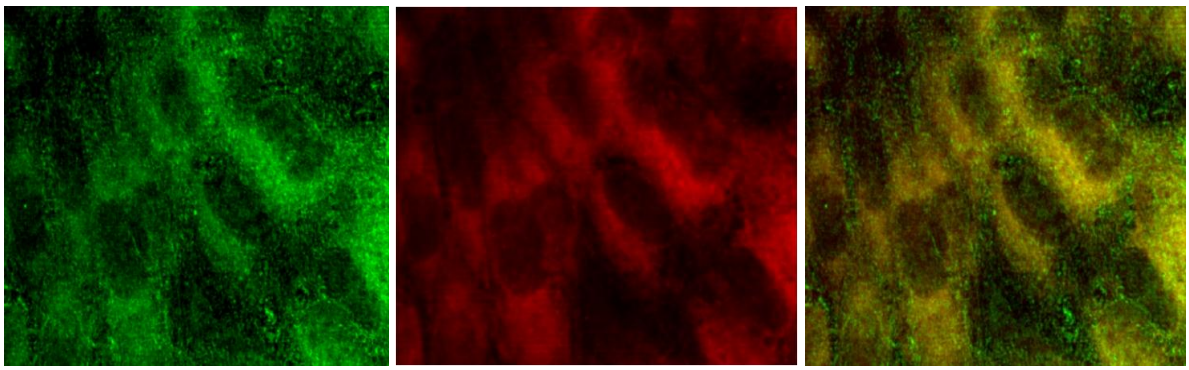

(A) **(B)** **(C)**

Figure 38. Confocal immunofluorescence analysis of mitochondrial localization of MDR1 (A-C). rPCECs cultured on glass coverslips were incubated with 5 nm of MitoTracker® red to label mitochondria (red), fixed and processed for MDR1 protein (green) using mdr-1 mouse monoclonal IgG. (A) MDR1(green); (B) mitochondria (red); (C) image of colocalized points (yellow) between red (mitochondria) and green (MDR1). Fluorescence signals obtained using ImageJ colocalization Plugin Software (NIH). The images are representative of at least three independent experiments with similar results. Mean value of Pearson's correlation coefficient (R_r) = 0.58 and overlap coefficient (R) = 0.99.

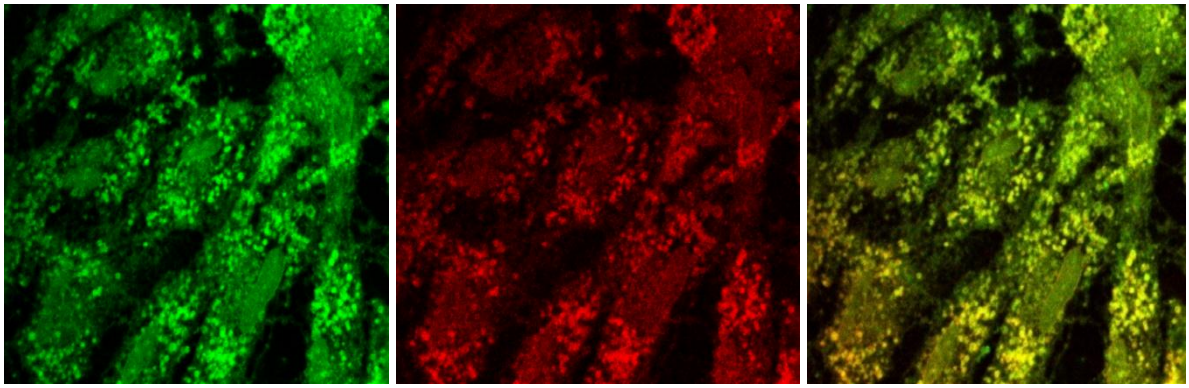

(A) **(B)** **(C)**

Figure 39. Confocal immunofluorescence analysis of mitochondrial localization of PepT-1 (D-F) protein. rPCECs cultured on glass coverslips were incubated with 5 nm of MitoTracker® red to label mitochondria (red), fixed and processed for PepT-1 protein (green) using pepT-1 rabbit polyclonal IgG. (A) PepT-1 (green); (B) mitochondria (red); (C) image of colocalized points (yellow) between red (mitochondria) and green (PepT-1). Fluorescence signals obtained using ImageJ colocalization Plugin Software (NIH). The images are representative of at least three independent experiments with similar results. Mean value of Pearson's correlation coefficient (R_r) = 0.69 and overlap coefficient (R) = 0.99.

7.4 Discussion

The most recognized MDR mechanism correlates well with the expression of an adenosine triphosphate (ATP)–dependent drug efflux pump. This efflux pump is caused by an over-expression of several efflux proteins such as MDR1, MRP, and BCRP. A 170-kDa MDR1, with 1280 amino acids is a member of the ATP-binding cassette (ABC) protein super family and encoded by the MDR gene [239,245,261]. Earlier our laboratory has reported peptide transporter mediated enhanced translocation of various altered compounds were originally substrates of MDR1 [255,256,262,263]. The MDR1 efflux transporter is generally considered to be cell surface localized. However, several intracellular compartments may also be potential site for MDR1 functional activity.

Mitochondria are attractive targets for ocular drug-delivery because of growing confirmation to support an association between mitochondrial dysfunction and a number of ocular diseases [234]. Few studies have demonstrated the mitochondrial localization of MDR1 efflux transporter as a possible reason for intracellular sub-therapeutic drug distribution [235,236,249-252]. A primary objective of this project was to identify functional localization of MDR1 efflux and PepT-1 influx transporters on mitochondrial surface of corneal epithelial cells (rPCECs) by using *in vitro* uptake experiments, flow cytometry, western blot, and confocal microscopy.

Mitochondrial isolation and purification using differential centrifugation principle is a widely used technique and similar to other reports [235,257,258], we have also obtained the high degree of mitochondrial purity and integrity. Using JC-1 staining, we first verified the integrity of isolated mitochondria by fluorescence microplate assay. Higher JC-1 accumulation in the isolated mitochondrial fraction, over that obtained with the valinomycin treated control mitochondria sample, indicated that the isolated fraction was enriched in

intact mitochondria (Fig. 32). In addition, the purity of mitochondria was also confirmed by transmission electron microscopy (TEM). Figure 33 illustrates typical morphology of the mitochondria obtained from the cell fractionation method. TEM images clearly depict the purity and preservation of mitochondrial structure, both of which are important for functional and structural studies.

To investigate mitochondrial MDR1 function, an accumulation and efflux of Rho 123 was evaluated in isolated mitochondria of rPCECs in presence or absence of two different MDR1 inhibitors (quinidine and CsA). Rho 123 is a widely used mitochondrial fluorescent probe and has display strong analogy with anticancer agents. Rho 123 accumulation was significantly enhanced in the presence of different concentrations of quinidine in the isolated mitochondria compared to control mitochondria sample (Fig. 34). Reduced fluorescence of Rho 123 in control mitochondria was probably due to MDR1-mediated Rho 123 efflux. Quinidine mediated increased Rho 123 accumulation provides strong evidence that MDR1 is expressed and functionally active in mitochondria of rPCEC. Efflux activity of MDR1 on isolated mitochondria was further confirmed using another MDR1 inhibitor (CsA) by flow cytometry. When Rho 123 (500 nm) diffuses into the mitochondria, MDR1 actively pumps out Rho-123, and thereby showing lower fluorescence intensity (Fig. 36B). However, simultaneous treatment with CsA (10 μM) enhances accumulation of Rho 123 in the isolated mitochondria, resulting in higher fluorescence intensity (Fig. 36C, Table 11). In order to further confirm the functional activity of MDR1 on mitochondria, isolated samples of mitochondria were first subjected to Rho 123 for 60 min to allow maximum accumulation of Rho 123 followed by subsequent treatment with or without CsA for 30 min to determine the quantitative efflux of Rho 123 in response to MDR1 inhibitor (CsA). Significant reduction of

Rho 123 efflux in response to CsA confirms the functional activity of MDR1 on mitochondria of rPCECs (Fig. 36E, Table 12). Above results were found in complete agreement with the other report where reduced Rho 123 accumulation was observed in isolated mitochondria of MDR-positive cells [236].

Functional localization of PepT-1 transporter on mitochondria was also evaluated by performing radioactive uptake of [^{3}H]-Gly-Sar in the presence of two different (2.5 and 5 mM) concentration of dipeptide substrate Val-Val. Significant inhibition of [^{3}H]-Gly-Sar uptake in the presence of competing dipeptide substrate provides strong evidence of functional localization of PepT-1 transporter on mitochondria of rPCECs (Fig. 35). Similar results showing peptide transporter mediated uptake of [^{3}H]-Gly-Sar has already been observed in report showing characterization of peptide transporter across MDCKII-MDR1 cells [264].

Western blot was performed to confirm the expression of MDR1 and PepT-1 in mitochondria of rPCECs. MDR1 and PepT-1 bands detected approximately at 170 (Fig. 37A) and 85 kDa (Fig. 37B), respectively clearly confirm the presence of both efflux and influx transporter in mitochondria of rPCECs. Dey *et al.* previously reported the expression of MDR1 in human and rabbit cornea and corneal epithelial cell membrane and detected MDR1 with a molecular weight of approximately 170 kDa [256]. Moreover, PepT-1 expression with a molecular weight of approximately 80 kDa has been reported in small intestine confirming PepT1-mediated epithelial transport of dipeptides and cephalexin [265].

Dual fluorescence study allowed a positive approach of MDR1 and PepT-1 localization on mitochondria of rPCECs. Simultaneous labeling of MDR1/PepT-1 and mitochondria provided the green fluorescence signal corresponding to MDR1/PepT-1 (Fig.

38A and 39A), red fluorescence signal corresponding to mitochondria (Fig. 38B and 39B) and yellow fluorescence signal corresponding to mitochondrial co-expression of MDR1/PepT-1 (Figs. 38C and 39C), confirming the co-localization observation of other reports [235,236]. Co-localization coefficients (R_r and R) were used to estimate the level of co-localization between MDR1/Pept-1 and mitochondria marker MitoTracker® red. These coefficients represent the statistical relationship between fluorescence intensities. For MDR1 and PepT-1 transporters, higher values of $R_r > 0.5$ (0.58 and 0.69) and $R > 0.6$ (0.99 and 0.99) have confirmed the strong co-localization of these transporters on mitochondria of rPCECs.

Due to its critical functioning, mitochondrial dysfunction is associated with a number of cancerous as well as ocular diseases. Therefore, functional localization of MDR1 in mitochondria can play a crucial role in intracellular drug trafficking and intrinsic drug resistance [235,236,251,253,254]. MDR modulators blocking MDR1 function have been widely utilized presumably to evade cell membrane based efflux mechanisms. However, there is a need to explore alternative strategies which can also address MDR1 mediated intracellular drug sequestration and resistance. It has been shown that MDR1 expression inhibits cytochrome c release from mitochondria into cytosol following apoptotic stimuli, which otherwise is an important step to initiate cell apoptosis. This process ultimately hampers the anticancer drug induced apoptosis. It has been hypothesized that inhibition or cleavage of MDR1 can facilitates the cytochrome c release from mitochondria by sensitizing drug resistant cells for anticancer agents [236,266]. Moreover, several reports have shown that prodrug derivatization of therapeutic drugs that are MDR1 substrates can evade MDR1 mediated drug efflux [255,262]. Therefore, identification and utilization of influx

transporters such as Pept-1 on the mitochondria can be utilized as a promising strategy to evade mitochondrial MDR1 mediated drug efflux event.

Intracellular drug targeting is a potential area of research and therefore, continued research in the area of cell organelles (nucleus, mitochondria, golgi apparatus etc.) based transporter localization will undoubtedly provide a greater understanding of how these transporters can contribute to the intracellular drug trafficking and intrinsic drug resistance. Furthermore, it would be exciting to explore any possible differential expression of organelles localized transporters in diseased versus non-diseased state so that it can be utilize to develop intracellular drug targeting strategies.

7.5 Conclusion

This report provides evidence that MDR1 and PepT-1 are functionally expressed in the mitochondria of rPCECs. Mitochondrial dysfunctioning is associated with ocular diseases and have been considered as a potential target for drug delivery. According to the most probable hypothesis, MDR1 may be involved in protecting mitochondria by effluxing therapeutic drug molecules out from the intra-mitochondrial target site. This effect would lead to less opportunity for ocular drug molecules to enter into a desired mitochondrial site and thereby limit their therapeutic effect. In contrast, localization of peptide transporter on the mitochondria could be utilized for the evasion of mitochondrial localized MDR1 mediated drug efflux event. This process may result in higher drug accumulation at the mitochondrial target site to produce optimal therapeutic effects against targeted ocular diseases.

CHAPTER 8

SUMMARY AND RECOMMENDATIONS

8.1. Summary

Chemoresistance is the major cause of treatment failure in majority of cancer. Several strategies have been attempted to overcome MDR mediated chemoresistance. We have hypothesized and employed co-administration strategy using overlapping substrate of MDR1 and MRP2 efflux transporters to overcome challenges of chemotherapy. Three anticancer agents (topotecan, etoposide and vinblastine) have been tested for interaction studies with moxifloxacin for retinoblastoma. Retinoblastoma is the malignant tumors overexpressing multiple efflux proteins (MDR1 and MRP2) in the retinal cell layer of the eye.

In this study we show overlapping substrate specificity of moxifloxacin for MDR1 and MRP2 efflux transporters, which may endure a synergistic efflux action and develop resistance by lowering intracellular drug concentration and permeability. Furthermore, co-administration of moxifloxacin with therapeutic substrate of these efflux transporters (topotecan, etoposide and vinblastine) have been hypothesized and employed. Strategy of utilizing efflux pump inhibitors has its own limitations. Whereas, ocular cells have shown good tolerability against moxifloxacin, even at higher dose level. Overall, the drug interactions study attempted for the treatment of retinoblastoma shows a triple benefit in terms of overcoming chemoresistance, enhancing cytotoxic activity and inhibiting proinflammatory cytokines release. Knowing the fact that moxifloxacin is a clinically approved drug and cytochrome P450 metabolizing enzyme system is not involved in its metabolism, future implications of above research findings are very promising. If proven

clinically, our findings suggest that moxifloxacin may be a valuable new addition to chemotherapeutic armamentarium which may aid to reduce the chemotherapeutic dose and associated dose-limiting toxicities. Furthermore, we have also demonstrated moxifloxacin interaction with monocarbxylate influx transporter. Since, moxifloxacin is clinically delivered intravitreally for treating postoperative bacterial endophthalmitis, information about such interactions will be crucial in clinical settings and can further be explored to improve vitreous half-life and therapeutic efficacy of moxifloxacin.

Mitochondrion is an attractive target for drug-delivery because there is a growing confirmation to support an association between mitochondrial dysfunctions and a number of ocular diseases. We have provided direct evidence of peptide influx and MDR1 efflux transporter on mitochondria of corneal epithelial cells. Based on our finding, we hypothesized that functional localization of MDR1 may protect the mitochondria by effluxing therapeutics out from the intramitochondrial site. On the contrary, peptide transporter localization on mitochondria can be utilized for the evasion MDR1 mediated drug efflux event.

8.2. Recommendations

Based on results of this dissertation following recommendations can be made to further continue this work.

Though second (ciprofloxacin, ofloxacin) and third (levofloxacin) generation fluoroquinolones were known to be substrate of monocarboxylate influx transporter, study of moxifloxacin (fourth generation fluoroquinolone) interaction with monocarboxylate transporter was attempted for the first time. Further studies must be attempted for other

fourth generation fluoroquinolones (such as gatifloxacin and gemifloxacin) to uncover if it is common trend all over the generation.

In this dissertation, interaction of overlapping efflux transporter (MDR1 and MRP2) substrate was studied between moxifloxacin and three anticancer agents (topotecan, etoposide and vinblastine) for retinoblastoma management. Similar interaction studies should be undertaken using moxifloxacin and other anticancer agents which are also overlapping substrates of MDR1 and MRP2 (such as doxorubicin, paclitaxel, vincristine, methotrexate etc.), in order to identify weather moxifloxacin mediate modulation of anticancer cytotoxicity and chemoresistance is generalized phenomenon. Since MDR mediated chemoresistance is common phenomena in cancer therefore, moxifloxacin interaction with anticancer agents should be also undertaken for other cancers (such as breast cancer, ovarian cancer, lung cancer etc.) to determine moxifloxacin potential for treating multiple cancers.

Functional localization of influx and efflux transporters on cell membrane is commonly studied for various tissues and has been widely utilized for drug targeting. In this dissertation, mitochondrial localization of peptide influx and MDR1 efflux transporter was studied on corneal cells. Future studies must be attempted to determine mitochondrial localization of other influx (folate, biotin, riboflavin etc.) and efflux (breast cancer resistance protein) transporters. Since, intracellular drug targeting is a potential area of research therefore, similar studies should be also conducted on other cell organelles (such as nucleus, golgi apparatus etc.) to understand how these transporters can contribute to the intracellular drug trafficking and intrinsic drug resistance. Furthermore, it would be interesting to explore any possible differential expression of organelles localized transporters in diseased versus non-diseased state so that strategies should be developed for intracellular drug targeting.

Order Completed

Thank you very much for your order.

This is a License Agreement between Megha Barot ("You") and Informa Healthcare ("Informa Healthcare"). The license consists of your order details, the terms and conditions provided by Informa Healthcare, and the payment terms and conditions.

License number	Reference confirmation email for license number
License date	Oct 10, 2012
Licensed content publisher	Informa Healthcare
Licensed content publication	CURRENT EYE RESEARCH
Licensed content title	Mitochondrial Dysfunction in Retinal Diseases
Licensed content author	Megha Barot, Mitan R. Gokulgandhi, Ashim K. Mitra
Licensed content date	Dec 1, 2011
Type of Use	Dissertation/Thesis
Volume number	36
Issue number	12
Start page	1069
End page	1077
Requestor type	Author of this article
Format	print and electronic
Portion	Full article
Will you be translating?	no

References:

1 Barar J, Javadzadeh AR, Omidi Y. Ocular novel drug delivery: Impacts of membranes and barriers. Expert Opin Drug Deliv 2008;5:567-581.
2 Kim SH, Lutz RJ, Wang NS, Robinson MR. Transport barriers in transscleral drug delivery for retinal diseases. Ophthalmic Res 2007;39:244-254.
3 Gunda S, Mandava N, Mitra AK. Barriers in Ocular Drug Delivery. In: Tombran-Tink J, Barnstable CJ, Eds. Ocular Transporters, Ophthalmic Diseases and Drug Delivery. New Jersey, Humana Press, 2008:399-414.
4 Nicolo M, Ghiglione D, Calabria G. Retinal pigment epithelial tear following intravitreal injection of bevacizumab (avastin). Eur J Ophthalmol 2006;16:770-773.
5 Kralinger MT, Kieselbach GF, Voigt M, Hayden B, Hernandez E, Fernandez V, Parel JM. Experimental model for proliferative vitreoretinopathy by intravitreal dispase: Limited by zonulolysis and cataract. Ophthalmologica 2006;220:211-216.
6 Ozkiris A, Erkilic K. Complications of intravitreal injection of triamcinolone acetonide. Can J Ophthalmol 2005;40:63-68.
7 Nelson ML, Tennant MT, Sivalingam A, Regillo CD, Belmont JB, Martidis A. Infectious and presumed noninfectious endophthalmitis after intravitreal triamcinolone acetonide injection. Retina 2003;23:686-691.
8 Sutter FK, Gillies MC. Pseudo-endophthalmitis after intravitreal injection of triamcinolone. Br J Ophthalmol 2003;87:972-974.
9 Lee SB, Geroski DH, Prausnitz MR, Edelhauser HF. Drug delivery through the sclera: Effects of thickness, hydration, and sustained release systems. Exp Eye Res 2004;78:599-607.
10 Ambati J, Adamis AP. Transscleral drug delivery to the retina and choroid. Prog Retin Eye Res 2002;21:145-151.
11 Geroski DH, Edelhauser HF. Transscleral drug delivery for posterior segment disease. Adv Drug Deliv Rev 2001;52:37-48.
12 Olsen TW, Aaberg SY, Geroski DH, Edelhauser HF. Human sclera: Thickness and surface area. Am J Ophthalmol 1998;125:237-241.
13 Friberg TR, Lace JW. A comparison of the elastic properties of human choroid and sclera. Exp Eye Res 1988;47:429-436.
14 Boubriak OA, Urban JP, Bron AJ. Differential effects of aging on transport properties of anterior and posterior human sclera. Exp Eye Res 2003;76:701-713.
15 Jiang J, Geroski DH, Edelhauser HF, Prausnitz MR. Measurement and prediction of lateral diffusion within human sclera. Invest Ophthalmol Vis Sci 2006;47:3011-3016.
16 Madhu C, Rix P, Nguyen T, Chien DS, Woodward DF, Tang-Liu DD. Penetration of natural prostaglandins and their ester prodrugs and analogs across human ocular tissues in vitro. J Ocul Pharmacol Ther 1998;14:389-399.
17 Unlu N, Robinson JR. Scleral permeability to hydrocortisone and mannitol in the albino rabbit eye. J Ocul Pharmacol Ther 1998;14:273-281.
18 Hamalainen KM, Kananen K, Auriola S, Kontturi K, Urtti A. Characterization of paracellular and aqueous penetration routes in cornea, conjunctiva, and sclera. Invest Ophthalmol Vis Sci 1997;38:627-634.
19 Edelhauser HF, Maren TH. Permeability of human cornea and sclera to sulfonamide carbonic anhydrase inhibitors. Arch Ophthalmol 1988;106:1110-1115.

20 Ahmed I, Patton TF. Importance of the noncorneal absorption route in topical ophthalmic drug delivery. Invest Ophthalmol Vis Sci 1985;26:584-587.
21 Ambati J, Canakis CS, Miller JW, Gragoudas ES, Edwards A, Weissgold DJ, Kim I, Delori FC, Adamis AP. Diffusion of high molecular weight compounds through sclera. Invest Ophthalmol Vis Sci 2000;41:1181-1185.
22 Boubriak OA, Urban JP, Akhtar S, Meek KM, Bron AJ. The effect of hydration and matrix composition on solute diffusion in rabbit sclera. Exp Eye Res 2000;71:503-514.
23 Olsen TW, Edelhauser HF, Lim JI, Geroski DH. Human scleral permeability. Effects of age, cryotherapy, transscleral diode laser, and surgical thinning. Invest Ophthalmol Vis Sci 1995;36:1893-1903.
24 Ambati J, Gragoudas ES, Miller JW, You TT, Miyamoto K, Delori FC, Adamis AP. Transscleral delivery of bioactive protein to the choroid and retina. Invest Ophthalmol Vis Sci 2000;41:1186-1191.
25 Edwards A, Prausnitz MR. Fiber matrix model of sclera and corneal stroma for drug delivery to the eye. AIChE Journal 1998;44:214-225.
26 Kansara V, Mitra AK. Evaluation of an ex vivo model implication for carrier-mediated retinal drug delivery. Curr Eye Res 2006;31:415-426.
27 Cruysberg LP, Nuijts RM, Geroski DH, Koole LH, Hendrikse F, Edelhauser HF. In vitro human scleral permeability of fluorescein, dexamethasone-fluorescein, methotrexate-fluorescein and rhodamine 6g and the use of a coated coil as a new drug delivery system. J Ocul Pharmacol Ther 2002;18:559-569.
28 Chien DS, Homsy JJ, Gluchowski C, Tang-Liu DD. Corneal and conjunctival/scleral penetration of p-aminoclonidine, agn 190342, and clonidine in rabbit eyes. Curr Eye Res 1990;9:1051-1059.
29 Ahmed I, Gokhale RD, Shah MV, Patton TF. Physicochemical determinants of drug diffusion across the conjunctiva, sclera, and cornea. J Pharm Sci 1987;76:583-586.
30 Cheruvu NP, Kompella UB. Bovine and porcine transscleral solute transport: Influence of lipophilicity and the choroid-bruch's layer. Invest Ophthalmol Vis Sci 2006;47:4513-4522.
31 Church AL, Barza M, Baum J. An improved apparatus for transscleral iontophoresis of gentamicin. Invest Ophthalmol Vis Sci 1992;33:3543-3545.
32 Yoshizumi MO, Cohen D, Verbukh I, Leinwand M, Kim J, Lee DA. Experimental transscleral iontophoresis of ciprofloxacin. J Ocul Pharmacol 1991;7:163-167.
33 Cruysberg LP, Nuijts RM, Geroski DH, Gilbert JA, Hendrikse F, Edelhauser HF. The influence of intraocular pressure on the transscleral diffusion of high-molecular-weight compounds. Invest Ophthalmol Vis Sci 2005;46:3790-3794.
34 Rudnick DE, Noonan JS, Geroski DH, Prausnitz MR, Edelhauser HF. The effect of intraocular pressure on human and rabbit scleral permeability. Invest Ophthalmol Vis Sci 1999;40:3054-3058.
35 Pitkanen L, Ranta VP, Moilanen H, Urtti A. Permeability of retinal pigment epithelium: Effects of permeant molecular weight and lipophilicity. Invest Ophthalmol Vis Sci 2005;46:641-646.
36 Kadam RS, Kompella UB. Influence of lipophilicity on drug partitioning into sclera, choroid-retinal pigment epithelium, retina, trabecular meshwork, and optic nerve. J Pharmacol Exp Ther;332:1107-1120.
37 Maurice DM, Polgar J. Diffusion across the sclera. Exp Eye Res 1977;25:577-582.

38 Hogan J. Histology of the Human Eye. Philadelphia: WB Saunders;1971.
39 Robinson MR, Lee SS, Kim H, Kim S, Lutz RJ, Galban C, Bungay PM, Yuan P, Wang NS, Kim J, Csaky KG. A rabbit model for assessing the ocular barriers to the transscleral delivery of triamcinolone acetonide. Exp Eye Res 2006;82:479-487.
40 Hillenkamp J, Hussain AA, Jackson TL, Cunningham JR, Marshall J. The influence of path length and matrix components on ageing characteristics of transport between the choroid and the outer retina. Invest Ophthalmol Vis Sci 2004;45:1493-1498.
41 Ramrattan RS, van der Schaft TL, Mooy CM, de Bruijn WC, Mulder PG, de Jong PT. Morphometric analysis of bruch's membrane, the choriocapillaris, and the choroid in aging. Invest Ophthalmol Vis Sci 1994;35:2857-2864.
42 Hussain AA, Rowe L, Marshall J. Age-related alterations in the diffusional transport of amino acids across the human bruch's-choroid complex. J Opt Soc Am A Opt Image Sci Vis 2002;19:166-172.
43 Moore DJ, Hussain AA, Marshall J. Age-related variation in the hydraulic conductivity of bruch's membrane. Invest Ophthalmol Vis Sci 1995;36:1290-1297.
44 Moore DJ, Clover GM. The effect of age on the macromolecular permeability of human bruch's membrane. Invest Ophthalmol Vis Sci 2001;42:2970-2975.
45 Cunha-Vaz JG. The blood-retinal barriers. Doc Ophthalmol 1976;41:287-327.
46 Zinn KM, Benjamin-Henkind J. Retinal pigment epithelium. In:Tasman W, ed. Duane’s Foundations of Clinical Ophthalmology. Philadelphia: Lippincott-Raven; 1995:Chap 21:1-20.
47 Amaral J, Fariss RN, Campos MM, Robison WG, Jr., Kim H, Lutz R, Becerra SP. Transscleral-rpe permeability of pedf and ovalbumin proteins: Implications for subconjunctival protein delivery. Invest Ophthalmol Vis Sci 2005;46:4383-4392.
48 Kennedy BG, Mangini NJ. P-glycoprotein expression in human retinal pigment epithelium. Mol Vis 2002;8:422-430.
49 Maurice DM, Mishima S. Ocular pharmacokinetics. In: Sears ML, ed. Pharmacology of the Eye. Berlin: Springler-Verlag; 1984:19-116.
50 Toris CB, Pederson JE. Experimental retinal detachment. Vii. Intravenous horseradish peroxidase diffusion across the blood-retinal barrier. Arch Ophthalmol 1984;102:752-756.
51 Peyman GA, Bok D. Peroxidase diffusion in the normal and laser-coagulated primate retina. Invest Ophthalmol 1972;11:35-45.
52 Hosoya K, Lee VH, Kim KJ. Roles of the conjunctiva in ocular drug delivery: A review of conjunctival transport mechanisms and their regulation. Eur J Pharm Biopharm 2005;60:227-240.
53 Dartt DA. Regulation of mucin and fluid secretion by conjunctival epithelial cells. Prog Retin Eye Res 2002;21:555-576.
54 Gukasyan HJ, Kim KJ, Lee VH. The Conjunctival Barrier in Ocular Drug Delivery. In: Ehrhardt C, Kim KJ, Eds. Drug Absorption Studies. New York, Springer, 2008;307-320.
55 Adson A, Raub TJ, Burton PS, Barsuhn CL, Hilgers AR, Audus KL, Ho NF. Quantitative approaches to delineate paracellular diffusion in cultured epithelial cell monolayers. J Pharm Sci 1994;83:1529-1536.
56 Huang AJ, Tseng SC, Kenyon KR. Paracellular permeability of corneal and conjunctival epithelia. Invest Ophthalmol Vis Sci 1989;30:684-689.

57 Gumbiner B. Structure, biochemistry, and assembly of epithelial tight junctions. Am J Physiol 1987;253:C749-758.
58 Horibe Y, Hosoya K, Kim KJ, Ogiso T, Lee VH. Polar solute transport across the pigmented rabbit conjunctiva: Size dependence and the influence of 8-bromo cyclic adenosine monophosphate. Pharm Res 1997;14:1246-1251.
59 Watsky MA, Jablonski MM, Edelhauser HF. Comparison of conjunctival and corneal surface areas in rabbit and human. Curr Eye Res 1988;7:483-486.
60 Kompella UB, Kim KJ, Lee VH. Active chloride transport in the pigmented rabbit conjunctiva. Curr Eye Res 1993;12:1041-1048.
61 Crosson CE, Beuerman RW, Klyce SD. Dopamine modulation of active ion transport in rabbit corneal epithelium. Invest Ophthalmol Vis Sci 1984;25:1240-1245.
62 Klyce SD. Electrical profiles in the corneal epithelium. J Physiol 1972;226:407-429.
63 Maurice DM. Electrical potential and ion transport across the conjunctiva. Exp Eye Res 1973;15:527-532.
64 Lee VH, Carson LW, Kashi SD, Stratford RE, Jr. Metabolic and permeation barriers to the ocular absorption of topically applied enkephalins in albino rabbits. J Ocul Pharmacol 1986;2:345-352.
65 Hayakawa E, Chien DS, Inagaki K, Yamamoto A, Wang W, Lee VH. Conjunctival penetration of insulin and peptide drugs in the albino rabbit. Pharm Res 1992;9:769-775.
66 Stratford RE, Jr., Carson LW, Dodda-Kashi S, Lee VH. Systemic absorption of ocularly administered enkephalinamide and inulin in the albino rabbit: Extent, pathways, and vehicle effects. J Pharm Sci 1988;77:838-842.
67 Sun L, Basu SK, Kim KJ, Lee VH. Arginine vasopressin transport and metabolism in the pigmented rabbit conjunctiva. Eur J Pharm Sci 1998;6:47-52.
68 Prince JH, Diesem CD, Eglitis I, Ruskell GL: The rabbit. In: Prince JH, Ed. Anatomy and histology of the eye and orbit in domestic animals. Springfield, Charles c Thomas, 1960:268-269.
69 Amrite AC, Kompella UB. Size-dependent disposition of nanoparticles and microparticles following subconjunctival administration. J Pharm Pharmacol 2005;57:1555-1563.
70 Maurice DM. Ota Y. The kinetics of subconjunctival injections. Jpn J Ophthalmol 1978;22:95-100.
71 Kim H, Robinson MR, Lizak MJ, Tansey G, Lutz RJ, Yuan P, Wang NS, Csaky KG. Controlled drug release from an ocular implant: An evaluation using dynamic three-dimensional magnetic resonance imaging. Invest Ophthalmol Vis Sci 2004;45:2722-2731.
72 Pontes de Carvalho RA, Krausse ML, Murphree AL, Schmitt EE, Campochiaro PA, Maumenee IH. Delivery from episcleral exoplants. Invest Ophthalmol Vis Sci 2006;47:4532-4539.
73 Balachandran RK, Barocas VH. Computer modeling of drug delivery to the posterior eye: Effect of active transport and loss to choroidal blood flow. Pharm Res 2008;25:2685-2696.
74 Bill A, Tornquist P, Alm A. Permeability of the intraocular blood vessels. Trans Ophthalmol Soc U K 1980;100:332-336.
75 Gardner TW, Antonetti DA, Barber AJ, Lieth E, Tarbell JA. The molecular structure and function of the inner blood-retinal barrier. Penn state retina research group. Doc Ophthalmol 1999;97:229-237.

76 Lang JC, Stiemke MM. Biological Barriers to Ocular Delivery. In: Reddy IK, Ed. Ocular Therapeutics and Drug Delivery: A Multidisciplinary Approach. Pennsylvania, Technomic Publishing Company, Inc. 1996;85-88.
77 Miller S, Steinberg RH. Transport of taurine, L-methionine and 3-o-methyl-D-glucose across frog retinal pigment epithelium. Exp Eye Res. 1976;23:177-89.
78 Tornquist P, Alm A, Bill A. Studies on ocular blood flow and retinal capillary permeability to sodium in pigs. Acta Physiol Scand 1979;106:343-350.
79 Grayson MC, Laties AM. Ocular localization of sodium fluorescein. Effects of administration in rabbit and monkey. Arch Ophthalmol 1971;85:600-603.
80 Stewart PA, Tuor UI. Blood-eye barriers in the rat: Correlation of ultrastructure with function. J Comp Neurol 1994;340:566-576.
81 de Oliveira F. Pericytes in diabetic retinopathy. Br J Ophthalmol 1966;50:134-143.
82 Larsen M. Ocular fluorometry methodological improvements and clinical studies--with special reference to the blood-retina barrier permeability to fluorescein and fluorescein glucuronide. Acta Ophthalmol Suppl 1993:1-52.
83 Cumha-Vaz JG. The blood-ocular barriers. Invest Ophthalmol Vis Sci 1978;17:1037-1039.
84 Korte GE, Bellhorn RW, Burns MS. Ultrastructure of blood-retinal barrier permeability in rat phototoxic retinopathy. Invest Ophthalmol Vis Sci 1983;24:962-971.
85 Bellhorn RW, Burns MS, Benjamin JV. Retinal vessel abnormalities of phototoxic retinopathy in rats. Invest Ophthalmol Vis Sci 1980;19:584-595.
86 Lee VH. Membrane transporters. Eur J Pharm Sci 2000;11 Suppl 2:S41-50.
87 Barot M, Gokulgandhi MR, Haghnegahdar M, Dalvi P, Mitra AK. Effect of emergence of fluoroquinolone resistance on intrinsic expression of p-glycoprotein phenotype in corneal epithelial cells. J Ocul Pharmacol Ther;27:553-559.
88 Cannon RD, Lamping E, Holmes AR, Niimi K, Baret PV, Keniya MV, Tanabe K, Niimi M, Goffeau A, Monk BC. Efflux-mediated antifungal drug resistance. Clin Microbiol Rev 2009;22:291-321, Table of Contents.
89 Dilger K, Schwab M, Fromm MF. Identification of budesonide and prednisone as substrates of the intestinal drug efflux pump p-glycoprotein. Inflamm Bowel Dis 2004;10:578-583.
90 Tsuji A. P-glycoprotein-mediated efflux transport of anticancer drugs at the blood-brain barrier. Ther Drug Monit 1998;20:588-590.
91 Barot M, Bagui M, Gokulgandhi MR, Mitra AK. Prodrug strategies in ocular drug delivery. Med Chem;8:753-768.
92 Gokulgandhi MR, Barot M, Bagui M, Pal D, Mitra AK. Transporter-targeted lipid prodrugs of cyclic cidofovir: A potential approach for the treatment of cytomegalovirus retinitis. J Pharm Sci;101:3249-3263.
93 www.cancer.gov.
94 de Graaf P, Goricke S, Rodjan F, Galluzzi P, Maeder P, Castelijns JA, Brisse HJ. Guidelines for imaging retinoblastoma: Imaging principles and mri standardization. Pediatr Radiol;42:2-14.
95 Ray A, Gombos DS, Vats TS. Retinoblastoma: An overview. Indian J Pediatr;79:916-921.
96 Khetan V, Gupta A, Gopal L. Retinoblastoma: Recent trends a mini review based on published literature. Oman J Ophthalmol;4:108-115.

97 Wilson MW, Fraga CH, Rodriguez-Galindo C, Hagedorn N, Leggas ML, Stewart C. Expression of the multi-drug resistance proteins and the pregnane x receptor in treated and untreated retinoblastoma. Curr Eye Res 2009;34:386-394.
98 Krishnakumar S, Mallikarjuna K, Desai N, Muthialu A, Venkatesan N, Sundaram A, Khetan V, Shanmugam MP. Multidrug resistant proteins: P-glycoprotein and lung resistance protein expression in retinoblastoma. Br J Ophthalmol 2004;88:1521-1526.
99 Chan HS, Lu Y, Grogan TM, Haddad G, Hipfner DR, Cole SP, Deeley RG, Ling V, Gallie BL. Multidrug resistance protein (mrp) expression in retinoblastoma correlates with the rare failure of chemotherapy despite cyclosporine for reversal of p-glycoprotein. Cancer Res 1997;57:2325-2330.
100 Filho JP, Correa ZM, Odashiro AN, Coutinho AB, Martins MC, Erwenne CM, Burnier MN, Jr. Histopathological features and p-glycoprotein expression in retinoblastoma. Invest Ophthalmol Vis Sci 2005;46:3478-3483.
101 Hodgetts B, Jones DR, Binstead JA. The response of broiler chicks to vitamin drenches immediately after hatching. Vet Rec 1977;101:268.
102 Aylward GW. Progressive changes in diabetics and their management. Eye (Lond) 2005;19:1115-1118.
103 Frank RN. Diabetic retinopathy. N Engl J Med 2004;350:48-58.
104 Cheung N, Mitchell P, Wong TY. Diabetic retinopathy. Lancet;376:124-136.
105 Fong DS, Aiello L, Gardner TW, King GL, Blankenship G, Cavallerano JD, Ferris FL, 3rd, Klein R. Retinopathy in diabetes. Diabetes Care 2004;27 Suppl 1:S84-87.
106 Kowluru RA, Tang J, Kern TS. Abnormalities of retinal metabolism in diabetes and experimental galactosemia. Vii. Effect of long-term administration of antioxidants on the development of retinopathy. Diabetes 2001;50:1938-1942.
107 Xia P, Inoguchi T, Kern TS, Engerman RL, Oates PJ, King GL. Characterization of the mechanism for the chronic activation of diacylglycerol-protein kinase c pathway in diabetes and hypergalactosemia. Diabetes 1994;43:1122-1129.
108 Kowluru RA, Chan PS. Oxidative stress and diabetic retinopathy. Exp Diabetes Res 2007;2007:43603.
109 Anderson RE, Rapp LM, Wiegand RD. Lipid peroxidation and retinal degeneration. Curr Eye Res 1984;3:223-227.
110 Du Y, Miller CM, Kern TS. Hyperglycemia increases mitochondrial superoxide in retina and retinal cells. Free Radic Biol Med 2003;35:1491-1499.
111 Ellis EA, Guberski DL, Somogyi-Mann M, Grant MB. Increased h2o2, vascular endothelial growth factor and receptors in the retina of the bbz/wor diabetic rat. Free Radic Biol Med 2000;28:91-101.
112 Li W, Yanoff M, Jian B, He Z. Altered mrna levels of antioxidant enzymes in pre-apoptotic pericytes from human diabetic retinas. Cell Mol Biol (Noisy-le-grand) 1999;45:59-66.
113 Kowluru RA, Kern TS, Engerman RL. Abnormalities of retinal metabolism in diabetes or experimental galactosemia. Iv. Antioxidant defense system. Free Radic Biol Med 1997;22:587-592.
114 Colantuoni A, Longoni B, Marchiafava PL. Retinal photoreceptors of syrian hamsters undergo oxidative stress during streptozotocin-induced diabetes. Diabetologia 2002;45:121-124.

115 Kowluru RA. Effect of reinstitution of good glycemic control on retinal oxidative stress and nitrative stress in diabetic rats. Diabetes 2003;52:818-823.
116 Kong GY, Van Bergen NJ, Trounce IA, Crowston JG. Mitochondrial dysfunction and glaucoma. J Glaucoma 2009;18:93-100.
117 Barron MJ, Griffiths P, Turnbull DM, Bates D, Nichols P. The distributions of mitochondria and sodium channels reflect the specific energy requirements and conduction properties of the human optic nerve head. Br J Ophthalmol 2004;88:286-290.
118 Fine SL, Berger JW, Maguire MG, Ho AC. Age-related macular degeneration. N Engl J Med 2000;342:483-492.
119 Young RW. Pathophysiology of age-related macular degeneration. Surv Ophthalmol 1987;31:291-306.
120 Sarks SH. Ageing and degeneration in the macular region: A clinico-pathological study. Br J Ophthalmol 1976;60:324-341.
121 Beatty S, Koh H, Phil M, Henson D, Boulton M. The role of oxidative stress in the pathogenesis of age-related macular degeneration. Surv Ophthalmol 2000;45:115-134.
122 Winkler BS, Boulton ME, Gottsch JD, Sternberg P. Oxidative damage and age-related macular degeneration. Mol Vis 1999;5:32.
123 A randomized, placebo-controlled, clinical trial of high-dose supplementation with vitamins c and e, beta carotene, and zinc for age-related macular degeneration and vision loss: Areds report no. 8. Arch Ophthalmol 2001;119:1417-1436.
124 Jarrett SG, Cuenco J, Boulton M. Dietary antioxidants provide differential subcellular protection in epithelial cells. Redox Rep 2006;11:144-152.
125 Jarrett SG, Lin H, Godley BF, Boulton ME. Mitochondrial DNA damage and its potential role in retinal degeneration. Prog Retin Eye Res 2008;27:596-607.
126 Druzhyna NM, Wilson GL, LeDoux SP. Mitochondrial DNA repair in aging and disease. Mech Ageing Dev 2008;129:383-390.
127 Golden TR, Melov S. Mitochondrial DNA mutations, oxidative stress, and aging. Mech Ageing Dev 2001;122:1577-1589.
128 Sastre J, Pallardo FV, Vina J. Mitochondrial oxidative stress plays a key role in aging and apoptosis. IUBMB Life 2000;49:427-435.
129 Green DR, Amarante-Mendes GP. The point of no return: Mitochondria, caspases, and the commitment to cell death. Results Probl Cell Differ 1998;24:45-61.
130 Kowluru RA. Diabetic retinopathy: Mitochondrial dysfunction and retinal capillary cell death. Antioxid Redox Signal 2005;7:1581-1587.
131 Kanwar M, Chan PS, Kern TS, Kowluru RA. Oxidative damage in the retinal mitochondria of diabetic mice: Possible protection by superoxide dismutase. Invest Ophthalmol Vis Sci 2007;48:3805-3811.
132 Kowluru RA, Kowluru V, Xiong Y, Ho YS. Overexpression of mitochondrial superoxide dismutase in mice protects the retina from diabetes-induced oxidative stress. Free Radic Biol Med 2006;41:1191-1196.
133 Kowluru RA, Atasi L, Ho YS. Role of mitochondrial superoxide dismutase in the development of diabetic retinopathy. Invest Ophthalmol Vis Sci 2006;47:1594-1599.
134 Madsen-Bouterse SA, Mohammad G, Kanwar M, Kowluru RA. Role of mitochondrial DNA damage in the development of diabetic retinopathy, and the metabolic memory phenomenon associated with its progression. Antioxid Redox Signal;13:797-805.

135 Kowluru RA, Abbas SN. Diabetes-induced mitochondrial dysfunction in the retina. Invest Ophthalmol Vis Sci 2003;44:5327-5334.
136 Sheu SS, Nauduri D, Anders MW. Targeting antioxidants to mitochondria: A new therapeutic direction. Biochim Biophys Acta 2006;1762:256-265.
137 Ju WK, Liu Q, Kim KY, Crowston JG, Lindsey JD, Agarwal N, Ellisman MH, Perkins GA, Weinreb RN. Elevated hydrostatic pressure triggers mitochondrial fission and decreases cellular atp in differentiated rgc-5 cells. Invest Ophthalmol Vis Sci 2007;48:2145-2151.
138 Abu-Amero KK, Morales J, Bosley TM. Mitochondrial abnormalities in patients with primary open-angle glaucoma. Invest Ophthalmol Vis Sci 2006;47:2533-2541.
139 Calandrella N, Scarsella G, Pescosolido N, Risuleo G. Degenerative and apoptotic events at retinal and optic nerve level after experimental induction of ocular hypertension. Mol Cell Biochem 2007;301:155-163.
140 Kerrigan LA, Zack DJ, Quigley HA, Smith SD, Pease ME. Tunel-positive ganglion cells in human primary open-angle glaucoma. Arch Ophthalmol 1997;115:1031-1035.
141 Moreno MC, Campanelli J, Sande P, Sanez DA, Keller Sarmiento MI, Rosenstein RE. Retinal oxidative stress induced by high intraocular pressure. Free Radic Biol Med 2004;37:803-812.
142 Bonne C, Muller A, Villain M. Free radicals in retinal ischemia. Gen Pharmacol 1998;30:275-280.
143 Farkas RH, Chowers I, Hackam AS, Kageyama M, Nickells RW, Otteson DC, Duh EJ, Wang C, Valenta DF, Gunatilaka TL, Pease ME, Quigley HA, Zack DJ. Increased expression of iron-regulating genes in monkey and human glaucoma. Invest Ophthalmol Vis Sci 2004;45:1410-1417.
144 Tezel G, Seigel GM, Wax MB. Autoantibodies to small heat shock proteins in glaucoma. Invest Ophthalmol Vis Sci 1998;39:2277-2287.
145 Murphy MP, Smith RA. Targeting antioxidants to mitochondria by conjugation to lipophilic cations. Annu Rev Pharmacol Toxicol 2007;47:629-656.
146 Neroev VV, Archipova MM, Bakeeva LE, Fursova A, Grigorian EN, Grishanova AY, Iomdina EN, Ivashchenko Zh N, Katargina LA, Khoroshilova-Maslova IP, Kilina OV, Kolosova NG, Kopenkin EP, Korshunov SS, Kovaleva NA, Novikova YP, Philippov PP, Pilipenko DI, Robustova OV, Saprunova VB, Senin, II, Skulachev MV, Sotnikova LF, Stefanova NA, Tikhomirova NK, Tsapenko IV, Shchipanova AI, Zinovkin RA, Skulachev VP. Mitochondria-targeted plastoquinone derivatives as tools to interrupt execution of the aging program. 4. Age-related eye disease. Skq1 returns vision to blind animals. Biochemistry (Mosc) 2008;73:1317-1328.
147 Fritsche LG, Loenhardt T, Janssen A, Fisher SA, Rivera A, Keilhauer CN, Weber BH. Age-related macular degeneration is associated with an unstable arms2 (loc387715) mrna. Nat Genet 2008;40:892-896.
148 Schmidt S, Hauser MA, Scott WK, Postel EA, Agarwal A, Gallins P, Wong F, Chen YS, Spencer K, Schnetz-Boutaud N, Haines JL, Pericak-Vance MA. Cigarette smoking strongly modifies the association of loc387715 and age-related macular degeneration. Am J Hum Genet 2006;78:852-864.
149 Rivera A, Fisher SA, Fritsche LG, Keilhauer CN, Lichtner P, Meitinger T, Weber BH. Hypothetical loc387715 is a second major susceptibility gene for age-related macular

degeneration, contributing independently of complement factor h to disease risk. Hum Mol Genet 2005;14:3227-3236.
150 Hageman GS, Anderson DH, Johnson LV, Hancox LS, Taiber AJ, Hardisty LI, Hageman JL, Stockman HA, Borchardt JD, Gehrs KM, Smith RJ, Silvestri G, Russell SR, Klaver CC, Barbazetto I, Chang S, Yannuzzi LA, Barile GR, Merriam JC, Smith RT, Olsh AK, Bergeron J, Zernant J, Merriam JE, Gold B, Dean M, Allikmets R. A common haplotype in the complement regulatory gene factor h (hf1/cfh) predisposes individuals to age-related macular degeneration. Proc Natl Acad Sci U S A 2005;102:7227-7232.
151 Haines JL, Hauser MA, Schmidt S, Scott WK, Olson LM, Gallins P, Spencer KL, Kwan SY, Noureddine M, Gilbert JR, Schnetz-Boutaud N, Agarwal A, Postel EA, Pericak-Vance MA. Complement factor h variant increases the risk of age-related macular degeneration. Science 2005;308:419-421.
152 Kanda A, Chen W, Othman M, Branham KE, Brooks M, Khanna R, He S, Lyons R, Abecasis GR, Swaroop A. A variant of mitochondrial protein loc387715/arms2, not htra1, is strongly associated with age-related macular degeneration. Proc Natl Acad Sci U S A 2007;104:16227-16232.
153 Jones M, Mitchell P, Wang JJ, Sue C. Melas a3243g mitochondrial DNA mutation and age related maculopathy. Am J Ophthalmol 2004;138:1051-1053.
154 Jones MM, Manwaring N, Wang JJ, Rochtchina E, Mitchell P, Sue CM. Mitochondrial DNA haplogroups and age-related maculopathy. Arch Ophthalmol 2007;125:1235-1240.
155 Decanini A, Nordgaard CL, Feng X, Ferrington DA, Olsen TW. Changes in select redox proteins of the retinal pigment epithelium in age-related macular degeneration. Am J Ophthalmol 2007;143:607-615.
156 Nordgaard CL, Berg KM, Kapphahn RJ, Reilly C, Feng X, Olsen TW, Ferrington DA. Proteomics of the retinal pigment epithelium reveals altered protein expression at progressive stages of age-related macular degeneration. Invest Ophthalmol Vis Sci 2006;47:815-822.
157 Feher J, Kovacs I, Artico M, Cavallotti C, Papale A, Balacco Gabrieli C. Mitochondrial alterations of retinal pigment epithelium in age-related macular degeneration. Neurobiol Aging 2006;27:983-993.
158 Barreau E, Brossas JY, Courtois Y, Treton JA. Accumulation of mitochondrial DNA deletions in human retina during aging. Invest Ophthalmol Vis Sci 1996;37:384-391.
159 Wang AL, Lukas TJ, Yuan M, Neufeld AH. Increased mitochondrial DNA damage and down-regulation of DNA repair enzymes in aged rodent retinal pigment epithelium and choroid. Mol Vis 2008;14:644-651.
160 Ballinger SW, Van Houten B, Jin GF, Conklin CA, Godley BF. Hydrogen peroxide causes significant mitochondrial DNA damage in human rpe cells. Exp Eye Res 1999;68:765-772.
161 Jarrett SG, Boulton ME. Poly(adp-ribose) polymerase offers protection against oxidative and alkylation damage to the nuclear and mitochondrial genomes of the retinal pigment epithelium. Ophthalmic Res 2007;39:213-223.
162 Jarrett SG, Boulton ME. Antioxidant up-regulation and increased nuclear DNA protection play key roles in adaptation to oxidative stress in epithelial cells. Free Radic Biol Med 2005;38:1382-1391.

163 Liang FQ, Godley BF. Oxidative stress-induced mitochondrial DNA damage in human retinal pigment epithelial cells: A possible mechanism for rpe aging and age-related macular degeneration. Exp Eye Res 2003;76:397-403.
164 Graziewicz MA, Day BJ, Copeland WC. The mitochondrial DNA polymerase as a target of oxidative damage. Nucleic Acids Res 2002;30:2817-2824.
165 Jarrett SG, Milder JB, Liang LP, Patel M. The ketogenic diet increases mitochondrial glutathione levels. J Neurochem 2008;106:1044-1051.
166 Liang FQ, Alssadi R, Morehead P, Awasthi YC, Godley BF. Enhanced expression of glutathione-s-transferase a1-1 protects against oxidative stress in human retinal pigment epithelial cells. Exp Eye Res 2005;80:113-119.
167 Liang FQ, Green L, Wang C, Alssadi R, Godley BF. Melatonin protects human retinal pigment epithelial (rpe) cells against oxidative stress. Exp Eye Res 2004;78:1069-1075.
168 Godley BF, Jin GF, Guo YS, Hurst JS. Bcl-2 overexpression increases survival in human retinal pigment epithelial cells exposed to h(2)o(2). Exp Eye Res 2002;74:663-669.
169 Kennedy CJ, Rakoczy PE, Constable IJ. Lipofuscin of the retinal pigment epithelium: A review. Eye (Lond) 1995;9 (Pt 6):763-771.
170 Dunaief JL, Dentchev T, Ying GS, Milam AH. The role of apoptosis in age-related macular degeneration. Arch Ophthalmol 2002;120:1435-1442.
171 Feher J, Papale A, Mannino G, Gualdi L, Balacco Gabrieli C. Mitotropic compounds for the treatment of age-related macular degeneration. The metabolic approach and a pilot study. Ophthalmologica 2003;217:351-357.
172 Feher J, Kovacs B, Kovacs I, Schveoller M, Papale A, Balacco Gabrieli C. Improvement of visual functions and fundus alterations in early age-related macular degeneration treated with a combination of acetyl-l-carnitine, n-3 fatty acids, and coenzyme q10. Ophthalmologica 2005;219:154-166.
173 Broaddus E, Topham A, Singh AD. Incidence of retinoblastoma in the USA: 1975-2004. Br J Ophthalmol 2009;93:21-23.
174 Kernt M, Neubauer AS, Liegl RG, Lackerbauer CA, Eibl KH, Alge CS, Ulbig MW, A AK. Intracameral moxifloxacin: In vitro safety on human ocular cells. Cornea 2009;28:553-561.
175 Miller D. Review of moxifloxacin hydrochloride ophthalmic solution in the treatment of bacterial eye infections. Clin Ophthalmol 2008;2:77-91.
176 Balfour JA, Lamb HM. Moxifloxacin: A review of its clinical potential in the management of community-acquired respiratory tract infections. Drugs 2000;59:115-139.
177 Reuveni D, Halperin D, Shalit I, Priel E, Fabian I. Quinolones as enhancers of camptothecin-induced cytotoxic and anti-topoisomerase i effects. Biochem Pharmacol 2008;75:1272-1281.
178 Fabian I, Reuveni D, Levitov A, Halperin D, Priel E, Shalit I. Moxifloxacin enhances antiproliferative and apoptotic effects of etoposide but inhibits its proinflammatory effects in thp-1 and jurkat cells. Br J Cancer 2006;95:1038-1046.
179 Bromberg KD, Burgin AB, Osheroff N. Quinolone action against human topoisomerase iialpha: Stimulation of enzyme-mediated double-stranded DNA cleavage. Biochemistry 2003;42:3393-3398.

180 Reuveni D, Halperin D, Fabian I, Tsarfaty G, Askenasy N, Shalit I. Moxifloxacin increases anti-tumor and anti-angiogenic activity of irinotecan in human xenograft tumors. Biochem Pharmacol;79:1100-1107.
181 Weiss T, Shalit I, Blau H, Werber S, Halperin D, Levitov A, Fabian I. Anti-inflammatory effects of moxifloxacin on activated human monocytic cells: Inhibition of nf-kappab and mitogen-activated protein kinase activation and of synthesis of proinflammatory cytokines. Antimicrob Agents Chemother 2004;48:1974-1982.
182 Dalhoff A, Shalit I. Immunomodulatory effects of quinolones. Lancet Infect Dis 2003;3:359-371.
183 Shalit I, Horev-Azaria L, Fabian I, Blau H, Kariv N, Shechtman I, Alteraz H, Kletter Y. Immunomodulatory and protective effects of moxifloxacin against candida albicans-induced bronchopneumonia in mice injected with cyclophosphamide. Antimicrob Agents Chemother 2002;46:2442-2449.
184 Shalit I, Kletter Y, Halperin D, Waldman D, Vasserman E, Nagler A, Fabian I. Immunomodulatory effects of moxifloxacin in comparison to ciprofloxacin and g-csf in a murine model of cyclophosphamide-induced leukopenia. Eur J Haematol 2001;66:287-296.
185 Polachek H, Holcberg G, Polachek J, Rubin M, Feinshtein V, Sheiner E, Ben-Zvi Z. Carrier-mediated uptake of levofloxacin by bewo cells, a human trophoblast cell line. Arch Gynecol Obstet;281:833-838.
186 Horibe Y, Hosoya K, Kim KJ, Lee VH. Carrier-mediated transport of monocarboxylate drugs in the pigmented rabbit conjunctiva. Invest Ophthalmol Vis Sci 1998;39:1436-1443.
187 Gokulgandhi MR, Vadlapudi AD, Mitra AK. Ocular toxicity from systemically administered xenobiotics. Expert Opin Drug Metab Toxicol;8:1277-1291.
188 Raghava S, Hammond M, Kompella UB. Periocular routes for retinal drug delivery. Expert Opin Drug Deliv 2004;1:99-114.
189 O'Brien TP, Arshinoff SA, Mah FS. Perspectives on antibiotics for postoperative endophthalmitis prophylaxis: Potential role of moxifloxacin. J Cataract Refract Surg 2007;33:1790-1800.
190 Iyer MN, He F, Wensel TG, Mieler WF, Benz MS, Holz ER. Clearance of intravitreal moxifloxacin. Invest Ophthalmol Vis Sci 2006;47:317-319.
191 Ozturk F, Kortunay S, Kurt E, Ubeyt Inan U, Sami Ilker S, Basci NE, Bozkurt A, Oguz Kayaalp S. Ofloxacin levels after intravitreal injection. Effects of trauma and inflammation. Ophthalmic Res 1999;31:446-451.
192 Pearson PA, Hainsworth DP, Ashton P. Clearance and distribution of ciprofloxacin after intravitreal injection. Retina 1993;13:326-330.
193 Hughes PM, Krishnamoorthy R, Mitra AK. Vitreous disposition of two acycloguanosine antivirals in the albino and pigmented rabbit models: A novel ocular microdialysis technique. J Ocul Pharmacol Ther 1996;12:209-224.
194 Philp NJ, Wang D, Yoon H, Hjelmeland LM. Polarized expression of monocarboxylate transporters in human retinal pigment epithelium and arpe-19 cells. Invest Ophthalmol Vis Sci 2003;44:1716-1721.
195 Enerson BE, Drewes LR. Molecular features, regulation, and function of monocarboxylate transporters: Implications for drug delivery. J Pharm Sci 2003;92:1531-1544.

196 Majumdar S, Gunda S, Pal D, Mitra AK. Functional activity of a monocarboxylate transporter, mct1, in the human retinal pigmented epithelium cell line, arpe-19. Mol Pharm 2005;2:109-117.
197 Kenyon E, Yu K, La Cour M, Miller SS. Lactate transport mechanisms at apical and basolateral membranes of bovine retinal pigment epithelium. Am J Physiol 1994;267:C1561-1573.
198 Lin H, la Cour M, Andersen MV, Miller SS. Proton-lactate cotransport in the apical membrane of frog retinal pigment epithelium. Exp Eye Res 1994;59:679-688.
199 Giasson C, Bonanno JA. Facilitated transport of lactate by rabbit corneal endothelium. Exp Eye Res 1994;59:73-81.
200 Poole RC, Halestrap AP. Transport of lactate and other monocarboxylates across mammalian plasma membranes. Am J Physiol 1993;264:C761-782.
201 Bonanno JA. Lactate-proton cotransport in rabbit corneal epithelium. Curr Eye Res 1990;9:707-712.
202 Callegan MC, Ramirez R, Kane ST, Cochran DC, Jensen H. Antibacterial activity of the fourth-generation fluoroquinolones gatifloxacin and moxifloxacin against ocular pathogens. Adv Ther 2003;20:246-252.
203 Kowalski RP, Dhaliwal DK, Karenchak LM, Romanowski EG, Mah FS, Ritterband DC, Gordon YJ. Gatifloxacin and moxifloxacin: An in vitro susceptibility comparison to levofloxacin, ciprofloxacin, and ofloxacin using bacterial keratitis isolates. Am J Ophthalmol 2003;136:500-505.
204 Mather R, Karenchak LM, Romanowski EG, Kowalski RP. Fourth generation fluoroquinolones: New weapons in the arsenal of ophthalmic antibiotics. Am J Ophthalmol 2002;133:463-466.
205 Emoto A, Ushigome F, Koyabu N, Kajiya H, Okabe K, Satoh S, Tsukimori K, Nakano H, Ohtani H, Sawada Y. H(+)-linked transport of salicylic acid, an nsaid, in the human trophoblast cell line bewo. Am J Physiol Cell Physiol 2002;282:C1064-1075.
206 Halestrap AP, Price NT. The proton-linked monocarboxylate transporter (mct) family: Structure, function and regulation. Biochem J 1999;343 Pt 2:281-299.
207 Defoe DM, Ahmad A, Chen W, Hughes BA. Membrane polarity of the na(+)-k+ pump in primary cultures of xenopus retinal pigment epithelium. Exp Eye Res 1994;59:587-596.
208 Korte GE, Wanderman MC. Distribution of na+ k(+)-atpase in regenerating retinal pigment epithelium in the rabbit. A study by electron microscopic cytochemistry. Exp Eye Res 1993;56:219-229.
209 Hadjiagapiou C, Schmidt L, Dudeja PK, Layden TJ, Ramaswamy K. Mechanism(s) of butyrate transport in caco-2 cells: Role of monocarboxylate transporter 1. Am J Physiol Gastrointest Liver Physiol 2000;279:G775-780.
210 Lin RY, Vera JC, Chaganti RS, Golde DW. Human monocarboxylate transporter 2 (mct2) is a high affinity pyruvate transporter. J Biol Chem 1998;273:28959-28965.
211 Orsenigo MN, Tosco M, Bazzini C, Laforenza U, Faelli A. A monocarboxylate transporter mct1 is located at the basolateral pole of rat jejunum. Exp Physiol 1999;84:1033-1042.
212 Scoper SV. Review of third-and fourth-generation fluoroquinolones in ophthalmology: In-vitro and in-vivo efficacy. Adv Ther 2008;25:979-994.

213 Saravolatz LD, Leggett J. Gatifloxacin, gemifloxacin, and moxifloxacin: The role of 3 newer fluoroquinolones. Clin Infect Dis 2003;37:1210-1215.
214 Benitez-Del-Castillo J, Verboven Y, Stroman D, Kodjikian L. The role of topical moxifloxacin, a new antibacterial in europe, in the treatment of bacterial conjunctivitis. Clin Drug Investig;31:543-557.
215 Bertino JS, Jr. Impact of antibiotic resistance in the management of ocular infections: The role of current and future antibiotics. Clin Ophthalmol 2009;3:507-521.
216 Asbell PA, Colby KA, Deng S, McDonnell P, Meisler DM, Raizman MB, Sheppard JD, Jr., Sahm DF. Ocular trust: Nationwide antimicrobial susceptibility patterns in ocular isolates. Am J Ophthalmol 2008;145:951-958.
217 Hariharan S, Minocha M, Mishra GP, Pal D, Krishna R, Mitra AK. Interaction of ocular hypotensive agents (pgf2 alpha analogs-bimatoprost, latanoprost, and travoprost) with mdr efflux pumps on the rabbit cornea. J Ocul Pharmacol Ther 2009;25:487-498.
218 Chintagumpala M, Chevez-Barrios P, Paysse EA, Plon SE, Hurwitz R. Retinoblastoma: Review of current management. Oncologist 2007;12:1237-1246.
219 Shields JA, Shields CL, Parsons HM. Differential diagnosis of retinoblastoma. Retina 1991;11:232-243.
220 Shields JA, Augsburger JJ. Current approaches to the diagnosis and management of retinoblastoma. Surv Ophthalmol 1981;25:347-372.
221 Chan HS, Thorner PS, Haddad G, Gallie BL. Multidrug-resistant phenotype in retinoblastoma correlates with p-glycoprotein expression. Ophthalmology 1991;98:1425-1431.
222 Jain R, Agarwal S, Majumdar S, Zhu X, Pal D, Mitra AK. Evasion of p-gp mediated cellular efflux and permeability enhancement of hiv-protease inhibitor saquinavir by prodrug modification. Int J Pharm 2005;303:8-19.
223 Dimaras H, Heon E, Doyle J, Strahlendorf C, Paton KE, Halliday W, Babyn P, Gallie BL, Chan HS. Multifaceted chemotherapy for trilateral retinoblastoma. Arch Ophthalmol;129:362-365.
224 Chan HS, DeBoer G, Thiessen JJ, Budning A, Kingston JE, O'Brien JM, Koren G, Giesbrecht E, Haddad G, Verjee Z, Hungerford JL, Ling V, Gallie BL. Combining cyclosporin with chemotherapy controls intraocular retinoblastoma without requiring radiation. Clin Cancer Res 1996;2:1499-1508.
225 Lee TW, Yang SW, Kim CM, Hong WS, Youn DH. Chemosensitization to adriamycin by cyclosporin a and verapamil in human retinoblastoma cell lines. J Korean Med Sci 1993;8:104-109.
226 Wang Q, Strab R, Kardos P, Ferguson C, Li J, Owen A, Hidalgo IJ. Application and limitation of inhibitors in drug-transporter interactions studies. Int J Pharm 2008;356:12-18.
227 Pal D, Mitra AK. Mdr- and cyp3a4-mediated drug-drug interactions. J Neuroimmune Pharmacol 2006;1:323-339.
228 McGee DH, Holt WF, Kastner PR, Rice RL. Safety of moxifloxacin as shown in animal and in vitro studies. Surv Ophthalmol 2005;50 Suppl 1:S46-54.
229 Vene R, Arena G, Poggi A, D'Arrigo C, Mormino M, Noonan DM, Albini A, Tosetti F. Novel cell death pathways induced by n-(4-hydroxyphenyl)retinamide: Therapeutic implications. Mol Cancer Ther 2007;6:286-298.
230 Gruss-Fischer T, Fabian I. Protection by ascorbic acid from denaturation and release of cytochrome c, alteration of mitochondrial membrane potential and activation of multiple

caspases induced by h(2)o(2), in human leukemia cells. Biochem Pharmacol 2002;63:1325-1335.
231 Wu WC, Hu DN, Gao HX, Chen M, Wang D, Rosen R, McCormick SA. Subtoxic levels hydrogen peroxide-induced production of interleukin-6 by retinal pigment epithelial cells. Mol Vis;16:1864-1873.
232 Mizukami Y, Jo WS, Duerr EM, Gala M, Li J, Zhang X, Zimmer MA, Iliopoulos O, Zukerberg LR, Kohgo Y, Lynch MP, Rueda BR, Chung DC. Induction of interleukin-8 preserves the angiogenic response in hif-1alpha-deficient colon cancer cells. Nat Med 2005;11:992-997.
233 Brew R, Erikson JS, West DC, Kinsella AR, Slavin J, Christmas SE. Interleukin-8 as an autocrine growth factor for human colon carcinoma cells in vitro. Cytokine 2000;12:78-85.
234 Barot M, Gokulgandhi MR, Mitra AK. Mitochondrial dysfunction in retinal diseases. Curr Eye Res;36:1069-1077.
235 Munteanu E, Verdier M, Grandjean-Forestier F, Stenger C, Jayat-Vignoles C, Huet S, Robert J, Ratinaud MH. Mitochondrial localization and activity of p-glycoprotein in doxorubicin-resistant k562 cells. Biochem Pharmacol 2006;71:1162-1174.
236 Solazzo M, Fantappie O, Lasagna N, Sassoli C, Nosi D, Mazzanti R. P-gp localization in mitochondria and its functional characterization in multiple drug-resistant cell lines. Exp Cell Res 2006;312:4070-4078.
237 Karla PK, Earla R, Boddu SH, Johnston TP, Pal D, Mitra A. Molecular expression and functional evidence of a drug efflux pump (bcrp) in human corneal epithelial cells. Curr Eye Res 2009;34:1-9.
238 Karla PK, Pal D, Mitra AK. Molecular evidence and functional expression of multidrug resistance associated protein (mrp) in rabbit corneal epithelial cells. Exp Eye Res 2007;84:53-60.
239 Gottesman MM. Mechanisms of cancer drug resistance. Annu Rev Med 2002;53:615-627.
240 Gillet JP, Gottesman MM. Mechanisms of multidrug resistance in cancer. Methods Mol Biol;596:47-76.
241 Pommier Y, Sordet O, Antony S, Hayward RL, Kohn KW. Apoptosis defects and chemotherapy resistance: Molecular interaction maps and networks. Oncogene 2004;23:2934-2949.
242 Hendrich AB, Michalak K. Lipids as a target for drugs modulating multidrug resistance of cancer cells. Curr Drug Targets 2003;4:23-30.
243 Liscovitch M, Lavie Y. Multidrug resistance: A role for cholesterol efflux pathways? Trends Biochem Sci 2000;25:530-534.
244 Lage H, Dietel M. Involvement of the DNA mismatch repair system in antineoplastic drug resistance. J Cancer Res Clin Oncol 1999;125:156-165.
245 Gottesman MM, Fojo T, Bates SE. Multidrug resistance in cancer: Role of atp-dependent transporters. Nat Rev Cancer 2002;2:48-58.
246 Duvvuri M, Krise JP. Intracellular drug sequestration events associated with the emergence of multidrug resistance: A mechanistic review. Front Biosci 2005;10:1499-1509.
247 Slapak CA, Lecerf JM, Daniel JC, Levy SB. Energy-dependent accumulation of daunorubicin into subcellular compartments of human leukemia cells and cytoplasts. J Biol Chem 1992;267:10638-10644.

248 Hindenburg AA, Gervasoni JE, Jr., Krishna S, Stewart VJ, Rosado M, Lutzky J, Bhalla K, Baker MA, Taub RN. Intracellular distribution and pharmacokinetics of daunorubicin in anthracycline-sensitive and -resistant hl-60 cells. Cancer Res 1989;49:4607-4614.
249 Solazzo M, Fantappie O, D'Amico M, Sassoli C, Tani A, Cipriani G, Bogani C, Formigli L, Mazzanti R. Mitochondrial expression and functional activity of breast cancer resistance protein in different multiple drug-resistant cell lines. Cancer Res 2009;69:7235-7242.
250 Rajagopal A, Simon SM. Subcellular localization and activity of multidrug resistance proteins. Mol Biol Cell 2003;14:3389-3399.
251 Meschini S, Calcabrini A, Monti E, Del Bufalo D, Stringaro A, Dolfini E, Arancia G. Intracellular p-glycoprotein expression is associated with the intrinsic multidrug resistance phenotype in human colon adenocarcinoma cells. Int J Cancer 2000;87:615-628.
252 Shapiro AB, Fox K, Lee P, Yang YD, Ling V. Functional intracellular p-glycoprotein. Int J Cancer 1998;76:857-864.
253 Ling X, He Y, Zhang G, Zhou Y, Yan B. Increased p-glycoprotein expression in mitochondria is related to acquired multidrug resistance in human hepatoma cells depleted of mitochondrial DNA. Int J Oncol;40:109-118.
254 Shen Y, Chu Y, Yang Y, Wang Z. Mitochondrial localization of p-glycoprotein in the human breast cancer cell line mcf-7/adm and its functional characterization. Oncol Rep;27:1535-1540.
255 Janoria KG, Boddu SH, Natesan S, Mitra AK. Vitreal pharmacokinetics of peptide-transporter-targeted prodrugs of ganciclovir in conscious animals. J Ocul Pharmacol Ther;26:265-271.
256 Dey S, Patel J, Anand BS, Jain-Vakkalagadda B, Kaliki P, Pal D, Ganapathy V, Mitra AK. Molecular evidence and functional expression of p-glycoprotein (mdr1) in human and rabbit cornea and corneal epithelial cell lines. Invest Ophthalmol Vis Sci 2003;44:2909-2918.
257 Chaiyarit S, Thongboonkerd V. Comparative analyses of cell disruption methods for mitochondrial isolation in high-throughput proteomics study. Anal Biochem 2009;394:249-258.
258 Bourgeron T, Chretien D, Rotig A, Munnich A, Rustin P. Isolation and characterization of mitochondria from human b lymphoblastoid cell lines. Biochem Biophys Res Commun 1992;186:16-23.
259 Reers M, Smith TW, Chen LB. J-aggregate formation of a carbocyanine as a quantitative fluorescent indicator of membrane potential. Biochemistry 1991;30:4480-4486.
260 Zinchuk V, Zinchuk O. Quantitative colocalization analysis of confocal fluorescence microscopy images. Curr Protoc Cell Biol 2008;Chapter 4:Unit 4 19.
261 Anand BS, Dey S, Mitra AK. Current prodrug strategies via membrane transporters/receptors. Expert Opin Biol Ther 2002;2:607-620.
262 Gunda S, Hariharan S, Mitra AK. Corneal absorption and anterior chamber pharmacokinetics of dipeptide monoester prodrugs of ganciclovir (gcv): In vivo comparative evaluation of these prodrugs with val-gcv and gcv in rabbits. J Ocul Pharmacol Ther 2006;22:465-476.
263 Katragadda S, Talluri RS, Mitra AK. Modulation of p-glycoprotein-mediated efflux by prodrug derivatization: An approach involving peptide transporter-mediated influx across rabbit cornea. J Ocul Pharmacol Ther 2006;22:110-120.

264 Agarwal S, Jain R, Pal D, Mitra AK. Functional characterization of peptide transporters in mdckii-mdr1 cell line as a model for oral absorption studies. Int J Pharm 2007;332:147-152.
265 Buyse M, Berlioz F, Guilmeau S, Tsocas A, Voisin T, Peranzi G, Merlin D, Laburthe M, Lewin MJ, Roze C, Bado A. Pept1-mediated epithelial transport of dipeptides and cephalexin is enhanced by luminal leptin in the small intestine. J Clin Invest 2001;108:1483-1494.
266 Mantovani I, Cappellini A, Tazzari PL, Papa V, Cocco L, Martelli AM. Caspase-dependent cleavage of 170-kda p-glycoprotein during apoptosis of human t-lymphoblastoid cem cells. J Cell Physiol 2006;207:836-844.

VITA

Megha Barot was born on July 14, 1983, in Kalol, Gujarat, India. She completed her secondary education from Dayalbagh Educational Institute, Agra. Later she obtained her Bachelor of Pharmacy and Masters in Pharmaceutical Science degrees from Barkatullah University (Bhopal) and Sardar Patel University (Vallabh Vidyanagar), respectively. After completion of M.Pharm., she worked as a Lecturer in R. P. College of Pharmacy, Gujarat, India.

Megha joined Interdisciplinary Ph.D. program at UMKC in fall 2008. She served as a Librarian of Pharmaceutical Sciences Graduate Students Association (PSGSA) during the academic year of 2009-10. She has received Ocular Drug Delivery and Disposition Focus Group (ODDDFG) student poster 1st place award for her work presented at 2012 AAPS annual meeting. She has also received a UMKC Interdisciplinary Doctoral Student Council-Community of Scholars best research poster award (2012), Women's Council Graduate Assistance Fund awards (2011 and 2012), and a Pharmacy Foundation Grant award (2011). Mrs. Barot is a member of the American Association of Pharmaceutical Scientists (AAPS) and the Association of Research in Vision and Ophthalmology (ARVO). She is currently serving as a student representative of the AAPS ODDDFG steering committee. She completed her doctoral studies in January 2013 under the guidance of Dr. Ashim K. Mitra. She has authored and co-authored several peer reviewed publications, and has presented at several national conferences. She has currently accepted a position at United States Pharmacopeia, Rockville, MD.